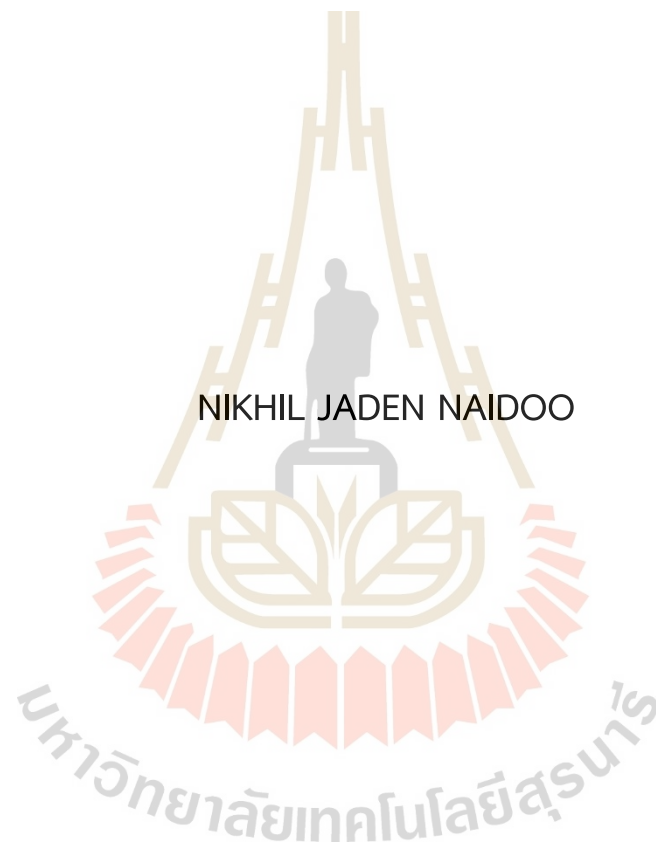


ENHANCEMENT OF POWER CONVERSION EFFICIENCY OF BULK
CRYSTALLINE SOLAR CELLS THROUGH CADMIUM SULPHIDE
WINDOW LAYER WITH BISMUTH DOPED ZINC OXIDE BUFFER
LAYER



A Thesis Submitted in Partial Fulfilment of the Requirements for the
Degree of Master of Engineering in Electrical Engineering
Suranaree University of Technology
Academic Year 2021

การเพิ่มประสิทธิภาพการแปลงพลังงานของเซลล์แสงอาทิตย์ชนิดผลึก
ซิลิคอนด้วยชั้นหน้าต่างแคดเมียมซัลไฟด์ที่มีชั้นบัฟเฟอร์ของซิงค์ออกไซด์เจือ
บิสมีท



วิทยานิพนธ์นี้เป็นส่วนหนึ่งของการศึกษาตามหลักสูตรปริญญาวิศวกรรมศาสตรมหาบัณฑิต
สาขาวิชาวิศวกรรมไฟฟ้า
มหาวิทยาลัยเทคโนโลยีสุรนารี
ปีการศึกษา 2564

ENHANCEMENT OF POWER CONVERSION EFFICIENCY OF BULK
CRYSTALLINE SOLAR CELLS THROUGH CADMIUM SULPHIDE
WINDOW LAYER WITH BISMUTH DOPED ZINC OXIDE BUFFER
LAYER

Suranaree University of Technology has approved this thesis submitted in
partial fulfilment of the requirements for a Master's Degree.

Thesis Examining Committee



(Dr. Rungrueng Pattanakul)
Chairperson



(Asst. Prof. Dr. Thipwan Fangsuwannarak)
Member (Thesis Advisor)



(Asst. Prof. Dr. Boonsong Sutaphan)
Member



(Assoc. Prof. Dr. Chatchai Jothityangkoon)
Vice Rector for Academic Affairs and
Quality Assurance



(Assoc. Prof. Dr. Pornsiri Jongkol)
Dean of Institute of Engineering

NIKHIL JADEN NAIDOO : การเพิ่มประสิทธิภาพการแปลงพลังงานของเซลล์แสงอาทิตย์ชนิดผลึกซิลิคอนด้วยชั้นหน้าต่างแคดเมียมซัลไฟด์ที่มีชั้นบัฟเฟอร์ของซิงค์ออกไซด์เจือบิสมัท (ENHANCEMENT OF POWER CONVERSION EFFICIENCY OF BULK CRYSTALLINE SOLAR CELLS THROUGH CADMIUM SULPHIDE WINDOW LAYER WITH BISMUTH DOPED ZINC OXIDE BUFFER LAYER)

อาจารย์ที่ปรึกษา : ผู้ช่วยศาสตราจารย์ ดร.ทิพย์วรรณ พิงสุวรรณ์รักษ์, 102 หน้า.

คำสำคัญ : फिल्मบาง แคดเมียมซัลไฟด์ ซิงค์ออกไซด์ แถบพลังงานช่องว่าง ความยาวคลื่น

วิทยานิพนธ์เล่มนี้ได้ศึกษาการประยุกต์ใช้ฟิล์มบางควอนตัมต่อทจากแคดเมียมซัลไฟด์และซิงค์ออกไซด์เจือบิสมัทเพื่อพัฒนาประสิทธิภาพเซลล์แสงอาทิตย์ เนื่องจากเซลล์แสงอาทิตย์ในปัจจุบันมีการใช้งานจากวัสดุซิลิคอน ซึ่งซิลิคอนมีขีดจำกัดในการแปลงพลังงานแสงเป็นพลังงานไฟฟ้า ดังนั้นการปรับปรุงคุณภาพจึงมีความจำเป็นอย่างยิ่งในการเพิ่มประสิทธิภาพการแปลงพลังงานแสงเป็นพลังงานไฟฟ้า หนึ่งใน การปรับปรุงคือการสร้างชั้นฟิล์มบางบนเซลล์แสงอาทิตย์ เพื่อลดการสูญเสียพลังงานทางแสงที่ตกกระทบลงบนเซลล์แสงอาทิตย์และลดการรวมตัวกันของพาหะ และยังสามารถเป็นหน้าต่างรับแสงเพื่อลดการสะท้อนแสงกลับของแสงและช่วยเพิ่มการดูดกลืนพลังงานจากแสงอาทิตย์

ฟิล์มบางแคดเมียมบนซิงค์ออกไซด์ถูกสร้างขึ้นจากกระบวนการหมุนเหวี่ยงบนแผ่นควอตซ์ที่มีชั้นซิงค์ออกไซด์เป็นชั้นบัฟเฟอร์ และได้ถูกวิเคราะห์คุณสมบัติต่างๆ พบว่าจากการวิเคราะห์ทางแสงด้วยเครื่อง UV-VIS ฟิล์มบางแคดเมียมบนซิงค์ออกไซด์มีค่าการสะท้อนแสงกลับที่ต่ำในช่วงความยาวคลื่นช่วงคลื่นตามองเห็น แต่ในขณะที่ค่าการทะลุผ่านของแสงของฟิล์มบางมีค่าที่มากในช่วงความยาวคลื่นช่วงตามองเห็น และมีค่าการทะลุผ่านของแสงในช่วงความยาวคลื่นเหนือม่วงที่น้อยกว่า 400 nm จากการวิเคราะห์การเกาะเกี่ยวทางเคมีด้วยเครื่อง FTIR พบว่าฟิล์มบางเกิดการเกาะเกี่ยวพันธะระหว่างแคดเมียมและซัลเฟอร์ ซึ่งกล่าวได้ว่าสามารถสร้างฟิล์มบางแคดเมียมซัลไฟด์ด้วยวิธีการหมุนเหวี่ยงได้

จากการวิเคราะห์พื้นผิวฟิล์มบางด้วยภาพถ่ายจากเครื่อง FESEM พบว่าฟิล์มบางที่มีชั้นซิงค์ออกไซด์สามารถปรับปรุงพื้นผิวให้ฟิล์มบางแคดเมียมซัลไฟด์เกาะอยู่บนพื้นผิวได้ดีขึ้น เรียบเนียนเป็นเนื้อเดียวกัน และลดรอยแตกร้าวของฟิล์มบางลง ซึ่งผลจากการวัดเชิงโครงสร้างด้วยเครื่อง XRD แสดงให้เห็นถึงโครงสร้างของแคดเมียมซัลไฟด์ที่มีโครงสร้างผลึกเป็นรูปแบบของคิวบิก (Cubic) และโครงสร้างของซิงค์ออกไซด์ที่มีโครงสร้างผลึกแบบ Hexagonal wurtzite นอกจากนี้ยังพบอีกว่าเมื่อทำการ

อบฟิล์มที่อุณหภูมิสูงฟิล์มบางที่สังเคราะห์ขึ้นจะเกิดการแยกเฟส และจากการวัดคุณสมบัติทางไฟฟ้าด้วยวิธี Two-probe เพื่อนำค่าแรงดันไฟฟ้าและค่ากระแสไฟฟ้าที่วัดได้มาคำนวณหาค่าความต้านทานจำเพาะและค่าความนำไฟฟ้าจำเพาะของฟิล์มบางที่สร้างขึ้น โดยจากผลที่ได้พบว่าฟิล์มบางมีค่าความนำไฟฟ้าที่ดีมากขึ้น โดยเงื่อนไขที่มีชั้นซิงค์ออกไซด์และชั้นฟิล์มบางแคดเมียมจำนวนอย่างละ 3 ชั้น ให้ค่าความนำไฟฟ้าที่มากที่สุด และเหมาะสำหรับการนำมาประยุกต์ใช้เป็นชั้นหน้าต่างรับแสงสำหรับเซลล์แสงอาทิตย์



สาขาวิชา วิศวกรรมไฟฟ้า
ปีการศึกษา 2564

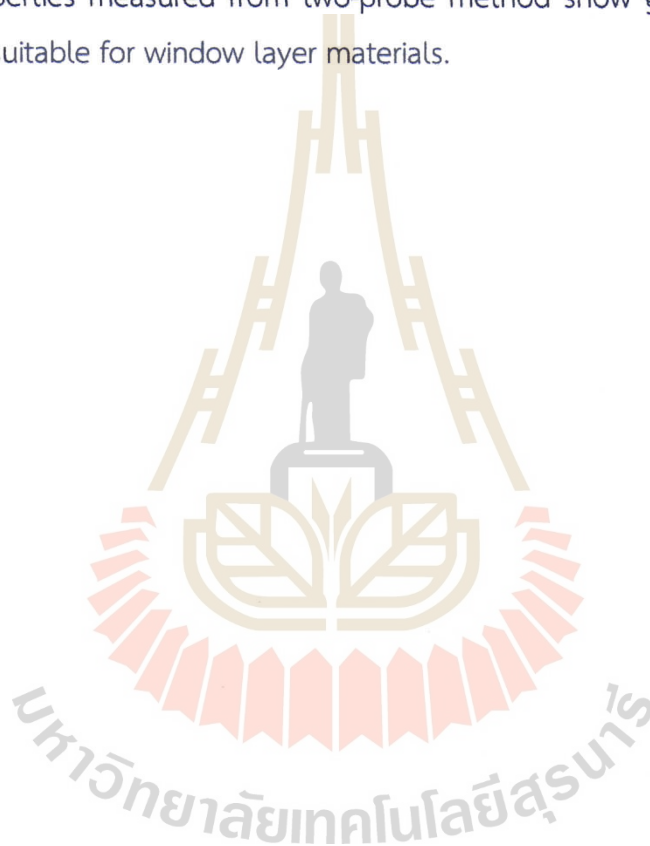
ลายมือชื่อนักศึกษา
ลายมือชื่ออาจารย์ที่ปรึกษา.....

NIKHIL JADEN NAIDOO : ENHANCEMENT OF POWER CONVERSION EFFICIENCY OF BULK CRYSTALLINE SOLAR CELLS THROUGH CADMIUM SULPHIDE WINDOW LAYER WITH BISMUTH DOPED ZINC OXIDE BUFFER LAYER. THESIS ADVISOR : ASST. PROF. THIPWAN FANGSUWANNARAK. Ph.D., 102 PP.

Keyword: THIN FILM/ CADMIUM SULPHIDE/ ZINC OXIDE/ QUANTUM DOT/ BAND GAP/ WAVELENGTH

This thesis presents an investigation into the use of quantum dot thin films as potential window layer materials in the improvement of photovoltaic solar cell efficiency. The materials studied are bismuth doped zinc oxide and cadmium sulphide. Methods of fabrication are studied to determine a simple method of synthesis and deposition. While other methods are studied, both materials used are deposited through spin coating, onto quartz substrates, for characterizations, and onto PN silicon in an attempt to create a prototype photovoltaic device. The properties of the thin films — optical, structural, and electrical — are studied through various means, including, UV-Vis, FTIR, XRD, FESEM, and two-probe technique. Together with the properties of the thin films, the factors affecting these properties are also studied in this research. The properties studied are to determine whether the materials would be a viable option for solar cell applications. Absorption, transmittance, reflectance, band gap, conductivity and resistivity, surface morphology and structural bonding are all investigate. Manipulation of the properties is also possible through the changing of certain factors like grain size, number of layers and temperature, which is documented in this thesis. To prove that the materials are suitable for improvement of efficiency, the properties are analysed with respect to those of crystalline silicon, attempting to limit the light that is wasted by the silicon solar cells, while also mitigating parasitic losses to the window layer materials. After characterizing the films, the films are deposited onto crystalline silicon and tested. Contacts are made through screen printing, with silver front contacts and aluminium rear contacts. Results obtained from UV-Vis analysis of the films, for optical properties show low reflectance in the wavelengths in the visible light region of the spectrum, while transmittance is high in

the visible light region of the spectrum, and low in the UV-region — $<400\text{nm}$. Structural analysis of the films through FTIR showed bonds formed between cadmium and sulphur, creating the cadmium sulphide particles, proving the method of deposition successful. The surface morphology data, studied through XRD and FESEM show improved homogeneity of the CdS film when deposited on a ZnO:Bi buffer layer, compared to deposition on plain quartz. Increased temperature was also shown to affect the surface morphology, with a higher temperature resulting in phase separation. Electrical properties measured from two-probe method show good conductivity on certain films, suitable for window layer materials.



School of Electrical Engineering
Academic Year 2021

Student's Signature
Advisor's Signature

[Handwritten Signature]
[Handwritten Signature]

ACKNOWLEDGEMENT

This thesis is a result of work made possible through the support of various individuals and institutions who I will forever be extremely grateful for.

Firstly, I would like to thank my academic advisor Asst. Prof. Dr Thipwan Fangsuwannarak, who has guided me and helped me grow as a researcher, for which I am extremely grateful. In addition, I would like to thank the committee members, Asst. Prof. Dr Boonsong Sutaphan and Dr Runrueang Pattanakul for their valuable advice. Also, I would like to acknowledge the assistance provided by Dr Colin Thomas Strine, with research and writing.

This thesis is also made possible by the funding provided by the Suranaree University of Technology, through the Nelson Mandela scholarship, and the Durban University of Technology co-operative education. My sincere thanks also go to the centre for international affairs (CIA) at Suranaree University for all their assistance.

Lastly, I would like to thank my family and friends who have played one of the most important roles during my time studying. My family for their continued support and faith in me, and friends, both in Thailand and South Africa, for their support, keeping me motivated.

Nikhil Jaden Naidoo

TABLE OF CONTENTS

	Page
ABSTRACT (THAI).....	I
ABSTRACT (ENGLISH).....	III
ACKNOWLEDGEMENT.....	V
TABLE OF CONTENTS.....	VI
LIST OF TABLES.....	IX
LIST OF FIGURES.....	X
CHAPTER	
1. INTRODUCTION	1
1.1 Background.....	1
1.2 Solar cells.....	10
1.3 Quantum dots.....	13
1.3.1 Quantum dot band gaps.....	13
1.3.2 Multiple exciton generation.....	14
1.4 Band gap.....	16
1.5 Window layers and heterojunctions	18
1.6 Cadmium sulphide.....	19
1.7 Zinc oxide.....	21
1.8 Research objectives	22
1.9 Scope and limitations.....	23
1.9.1 Preparation method	23
1.9.2 Characterisations	23
1.9.3 Power conversion efficiency (PCE) measurement of a prototype device	24

TABLE OF CONTENTS (Continued)

	Page
2. LITERATURE REVIEW	25
2.1 Background	25
2.2 CdS particle size	25
2.3 Band gap tuning.....	26
2.4 Temperature Variations.....	26
2.5 Crystal structure.....	28
2.6 Methods of deposition.....	29
2.7 Downshifting	30
2.8 Cadmium sulphide in heterojunction solar cells.....	31
2.8.1 Cadmium sulphide with crystalline silicon	31
2.8.2 Cadmium sulphide with cadmium tellurium.....	32
2.8.3 Cadmium sulphide with lead sulphide.....	32
2.8.4 Cadmium sulphide with perovskite	33
2.9 Zinc oxide thin films.....	33
2.10 Summary	34
3. METHODOLOGY.....	39
3.1 Introduction	39
3.2 Materials	39
3.3 Procedure.....	40
3.3.1 Zinc oxide preparation.....	40
3.3.2 Cadmium sulphide preparation	40
3.3.3 Characterizing thin films	42
3.4 Summary	47
4. RESULTS AND DISCUSSION.....	48
4.1 Introduction	48

TABLE OF CONTENTS (Continued)

	Page
4.2 Analysis of bismuth doped zinc oxide multilayers	48
4.3 Using bismuth doped zinc oxide as a buffer layer for cadmium sulphide	52
4.3.1 Determining the ideal number of layers of ZnO:Bi for the buffer layer.....	52
4.3.2 The effect of a varied temperature for drying cadmium sulphide	64
4.3.3 The effect of a varied number of layers for cadmium sulphide	66
4.4 Cadmium sulphide deposited by spin coating onto PN Silicon	71
4.5 Summary	73
5. Conclusions and recommendations.....	74
References.....	76
Vitae.....	. 87

LIST OF TABLES

Table	Page
1.1 Comparison of land required by different power plants to generate the same amount of power and their respective CO ₂ emissions.....	5
2.1 The band gap energy and particle size (diameter) of synthesized CdS NPs, obtained from absorption spectra.....	26
2.2 Properties of CdS thin films with and without annealing at different temperatures, using CBD technique.....	28
2.3 Energy band values for TiO ₂ , CdS, and TiO ₂ /CdS deposited by CBD and SILAR methods.....	29
2.4 Methods of deposition for P-Si/CdS.....	32
2.5 Summary of results achieved from previous experiments.....	35
4.1 Interpretation of the valleys obtained by the FTIR spectra of the synthesized CdS/ZnO:Bi nanostructures.....	54
4.2 Thickness and electrical properties of nanostructure thin films fabricated.....	58
4.3 Correlation between the number of layers of CdS and the grain size, absorption edge and band gap.....	71

LIST OF FIGURES

Figure	Page
1.1 Share among different fuel types, for electricity generated globally. Data.....	2
1.2 Carbon dioxide emissions by internal combustion engine vehicles (ICEV), hybrid engine vehicles (HEV) and electric vehicles (EV), per 100 kilometres (km) travelled, for grids containing various amounts of coal power generation in China.	3
1.3 Comparison of construction costs, with respect to generation capabilities, between generation plants of different sources.	6
1.4 Breakdown of construction costs of a 5MW PV generation plant.....	7
1.5 Spectrum of solar irradiance with absorbable light with Si and potential improvement with larger band gap window layer	9
1.6 Differently doped silicon making up the p-region and n-region of a PV cell.	11
1.7 Structure of the depletion region of the solar cell, together with the concentration of electrons and holes in each region before and after the diffusion process.....	12
1.8 Operation of PV cell.....	13
1.9 Varied Quantum dot energy band gaps vs quantum dot size for different materials.	14
1.10 Multiple exciton generation in a quantum dot.....	16
1.11 Energy vs crystal momentum for a semiconductor with (a) an indirect band gap and (b) a direct band gap.	17
1.12. Different layers making up the structure of a solar cell	19
1.13 Unit cell of CdS crystal, where the larger demonstrated atoms are that of Cd and the smaller are that of S, showing (a) wurtzite, (b) zinc blend and (c) rock salt phases.....	21
2.1 Optical absorption spectrum of bare TiO ₂ , CdS 9, 12, 15 and 18 SILAR cycles.	27
2.2 Absorbance and photoluminescence emission spectra of synthesized CdSe/CdS QD's.....	30

LIST OF FIGURES (CONTINUED)

Figure	Page
2.3 Absorbance and photoluminescence (PL) emission spectra of synthesized ZnO QDs with different pH values. The PL spectrum was obtained using an excitation wavelength of 340 nm.	31
3.1 Process for synthesizing bismuth doped zinc oxide.....	41
3.2 Process of depositing cadmium sulphide thin film by spin coating.....	42
3.3 Keithley a Tektronix Electrometer 2400 used for two-probe method to find current density.....	43
3.4 Screen-printing technique used for metal contacts.....	46
3.5 Diode behaviour when a bias voltage is applied to solar cell to test PN junction properties	46
4.1 Transmittance rates of bismuth doped zinc oxide with different number of layers, for varying wavelengths.	49
4.2 Reflectance rates of bismuth doped zinc oxide with different number of layers, for varying wavelengths.....	50
4.3 FTIR spectra of ZnO:Bi thin films on quartz with varied number of layers	50
4.4 FESEM image of 1 layer bismuth doped zinc oxide on quartz substrate magnified 1000 times.....	51
4.5 FESEM image of 4-layer bismuth doped zinc oxide on quartz substrate magnified 1000 times.....	51
4.6 Comparison of surface homogeneity between 3 CdS layer samples deposited (a) directly onto quartz substrate and (b) onto ZnO:Bi buffer layer	52
4.7 FTIR spectra of fabricated ZnO:Bi and CdS nanostructure thin films.....	53
4.8 J-V curve for all samples under dark vs illumination test for determination of ohmic/non-ohmic behaviour.	56
4.9. J-V plot in dark vs illumination test for photocurrent gain.	57
4.10 Transmittance spectra of CdS window layer and ZnO:Bi buffer layer with samples containing varying number of layers.	60

LIST OF FIGURES (CONTINUED)

Figure	Page
4.11 Reflectance spectra of CdS window layer and ZnO:Bi buffer layer with samples containing varying number of layers.	60
4.12 Absorption coefficients for fabricated samples at different wavelengths and inset are the estimated wavelengths for absorption edges	62
4.13 $(\alpha hv)^2$ versus (hv) curve for all samples (Tauc plot to determine band gap).....	63
4.14 Refractive index for all fabricated samples.....	63
4.15 FESEM images showing surface of ZnO:Bi_1L/CdS_5L prepared at a)100°C, b)200°C and c)300°C.	64
4.16 EDS data for film prepared at 300°C, showing the concentration of different elements on the ZnO_1L/CdS_5L film, proving the crystals formed are of sodium acetate.....	65
4.17 XRD analysis of ZnO:Bi_3L/CdS_5L at 100°C, 200°C and 300°C.....	66
4.18 SEM images of CdS films at 30000 x magnification; a) CdS_3L, b) CdS_5L, c) CdS_8L, d) CdS_11L.	67
4.19 XRD results from samples containing various number of layers of CdS on 3 ZnO:Bi layers.....	68
4.20 Absorption coefficients of CdS window layer and ZnO:Bi buffer layer with samples containing varying number of layers.	69
4.21 $(\alpha hv)^2$ versus (hv) curve for all samples (Tauc plot to determine band gap).....	70
4.22 Structure of prototype photovoltaic cell where metal makes a) contact on PN - junction, and b) non-firing contact	72
4.23 Curve from bias voltage applied to a PN-Si/ZnO:Bi diode	72
4.24 Current density and voltage of samples, with efficiencies, measured under solar simulator.....	74

CHAPTER 1

INTRODUCTION

1.1 Background

The entire world is currently heavily dependent on coal, oil, and gas, as these fossil fuels are responsible for electricity generation, depicted in figure 1.1. Coal and oil are widely used to generate electricity, while oil is also used as the preferred fuel for most vehicles (cars, trucks, ships, etc.), powering their internal combustion engines. As global electricity demand grows, through technological advancements and implementation in our daily lives, generation capacity needs to grow as well. However, fossil fuels, which have been used to generate electricity and mechanical power, since the dawn of industrialisation, do not satisfy the evolving requirements for a 21st century source of electricity; one that is clean, renewable, sustainable, and affordable. (BP, 2020; Breeze, 2019; Comello et al., 2018; Shalaeva et al., 2020)

Traditional power plants, using fuels like coal and oil, produce large amounts of carbon dioxide (CO₂), which remains in the Earth's atmosphere, contributing to the global warming crisis humans are currently battling. These fossil fuel plants aren't sustainable as fossil fuels aren't renewable resources, facing depletion if they are relentlessly used, with coal reserves expected to run out within the next 132 years, if the current rate of use persists, according to the world coal association. (*What Is Coal & Where Is It Found?*, 2020)

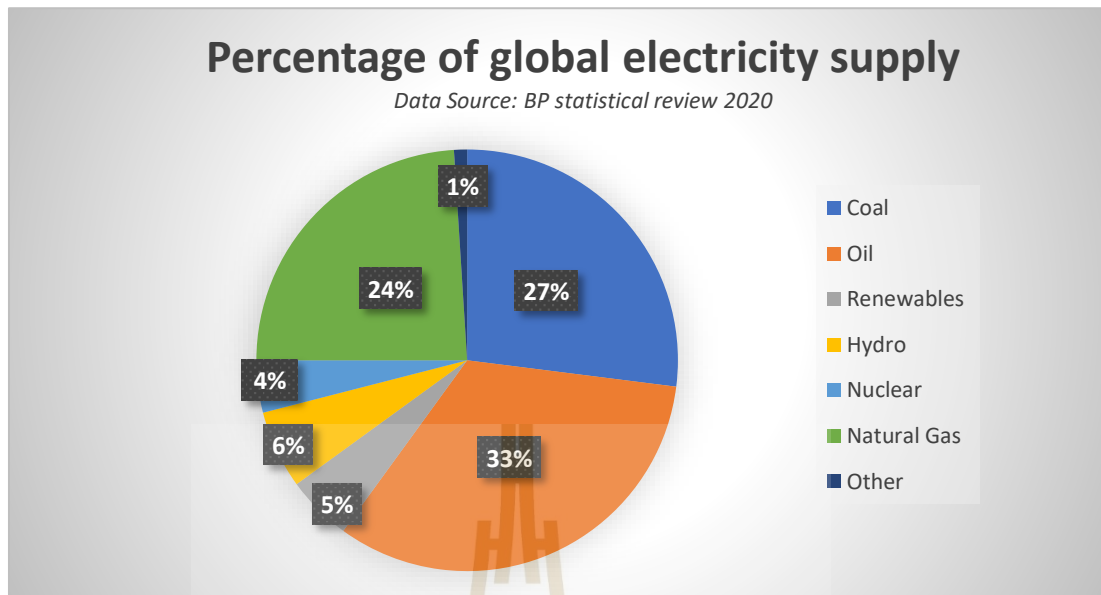


Figure 1.1 Share among different fuel types, for electricity generated globally. Data source:BP Statistical review 2020 (BP, 2020)

Electricity demand is expected to only grow as new technologies are developed, these include electric vehicles (EV's), which have also begun the transition of vehicles from fossil fuel powered internal combustion engines, to vehicles propelled by electric motors. With world oil reserves predicted to last just 50 more years, according to British petroleum energy reviews 2020 (BP, 2020), EV's could play an integral part in reducing carbon emissions from vehicles and power plants, through decreasing dependence on fossil fuels. However, at present the electricity that is needed to power EV's are mostly generated from fossil fuels, as seen in figure 1.1; hence, while EV's are taking us away from dependence on oil, they are still largely dependent on coal/gas/oil generated electricity, currently failing to achieve the goal of reducing carbon emissions. To fully reap the benefits of EV's, just like for household electricity demands, renewable energy needs to be more widely integrated into the global electricity supply. (BP, 2020; Huo et al., 2010)

While coal power plants are the main contributors to a grid; EV's will have little to no effect on carbon emissions. As seen in figure 1.2, a reduction in emissions will

only begin to occur when the grid from which EV's draw power, is comprised of at least 5% renewable energy.

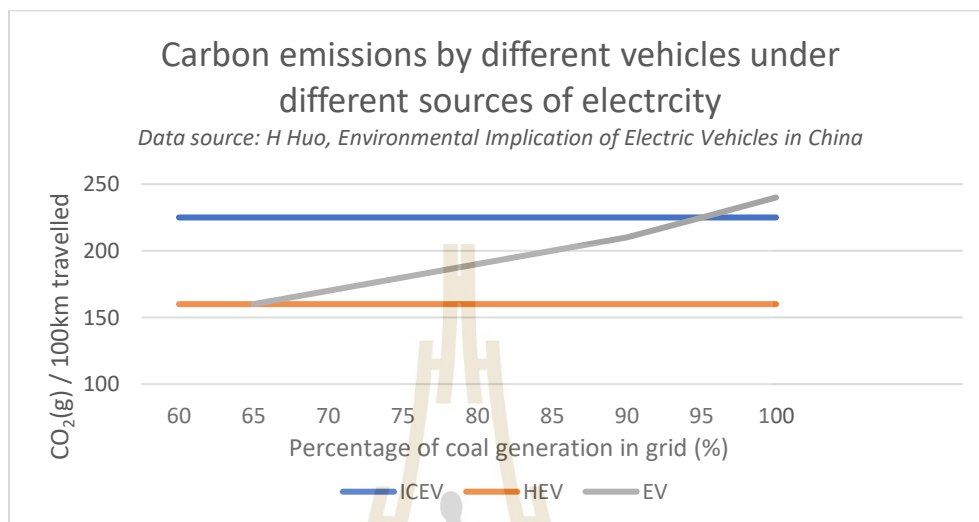


Figure 1.2 Carbon dioxide emissions by internal combustion engine vehicles (ICEV), hybrid engine vehicles (HEV) and electric vehicles (EV), per 100 kilometres (km) travelled, for grids containing various amounts of coal power generation in China. (Huo et al., 2010)

Solar power has the potential to solve carbon emission problems by harnessing sunlight to generate electricity. Over the span of a year, enough energy strikes the surface of the earth as solar irradiance, to meet 6000-8000 times the annual global electricity demand (Breeze, 2019). While the resource of sunlight is abundant, the harnessing capability is limited. The cost of manufacturing photovoltaic (PV) solar panels, together with storage systems, has been continuously decreasing, making PV solar power one of the fastest growing renewable energies, but solar power generation still pales in comparison to fossil fuel generation capacity (Comello et al., 2018; Molina, 2017).

Abundant solar irradiation, adequate slope and aspect, transmission lines that are within reasonable proximity to a populated area/road infrastructure, and a certain

type of land cover — short vegetation/shrublands, and free of mountains, forests, buildings — are the various requirements that need to be met for land to be used for a photovoltaic power plant (Kereush & Perovych, 2017). Research has been done into potentially using deserts or large bodies of water as alternatives, to solve the land requirement problem, however deserts present problems such as inoperable temperatures for PV cells, dust, and large transmission distances, while floating PV plants have increased costs related to floating structures (Abid et al., 2018; Bouraiou et al., 2015; Rosa-Clot & Tina, 2018; Saidan et al., 2016).

Lowered costs have improved the affordability of PV solar power, but the land/space required by solar farms is much greater than that of coal power plants (compared in table 1.1), lowering competitiveness for cost per kWh generated, due to the slow increase of efficiency in commercially available solar panels (Capellán-Pérez et al., 2017; Comello et al., 2018; Richter et al., 2013).

Figure 1.3 compares the average construction cost per kilowatt of capacity of different renewables, showing that the construction costs of solar power are relatively higher than that of wind and natural gas. Figure 1.4 shows the breakdown of the construction costs of a 5 MW PV plant, showing that the PV panels make up a large percentage of costs, while land also influences the cost.

To lower the construction costs of PV plants, the cost/number of solar panels will need to be reduced, together with the land requirements; these can only be achieved by increasing the efficiency of the panels while keeping costs low.

Table 1.1 Comparison of land required by different power plants to generate the same amount of power and their respective CO₂ emissions. (Kengpol et al., 2013)

Technology	Land in use (km ² /GW/year)	CO ₂ emissions (tonnes/GW/year)
Solar	630	600
Biomass	25600	600
Wind	9900	600
Hydro	7600	2000
Oil	20	700000
Natural Gas	20	400000
Coal	35	900000
Nuclear	10	2400

Despite major advancements in PV technology such as solar tracking (Awasthi et al., 2020) and floating solar farms (Abid et al., 2018; Rosa-Clot & Tina, 2018), which also have additional related costs, power conversion efficiencies of bulk silicon (Si) — Si whose band gap is dependent upon the material type — the most common PV's, are still limited by the size of the energy band gap (Saga, 2010; Sproul & Green, 1991). Si bulk material has an energy band gap in the range of 1.1-1.2 eV, which means that it can absorb light in the visible to near-infrared region of the solar spectrum (400-1100 nm), harnessing little to no conversion energy from photons that lie out of the range corresponding to the band gap (Green, 2008; Sproul & Green, 1991). This limitation is why current single junction crystalline Si solar cells can only reach efficiencies of 26.9%, falling short of the maximum theoretical efficiency of approximately 30% (Andreani et al., 2019; Richter et al., 2013; Shockley & Queisser, 1961; Zhao et al., 1999). To push the efficiencies of single-junction cells closer to the theoretical maximum, economical

solutions need to be found to enable the cells to better convert light in the visible to near-infrared range, in particular, higher energy photons at blue light wavelengths.

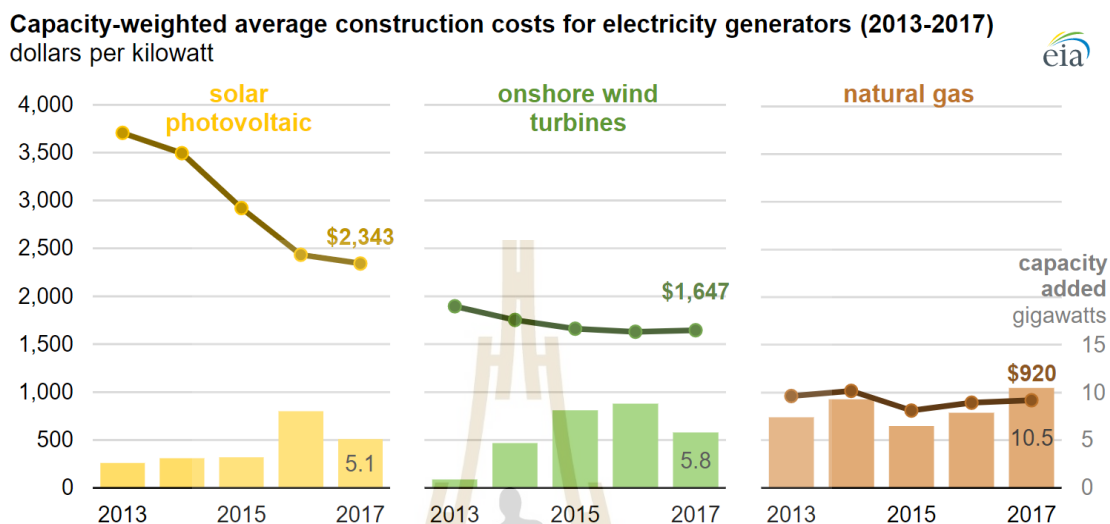


Figure 1.3 Comparison of construction costs, with respect to generation capabilities, between generation plants of different sources. (Mey, 2019)

Thinner silicon wafers can be made to possibly reduce surface recombination losses, converting higher energy photons to electricity, but these thinner wafers have lower power conversion efficiency (PCE) than bulk Si cells, as a result of being an indirect band gap material (Shah, Schade, Vanecek, Meier, Vallat-Sauvain, et al., 2004; Shockley & Queisser, 1961). Multijunction (tandem) solar cells are being developed with much higher efficiencies, due to having multiple energy band gaps, absorbing a wider range of light, however, they have not yet reached cost efficiency levels to compete with single-junction cells and hence, are not easily accessible (Jain & Hudait, 2014; Philipps et al., 2018).

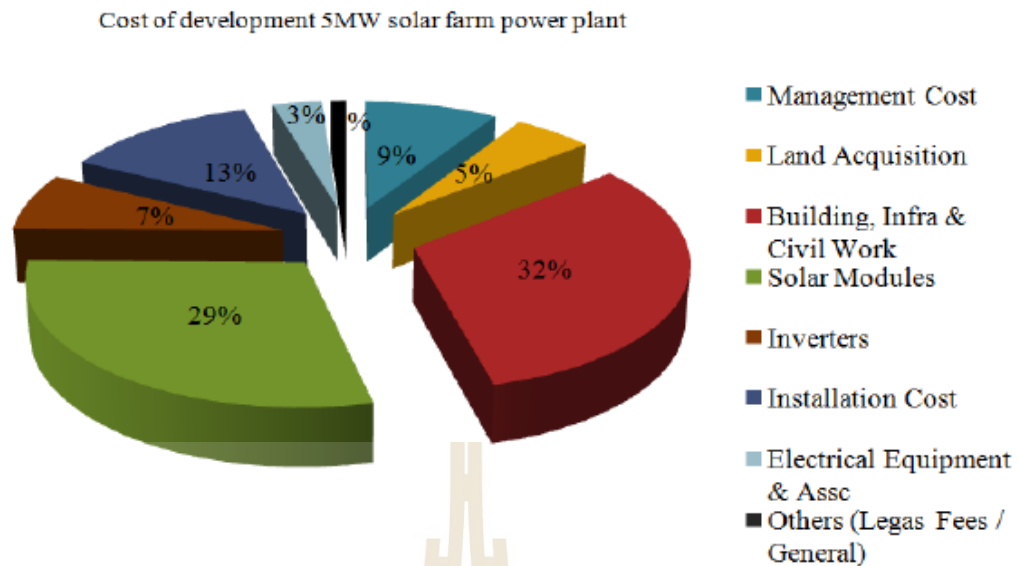


Figure 1.4 Breakdown of construction costs of a 5MW PV generation plant.

(Kassim et al., 2015)

Quantum dots (QD) are semiconducting nanoparticles that have various applications, including sensors and photovoltaics (Esteve-Turrillas & Abad-Fuentes, 2013). QD materials' band gaps can easily be tuned to correspond to light in the ultraviolet (UV) or infrared (IR) regions of the light spectrum, by selecting particle sizes and compositions, which can be synthesized using alloys of elements taken from the groups: 12-16, from which we get compounds such as cadmium sulphide (CdS) and oxide (ZnO) ZnS; 13-15, from which we get semiconductors like gallium arsenide (GaAs); or 14-16, from which we obtain semiconductor materials such as lead selenide (PbSe) (Ahmed et al., 2012; Esteve-Turrillas & Abad-Fuentes, 2013; Hod & Zaban, 2014; Lekha et al., 2013; Sui et al., 2013). These materials present an opportunity for improving the PCE of the already commercially available single-junction crystalline Si solar cells, while remaining cost-efficient, by being used as an economically viable window layer to improve the PCE through widening the range of light that is absorbable and improving the absorption of the visible to near-infrared light range (Hod & Zaban, 2014). QD materials are viable window layers to improve Si solar cells (efficiency) because of their strong light harvesting abilities, stability, high molar extinction coefficient, size-dependant optical properties and low fabrication costs (Ahmed et al.,

2012; Esteve-Turrillas & Abad-Fuentes, 2013; Hod & Zaban, 2014; Lekha et al., 2013; Sui et al., 2013).

A good candidate material for the window layer is CdS, being a direct band gap material with an energy band gap of $\approx 2.42\text{eV}$ (larger than Si) for bulk material and tuneable as quantum dot material. The window layer can be used to improve the absorption range of Si cells, allowing photons with energy lower than 2.42 eV to pass through to the Si solar cell and potentially downshift high-energy wavelengths above 2.42 eV. (Boakye & Nusenu, 1997a; Britt & Ferekides, 1993a; Hodgson et al., 2013; Jones et al., 2009; Qutub et al., 2016).

Zinc Oxide (ZnO) is another direct band gap QD material, that can be incorporated as a thin film nanostructure buffer layer between the absorber and CdS window layer, acting as a physical barrier for migrating dopants/impurities and potentially improving the film quality of the CdS layer, while also improving efficiency (Jones et al., 2009). With a direct band gap of 3.4 eV for bulk material at 300K, ZnO can further widen the absorption range of the solar cell with the CdS window layer (Jones et al., 2009; Krongarrom et al., 2012b; Nicolay et al., 2015). The effect of using a ZnO QD buffer layer, fabricated by sol-gel technique, is also investigated in this study, together with the CdS layer, using structural, optical, and electrical analyses. The band gap of ZnO that is wider than Si and CdS means that it can potentially widen to the absorption range for the window layer solar cell, resulting in an increased PCE.

Figure 1.5 shows the range of wavelengths that correspond to the band gaps of 2.42 eV and 3.4 eV for CdS and ZnO, respectively. A traditional Si solar cell responds efficiently to the photon energy at 1.1eV (1127 nm light wavelength). Thus a lot of energy from the total solar spectrum does not get efficiently absorbed by Si solar cells, often wasted in the form of heat, which further decreases solar cell performance and lifespan (Khalis et al., 2016; Park et al., 2013).

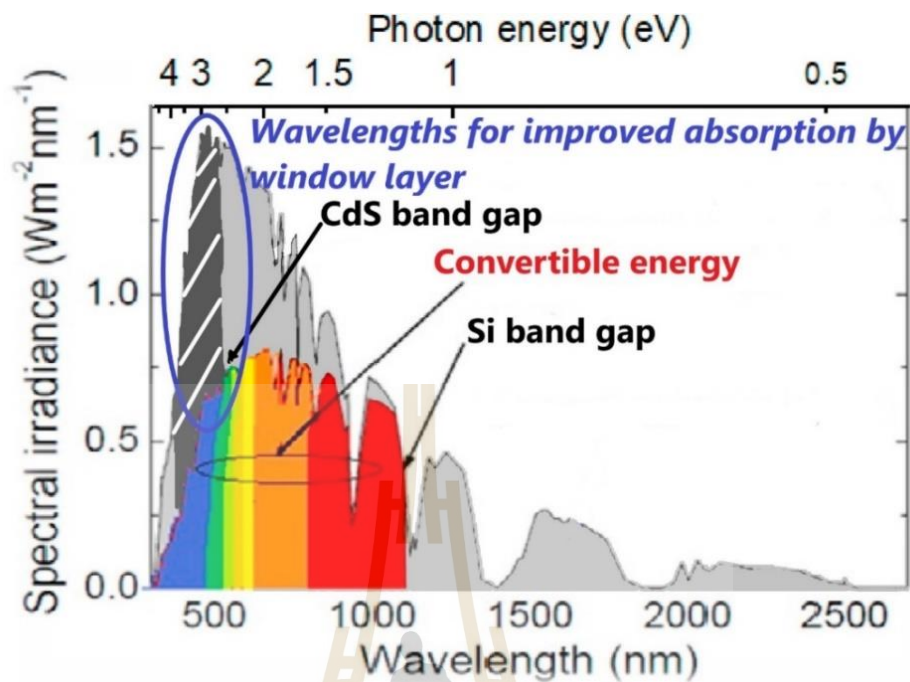


Figure 1.5 Spectrum of solar irradiance with absorbable light with Si and potential improvement with larger band gap window layer

Although CdS nanostructure thin film window layer studies exist, often for use in CdTe and other nanostructure thin film solar cells, research on the use of CdS together with ZnO as the potential window layer for crystalline Si solar cells is uncommon. In this study, we analyse nanostructured CdS window layer fabricated by inexpensive spin coating technique, for the efficiency improvement of commercial bulk Si solar cells. Through using an inexpensive technique such as spin coating, we ensure the economic viability of the solar cells. Applying the window layer to existing bulk Si solar cells, rather than new technologies, like multijunction or quantum dot cells, reduces implementation time, through enhancing solar cells that are already commercially available.

Incorporating the CdS/ZnO:Bi window layer onto already commercial bulk Si solar cells, we can improve the efficiency of these cells; the UV-visible absorption range would decrease losses from heat and Auger recombination caused by high-

energy photons ($>$ Energy band gap of Si), by improving the effective absorption of the higher energy photons through the window layer which has higher energy band gap (Boakye & Nusenu, 1997a). Improved efficiencies of solar cells would mean that required land space, and ultimately the cost per kilowatt hour (kWh) can be reduced, making solar power more appealing, leading to a higher adoption speed of photovoltaic technology.

1.2 Solar cells

Solar cells are electronic devices (semiconductors) with the ability to convert sunlight into electricity, delivering a portion of the energy absorbed from photons, to charge carriers. When light shines upon a solar cell, the cell produces a current and a voltage, to generate electric power. The process whereby light is converted into electricity requires a material in which the absorption of photons will separate an electron from a hole, within the solar cell, promoting electrons to a higher energy state, resulting in the movement of the higher energy state electron from the solar cell to the connected external circuit. The moving higher energy state electron will then dissipate energy in the external electrical devices and thereafter return to the solar cell, resulting in an electrical current. Various materials have the potential to be developed into solar cells due to their PV conversion abilities, however majority of PV energy conversions make use of semiconductor materials in the form of a p-n junction. (Gray, 2011; Jäger et al., 2016; Nelson & Starcher, 2015; Ramalingam & Indulkar, 2017)

Photovoltaic cells are made up of two layers of semiconductor material — most commonly silicon (crystalline, polycrystalline, and amorphous) — sandwiched together. Si is tetravalent material, meaning that it contains four valence electrons. Two layers with different concentrations of free electrons are created through doping the Si with different materials; the two layers are sandwiched together. A layer with an excess of positively charged holes, known as the p-type layer, is typically created by doping the Si with Boron (B) atoms, which are trivalent. A layer with an excess of negatively charged electrons, known as the n-type layer, is typically created by doping the Si with Phosphorous (P) atoms, which are pentavalent. Figure 1.6 shows how the added elements create holes and electrons; the trivalent atoms create additional

holes, while the pentavalent atoms add an additional free electron to the 4 valence electrons of the Si. (Gray, 2011; Jäger et al., 2016; Nelson & Starcher, 2015)

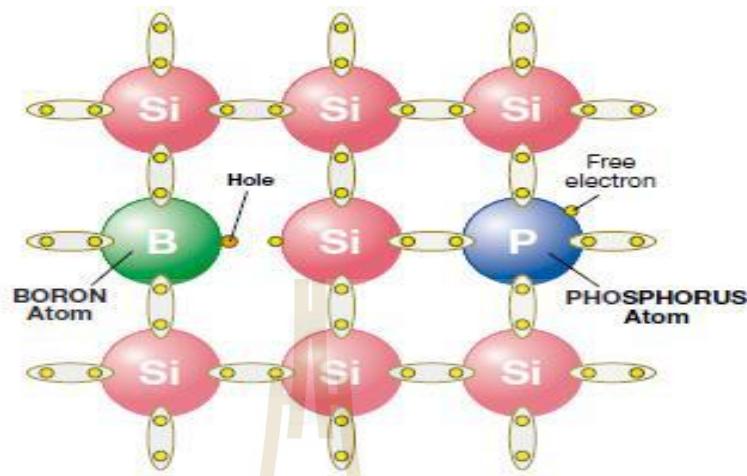


Figure 1.6 Differently doped silicon making up the p-region and n-region of a PV cell. (Jäger et al., 2016)

When the P-type and N-type materials are put together, the positively charged holes in the p-region and negatively charged electrons in the n-region migrate between the two materials. This process is known as diffusion; the movement of carriers creates the diffusion current (I_{Diff}). After diffusion, fewer electrons will be present in the n-region, therefore creating a net positive charge, whereas the p-region would have a net negative charge due to the increased concentration of electrons. An electric field between the two regions results from the combining of electrons and holes; the electric field repels holes on the side of the p-region, and electrons on the side of the n-region. Carrier movement caused by the electric field is known as the drift current (I_{Drift}). Diffusion will occur until the drift current is equal to the diffusion current. Due to the depletion region (area between the P and N regions), electrons and holes cannot cross the barrier and recombine, forcing electrons to flow through the external circuit, which will create the current. Figure 1.7 shows the structure of the depletion region of the solar cell, together with the concentration of electrons and holes in each region before and after the diffusion process. (Gray, 2011)

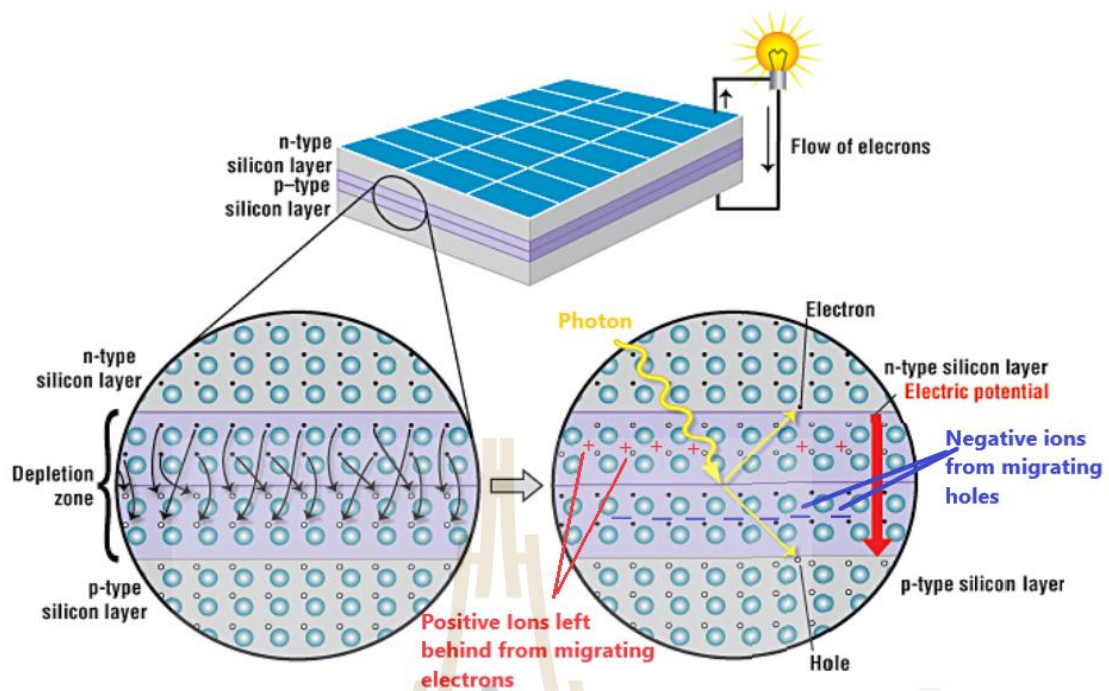


Figure 1.7 Structure of the depletion region of the solar cell, together with the concentration of electrons and holes in each region before and after the diffusion process (Fernandez, 2021)

The valence band of an atom is the outermost orbital that electrons occupy, when the valence electrons are excited, they jump into the conduction band, creating an electric current. Prior to being exposed to light (photons), the depletion layer contains no positive or negative charge carriers — the valence band is full and the conduction band is empty. When the cell is exposed to light energy, if the photon is of a wavelength with sufficient energy to overcome the gap between valence and conduction band, electrons would be excited, jumping from the valence to conduction band, separating electron and hole. The electron excited within the depletion layer gets attracted toward the n-region because of the positive charge, while the hole gets repelled toward the p-region. If the electrons are excited outside of the depletion layer, the electrons immediately recombine with the holes (not generating any current). This is known as the photovoltaic effect. (Gray, 2011; Jäger et al., 2016)

Due to the photovoltaic effect, valance electrons both in the P and N regions are promoted to the conduction band, resulting in excess electron/holes in both regions. The excess electrons present in N-region, move to the top metal contacts, while the excess holes presenting in P-region move to the rear metal contact. The internal electric field will only allow electrons to move in one direction, blocking movement the other way. Electrodes are each connected to the P and N layers, electrons will follow from the N-region to the P-region creating current, if photons strike the cell. Figure 1.8 shows the structure of a solar cell and the movement of electrons from the n-region to the p-region, through the external circuit. (Jäger et al., 2016; Nelson & Starcher, 2015; Ramalingam & Indulkar, 2017)

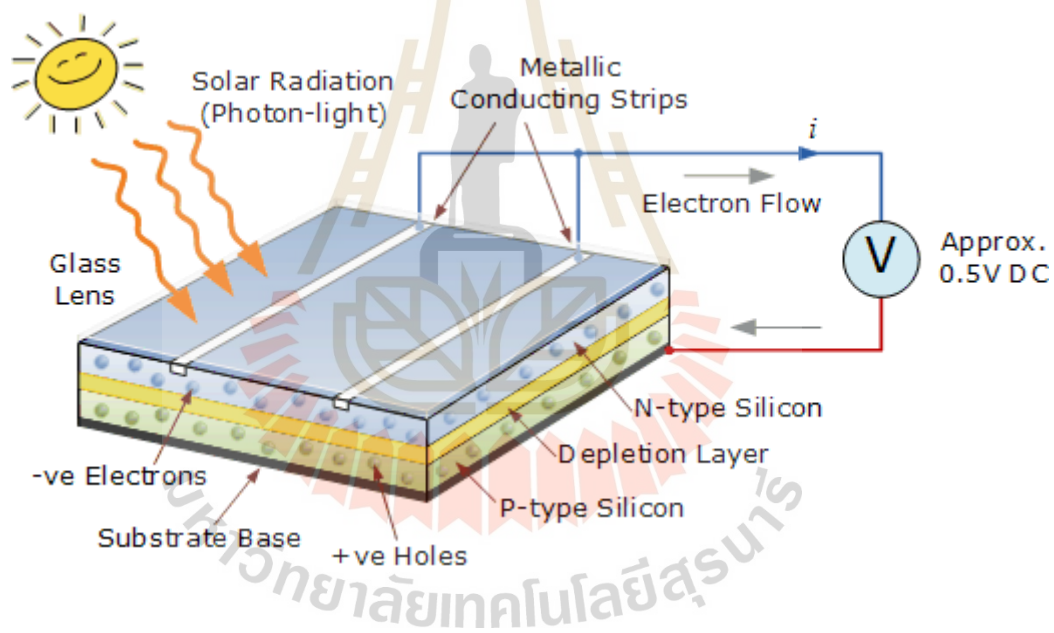


Figure 1.8 Operation of PV cell (Sainthiya & Beniwal, 2017)

1.3 Quantum dots

1.3.1 Quantum dot band gaps

Quantum dots (QDs) are semiconductor particles in the nano-scale, having optical and electrical properties that are different from larger particles of the same material. The band gaps on QD's, unlike bulk materials, are tuneable, due to the quantum size effect. The quantum size effect depends on the exciton Bohr radius

(distance in an electron-hole pair). When a particle's size is less than that of its Bohr radius, it experiences a splitting of energy levels, resulting in a larger band gap. Because a quantum dot is a semiconductor similar in size to its exciton Bohr radius, the band gap becomes adjustable, according to the size of the particle. Because of this property, band gaps can be adjusted by changing deposition techniques or levels of concentration when synthesizing. Figure 1.9 shows various QD materials and their band gaps according to particle size. (Al-Jawad, 2017; Balkus, 2013, p. 9; Veerathangam et al., 2017)

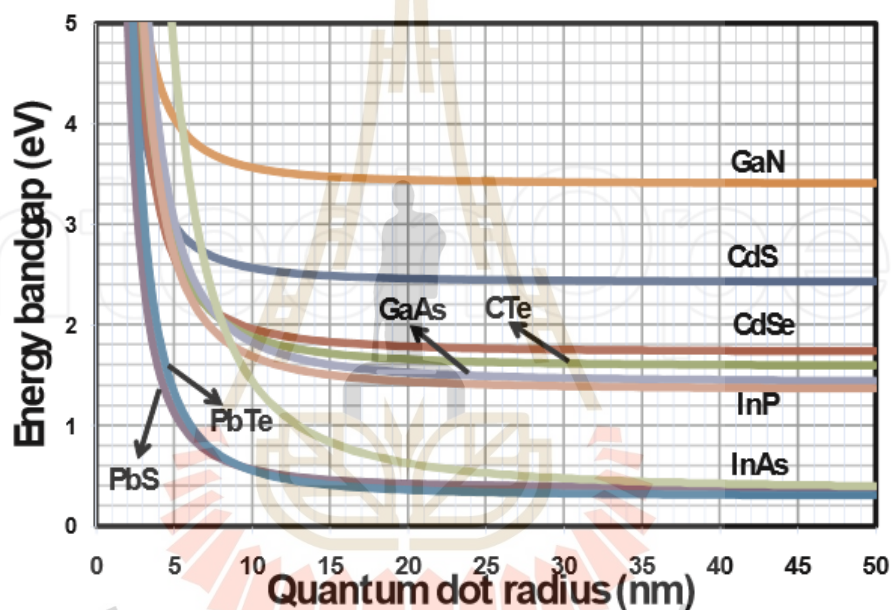


Figure 1.9 Varied Quantum dot energy band gaps vs quantum dot size for different materials. (Jasim, 2015)

1.3.2 Multiple exciton generation

Unlike bulk semiconductors such as crystalline silicon, quantum dots can generate multiple exciton (electron-hole pairs) after collision with one photon of energy exceeding the band gap. In bulk semiconductors, the absorption of a photon with energy exceeding the band gap promotes an electron from the valance band to a higher level in the conduction band, these electrons are called hot carriers. The excited electron (hot carrier) undergoes many nonradiative relaxation (thermalization:

multi-phonon emission) before reaching the bottom of the conduction band. However, in a quantum dot, the hot carrier undergoes an impact ionization process (carrier multiplication). (Chuu & Dai, 1992; Jasim, 2015)

Absorption of a single photon in QD's can generate multiple electron-hole pairs or electrons at a higher/lower energy level than the absorbed photon. When a photon of energy exceeding that of the band gap, is absorbed, the excess energy can generate an additional exciton, whereas in a bulk semiconductor, excess energy generates heat. This phenomenon is called multiple exciton generation (MEG). Figure 1.10 shows the process in a QD when a single photon is absorbed and two electron-hole pairs (excitons) are generated. (Jasim, 2015)

The Shockley-Queisser theoretical limit for a single junction solar cell works with the understanding that a single photon will produce one exciton. In the case of quantum dots, it is possible to generate more than one exciton per photon; this provides an opportunity to increase the efficiencies of single junction solar cells, beyond the previously accepted limits.

Down-converting is where a high-energy photon is absorbed and a lower energy photon is emitted; the opposite occurrence is known as up-conversion, where multiple emitted photons are of a higher energy level than the single absorbed photon. Another phenomenon associated with quantum dots is known as downshifting, where a photon is absorbed, and a single lower energy photon is emitted. Therefore, the absorption of UV photons in quantum dots can possibly produce more electron-hole pairs than near-infrared photons. By absorbing high-energy photons and emitting lower-energy photons, QD's can play a crucial role in solar cells, by reducing wasted light and heat losses. (Chuu & Dai, 1992; Jasim, 2015; Oreski et al., 2018)

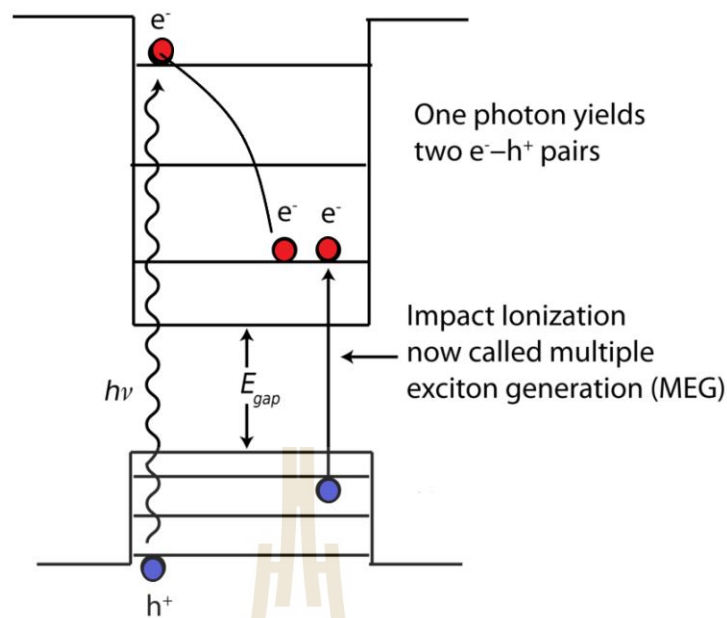


Figure 1.10 Multiple exciton generation in a quantum dot.

1.4 Band gap

In semiconductors, the band gap can be one of two types, namely, a direct band gap or an indirect band gap. The lowest energy state in the conduction band and the highest energy state in the valence band are each characterized by a crystal momentum (k -vector). The crystal momentum is a momentum-like vector associated with electrons in a crystal lattice. If the k -vectors are different, the material has an indirect band gap, in which a photon cannot be emitted because the electron must pass through an intermediate state and transfer momentum to the crystal lattice. If the crystal momentum of electrons and holes are the same in both the conduction band and the valence band, the band gap is a direct one, in which an electron can directly emit a photon. (Boakye & Nusenu, 1997b; Varghese et al., 2002)

Examples of direct band gap materials include CdS and ZnO. Indirect band gap materials include crystalline Si and Ge.

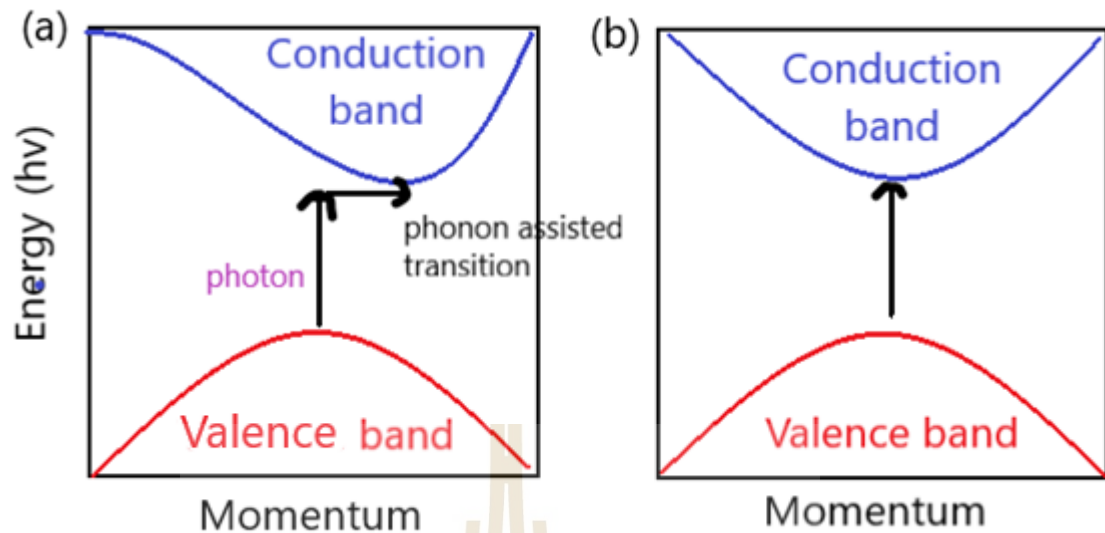


Figure 1.11 Energy vs crystal momentum for a semiconductor with (a) an indirect band gap and (b) a direct band gap.

Figure 1.11 shows the energy vs crystal momentum for the two types of band gaps. For the indirect band gap, an electron cannot shift from the highest energy state in the valence band (red) to the lowest energy state in the conduction band (blue) without a change in momentum. Most of the energy comes from a photon (vertical arrow), whilst all of the momentum comes from a phonon (horizontal arrow); Photons have relatively large energy and low momentum, whereas phonons have low energy but large momentum. For a direct band gap material, an electron can shift from the highest energy state in the valence band to the lowest energy state in the conduction band without a change in crystal momentum. Depicted (Figure 1.11b) is a transition in which a photon excites an electron from the valence band to the conduction band. (Bhandari et al., 2013; Chopra et al., 2004; Green, 1982; Shah, Schade, Vanecek, Meier, Vallat-Sauvain, et al., 2004)

Equation 1 gives the minimum photon energy (hf) required to excite an electron to the conduction band (Green, 1982):

$$hf = E_g - E_p \quad (1)$$

where E_p is the energy of an absorbed phonon with the required momentum to bridge the offset between the conduction band's lowest energy state and the highest energy state of the valence band. This equation demonstrates that the energy of the photon must be equal to the difference between the energy required to cross the band gap and the energy due to the phonon's momentum. This process involving two steps to move the electron, results in a much lower probability of absorption than in direct semiconductors, due to the fact that the process involves multiple particle interactions. (Green, 1982)

In an indirect band gap semiconductor, a photon must couple to a phonon to be absorbed. This makes the absorption coefficient drastically lower (and hence solar devices must be thicker). Since direct band gap materials can achieve higher absorption coefficients, the film can be made a lot thinner, which has many advantages — lower costs, reduced losses, and increased light absorption— in a solar cell. (Bhandari et al., 2013; Chopra et al., 2004; Shah, Schade, Vanecek, Meier, Vallat-Sauvain, et al., 2004)

1.5 Window layers and heterojunctions

Thin film solar cells usually have a structure consisting of a highly doped coating on a substrate, with a similar, but moderately doped absorber layer deposited on top of it. An oppositely conductive doped material is deposited on the absorber layer to form the emitter layer. The window layer in a heterojunction solar cell can be used to form the p-n junction with the absorber layer or used to improve performance of the already existing homogenous p-n junction. The structure of a solar cell incorporating a window layer is depicted in figure 1.12. There are two basic requirements for the window material, low electrical resistivity and high transmittance with an optimum band gap. CdS is widely used as a window or buffer layer material in photovoltaic devices due to its suitable band gap and enhancement properties in the interface chemistry between the light absorber and window layer, during fabrication. (Bin Rafiq et al., 2020; Özer & Köse, 2009)

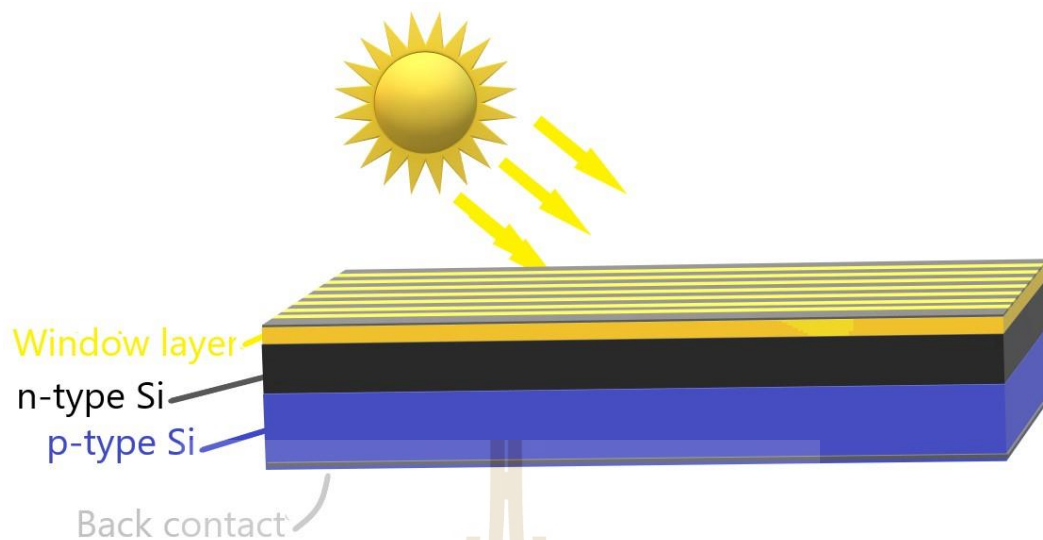


Figure 1.12. Different layers making up the structure of a solar cell

Methods of deposition for thin film window layers on solar cells include; CBD, SILAR, spin coating, RF sputtering, and electrodeposition.

1.6 Cadmium sulphide

CdS is an important II-VI semiconductor with a direct band gap of 2.42 eV which falls in the visible spectrum of light, at room temperature (300K), with absorption maxima at wavelength of 515nm and a melting point of CdS is 1475°C, imparting a bright yellow to maroon colour. Often synthesized using a sulphur source such as sodium sulphide (Na_2S) and a cadmium source such as cadmium acetate ($\text{Cd}(\text{CH}_3\text{COO})_2$), CdS can also be naturally occurring as hexagonal greenockite (wurtzite structure) or cubic hawleyite (zinc-blend structure). (Boakye & Nusenu, 1997b; Devamani et al., 2017a; Tan et al., 2011; Xiao et al., 2014)

With low electrical resistivity and high optical transmittance, CdS films are commonly used as a window or buffer layer material for many types of solar cells such as CdS/Cu(In,Ga)Se₂ (Singh & Patra, 2010), CdS/CdTe (Amin et al., 2007; Britt & Ferekides, 1993b; Ferekides et al., 2000), CdS/CuInS₂ (Olekseyuk et al., 2000) or CdS/CuInSe₂ (Ramanathan et al., 2003). Furthermore, CdS nanocrystals are also applied

for photosensors, transducers, optical wave-guides, non-linear integrated optical devices (Senthil et al., 2001), lasers laser materials (Klimov et al., 2000), biological labels (Bruchez et al., 1998), photo-conducting cells in sensors (Hur et al., 2008), paints and photo-electrocatalysis devices (Santos Andrade et al., 2019).

Sulphur vacancies caused by excess cadmium atoms result in intrinsic n-type conductivity for CdS. It can exist in three possible structures, wurtzite (wz); or zinc-blend (zb); or high-pressure rock-salt (rs) phase. From the possible structures, the wz structure is the most stable phase and easily synthesized. Under standard testing conditions, the wz-CdS is a stable phase, but under high temperature and pressure, rs-CdS is the stable phase. The zb-CdS is an intermediate phase between the transformation of wz-CdS to rs-CdS. (Devamani et al., 2017a; Xiao et al., 2014)

The wz phase had been observed in both the bulk and nanocrystalline CdS, while zb and rs phases are only observed in nanocrystalline CdS (Alkuam et al., 2017a; Balaji et al., 2018; Devamani et al., 2017a; Nagai et al., 2002; Raj & Rajendran, 2015). Band gaps vary for the different phases of CdS wz-CdS has a direct band gap of ≈ 2.4 eV, zb-CdS has a band gap of ≈ 2.55 eV, and rs-CdS has an indirect band gap of ≈ 1.5 eV (Xiao et al., 2014).

The wz-CdS form comprises of hexagonal close packing, while, the zb-CdS and rs-CdS structure have cubic close packing. In hexagonal wz-CdS and cubic zb-CdS, each atom is co-ordinated to four other atoms in tetrahedral fashion in a way that each atom has four neighbouring atoms of the opposite type, whereas in rs-CdS each atom is co-ordinated to six other atoms in octahedral fashion such that each atom has six neighbouring atoms of the opposite kind. Figure 1.13 shows the arrangement of the atoms in the different structures. (Qutub, 2013; Tan et al., 2011)

In heterojunction solar cells, the structure of the CdS can affect the efficiency by increasing or decreasing the lattice mismatch with the other material. (Arya et al., 1982)

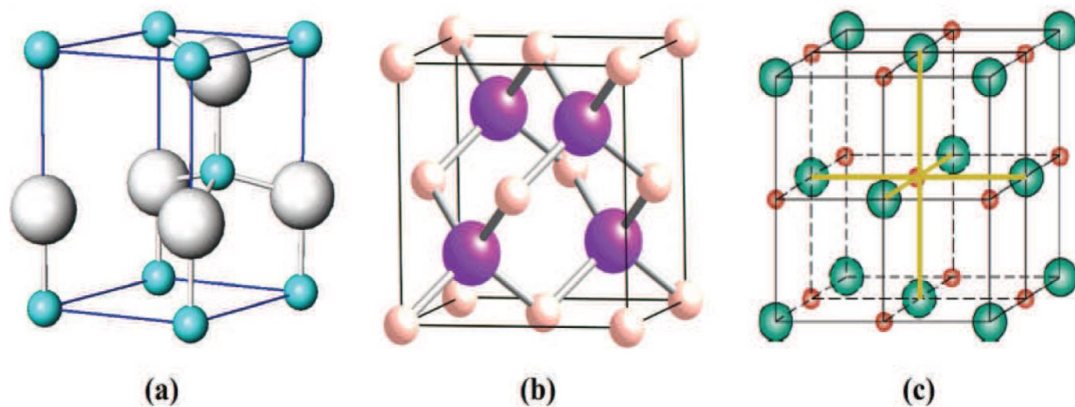


Figure 1.13 Unit cell of CdS crystal, where the larger demonstrated atoms are that of Cd and the smaller are that of S, showing (a) wurtzite, (b) zinc blend and (c) rock salt phases. (Qutub, 2013)

1.7 Zinc oxide

ZnO is a wide band gap (3.37 eV) II-VI semiconductor, typically showing n-type characteristics, even in the absence of intentional doping with low carrier concentration. While light absorption within the CdS at wavelengths below ≈ 512 nm does show a relatively poor EQE of $\approx 35\%$, such losses do not occur within ZnO films which exhibit a band gap energy close to 3.37 eV and therefore show better transparency in this spectral region. (Bhandari et al., 2013; Rattanawichai & Rattanachan, 2015)

Having great potential for applications in a wide array of fields, from medical to photovoltaics, due to its unique properties, ZnO has been and still is a widely researched compound. High chemical stability, a wide range of radiation absorption, good transparency, high coupling coefficient and high photo-stability, are some of the properties that justify the widespread utilization of ZnO. Due to its non-toxic, biocompatible, and biodegradable properties, ZnO nanoparticles have been also used, for targeted drug delivery and as a probe for bio-imaging as well as an anticancer and antimicrobial agent. (Akhtar et al., 2020; Rattanawichai & Rattanachan, 2015)

ZnO is one of the most interesting materials for optoelectronic applications because of its highly effective electrical and optoelectronic properties. In particular, its

wurtzite (wz) crystal structure with wide direct energy band gap (≈ 3.37 eV) and large excitation binding energy of ≈ 60 meV, at room temperature (300K). ZnO nanostructures have been extensively studied over the past years owing to the availability of a variety of growth methods resulting in a number of different morphologies and a wide range of material properties. In addition, ZnO nanostructures have attracted intensive research efforts due to high performance in micro-scale to nano-scale optoelectronic devices, such as transparent electronics and thin film solar cells. (Bhandari et al., 2013; Krongarrom et al., 2012a; Nicolay et al., 2015; Rattanawichai & Rattanachan, 2015)

1.8 Research objectives

This work aims at the development of a window layer for Si solar cells with a heterostructure acting as an additional light absorber, or filter. While the understanding of the power conversion efficiency limits of single Si junction solar cells has advanced, the formation mechanisms in alternative window layers such as ZnO or CdS are still a matter of debate. A window layer, which generates additional excited carriers, is especially promising as it offers efficient absorption at the UV-Visible wavelength range. Other than being an additional active layer, a window layer also offers efficiency improvement by downshifting high-energy photons to wavelengths that are better suited to the band gap of the active layers. This thesis covers 2 compound materials for a hetero-window layer: CdS, and ZnO:Bi, responding the green light wavelength (energy band gap of 2.4 eV), and the UV wavelength (energy band gap of 3.4 eV), respectively, but with less understood properties.

Interesting progress has been achieved towards the implementation of CdS or ZnO to a solar cell (Britt & Ferekides, 1993a; Fuhs, 2005; Gao et al., 2018; Krongarrom et al., 2012b; Rattanawichai et al., 2018) However, a characterisation of CdS/ZnO:Bi hetero films in a Si solar cell with appropriately designed layer thickness, has not yet been reported. Most studies were either restricted to structural and optical investigations or were limited by inherent shortcomings. Therefore, a systematic characterization of the CdS/ZnO:Bi top cell is identified as the first step towards the realization of a crystalline Si solar cell heterostructure. In these challenges, the

principal objective of this thesis is to explore the general feasibility of a Si junction solar cell incorporating CdS/ZnO:Bi window layer. The main objectives are;

- 1) A study of appropriate fabrication technique and number of CdS/ZnO:Bi layers and an enhanced understanding of nanocrystalline CdS formation on ZnO:Bi film for a crystalline Si solar cell heterostructure.
- 2) A systematic investigation of structural, optical, and electrical characterisations of CdS/ZnO:Bi window layer for the optimal solar cell properties.
- 3) A development and characterisation of crystalline Si photovoltaic device incorporating CdS/ZnO:Bi window layer.

1.9 Scope and limitations

1.9.1 Preparation method

Deposition techniques that will be considered for CdS and ZnO:Bi, in this thesis, include; SILAR, spin coating, and a hybrid of spin coating and SILAR. For the SILAR technique, a cation and an anion solution are prepared separately, the deposited in an alternating manner, to create a reaction between the two solutions, form CdS. For spin coating, a single CdS solution is prepared and deposited onto a substrate, then spun to create a homogenous layer. With a hybrid technique, a cation and an anion solution are prepared, similarly to SILAR, but instead of dip coating, spin coating is used to deposit the solutions.

1.9.2 Characterisations

For testing the properties of the window layer, the window layer first needs to be deposited onto a quartz substrate, instead of a Si wafer. Individual properties of the thin film such as transmission, reflection, absorption, and electrical characteristics, can only be determined if the film is analysed independently of Si. For structural properties, FTIR analysis is used to determine the type and strength of bonds created, while XRD analysis will be used to determine crystal structure. SEM imaging will be used to determine crystal size and film quality. The optical properties of the window layer film will be determined through analyses by UV-Vis spectroscopy.

Electrical properties such as current density will be determined using a two-probe method, passing a current through the film.

The structural properties of the window layer thin film will be analysed and optimised by varying the number of layers and the ZnO:Bi buffer layer properties. The structural properties of the Si wafer will be analysed and compared to Si with the window layer, however the structural properties of the Si wafer cannot be improved upon as it is manufactured externally and beyond scope of this research.

1.9.3 Power conversion efficiency (PCE) measurement of a prototype device

The PCE will be determined by measuring the electrical properties of the solar cell, once a p-n junction is created. Open circuit voltage and short circuit current can be used to determine the maximum generated power.

The PCE of the Si/window layer solar cell is analysed to determine the PCE improvement created by the window layer. Efficiency of the window layer will not be isolated, as no p-n junction will be developed using the window layer, aside from the Si solar cell.

CHAPTER 2

LITERATURE REVIEW

2.1 Background

Factors affecting the properties of CdS and ZnO:Bi have been extensively investigated over the years. During synthesis to deposition processes of quantum dots, factors like annealing temperature and/or deposition technique can affect particle size, crystal orientation and film thickness, which subsequently affects the film properties — band gap, transmittance, conductivity, and resistivity. To determine the viability of these materials, all factors need to be investigated. As an n-type quantum dot material, CdS can be used in heterojunction thin film solar cells, together with other p-type materials, such as PbS, CdTe, Si or perovskite. The different heterojunction structures and methods of depositions, related to cadmium sulphide solar cell applications have been reported and analysed in this chapter.

2.2 CdS particle size

The particle size of quantum dots may be the determining factor for many of the film's properties. Raj F.M, et al (2015) synthesized absorption coefficient CdS nanoparticles via chemical precipitation method, for analysis for use in dye sensitized solar cells. Particle size was controlled by adjusting the molar concentrations. 7 nm particles were synthesized, with a band gap of 3.81 eV, with optical absorption edge located at wavelength of 415 nm. Nida Qutub,et al. (2016), investigated the effect of particle size on the band gap of synthesized CdS nanoparticles. The particles varied in diameter, which affected the band gap and consequently the wavelength of light absorbed. Table 2.1 shows the data from the optical analysis of the different CdS nanoparticles:

Table 2.1 The band gap energy and particle size (diameter) of synthesized CdS NPs, obtained from absorption spectra. (Qutub et al., 2016)

	A	B	C	D	E	F
Absorption Wavelength (nm)	475	470	465	445	425	415
Band Gap (eV)	2.61	2.64	2.70	2.80	2.93	3.0
Particle size (nm)	10.18	8.06	7.04	5.16	4.26	3.9

2.3 Band gap tuning

CdS QD's to improve high-energy photon absorption and widen the band gap of TiO₂ solar cell, was investigated by K. Veerathangam, et al. (2017), showing the good optical properties of CdS QD needed for a window layer. Using SILAR technique CdS particles, sized between 3.05 to 9.07 nm were successfully deposited onto spin coated TiO₂. An increase in the number of SILAR cycles was proportional to the increase in particle size, showing a correlation between thickness of the CdS film and the size of particles (larger particles have smaller band gap), which will determine band gap. The absorption spectra of TiO₂ was below 410 nm, due to its band gap of 3.02 eV, but shifted to 550 nm (closer to visible light range) with the addition of the CdS film, as seen in figure 2.1.

2.4 Temperature Variations

The effect of annealing temperature on the properties of the CdS film — particle size and subsequently the band gap — has been previously investigated. C.T. Tsai, et al (1996) presented the effect on particle sizes of RF sputtered CdS thin films. The sizes grew as temperature increased, resulting in a decrease in band gap. Band gap for a 400 nm CdS film was at 2.45 eV. F. Boakye, et al. (1997), determined the energy band gap for CdS films prepared by thermal evaporation. This research showed that an increase in annealing temperature of the film, from 30°C to 200°C, resulted in band

gap decreasing from 3.24 eV to 2.46 eV. L. Arunraja, et al. (2016), also analyzed the effect of annealing temperature on synthesized CdS, obtained through precipitation method. Annealing temperatures between 300 °C -500°C were used and resulted in particle sizes of 25 – 41.5 nm. It was observed that higher annealing temperatures lowered the charge carrier resistance and sulphur concentration in the CdS. S. Varghese, et al. (2002) and Bakiyaraj, et al. (2011) investigated the correlation between annealing temperature and optical properties of CdS thin films that were deposited by chemical bath deposition (CBD) and analysed using UV-Vis spectrophotometer. An increase in annealing temperature showed a decrease in both the energy band gap and the absorption coefficient of the deposited CdS films. The resulting structural and optical properties from various annealing temperatures are presented in table 2.2:

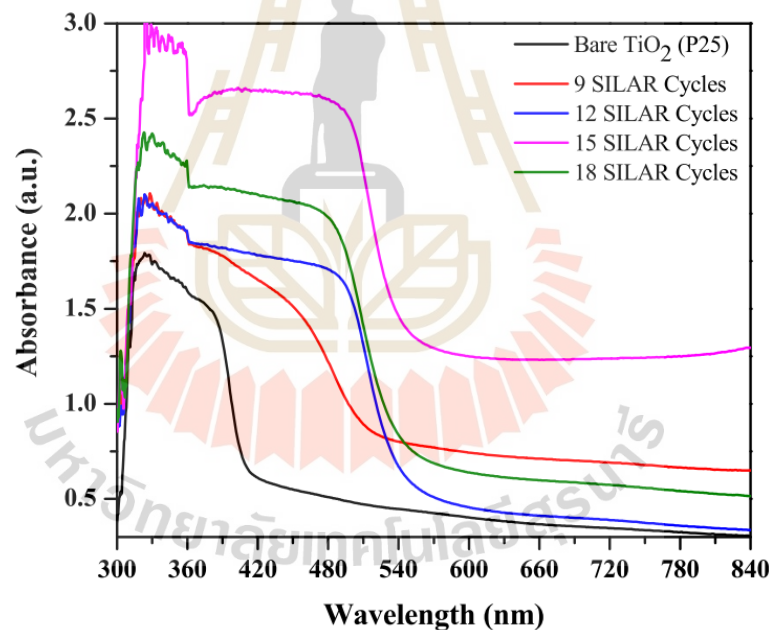


Figure 2.1 Optical absorption spectrum of bare TiO₂, CdS 9, 12, 15 and 18 SILAR cycles. (Veerathangam et al., 2017)

Table 2.2 Properties of CdS thin films with and without annealing at different temperatures, using CBD technique.
(Bakiyaraj et al., 2011; Varghese et al., 2002)

Source	Annealing temperature	Grain size (nm)	Conductivity ($\Omega \text{ cm}$) ⁻¹	Band Gap (eV)
S. Varghese, et al. (2002) (Varghese et al., 2002)	As deposited	-	-	2.4
	250°C	-	-	2.35
	300°C	-	-	2.25
Bakiyaraj, et al. (2011) (Bakiyaraj et al., 2011)	As deposited	6.48	6.7787×10^{-6}	3.5
	Annealed at 300°C	8.87	1.344×10^{-4}	3.3
	Annealed at 400°C	11.51	3.248×10^{-4}	3.15
	Annealed at 500°C	14.71	5.383×10^{-4}	2.9

2.5 Crystal structure

Crystal structure can affect the efficiency of a solar cell. Kodigala (2010) compared the cubic and hexagonal structures of CdS, concluding that hexagonal CdS would be preferred for thin film solar cells, owing to a larger band gap, allowing for increased light absorption. The band gap of CdS can change depending on the crystal structure. Soltani, et al. (2012) investigated the change in band gap for different crystal structures, finding that CdS with hexagonal closely packed (HCP) quantum dots have higher energy band gaps than that of face centred cubic (FCC) structured quantum dots. Particles were synthesized by microwave-hydrothermal method. Average particle size of CdS was 8.5 -12.5 nm, with particle size shown to increase with longer microwave exposure. Band gaps ranged from 2.54 -2.65 eV, decreasing with the increase of microwave exposure time. Nagai, et al (2002) synthesised CdS by CVD, finding that the absorption coefficient of HCP is higher than that FCC. Band gap was also found to

be higher for HCP than FCC. Devamani, et al. (2017) reported on synthesis of CdS nanoparticles via chemical co-precipitation method, achieving particles size of 31.54 nm and a hexagonal structure, with a band gap of 3.0 eV. Balaji, et al. (2018), studied hexagonal CdS nanoparticles deposited by hot wall technique. The studies carried out on the CdS thin films, analysing the optical properties, show transmittance of 80% and a direct band gap of 2.4 eV. The absorption edge of films annealed at 300°C shifted towards lower wavelength, which indicated the widening of the band gap, from 2.4 eV to 2.7 eV.

2.6 Methods of deposition

Alkuam, et al. (2017) used electrodeposition and CBD techniques to synthesize CdS thin films and CdS nanoparticles, respectively. Good hexagonal crystalline CdS thin films were achieved by electrodeposition method, having a PCE of 2.7%, when used with TiO₂. CdS nanoparticles synthesized by CBD and used with TiO₂ showed PCE of 0.86%. The most uniform thin film was achieved with a deposition time of 5 minutes when compared with the other films made by different deposition times. The results show that CdS can improve the performance of dye-sensitized solar cells (DSSC's). Al-Jawad, et al. (2017) achieved hexagonal structured CdS by both SILAR and CBD methods. TiO₂ thin films was deposited by chemical bath deposition (CBD) and SILAR methods, also using SILAR to deposit CdS. Absorption was shown by CdS for wavelengths larger than ≈500 nm. Photocurrent of both CBD and SILAR deposited TiO₂ was shown to increase with the addition of CdS, attributed to the increasing absorption ability of CdS, in visible light wavelengths. A hexagonal structure was observed for CdS deposited by SILAR and CBD methods. Reported band gaps are presented in table 2.3.

Table 2.3 Energy band values for TiO₂, CdS, and TiO₂/CdS deposited by CBD and SILAR methods. (Al-Jawad, 2017)

Method	Eg of TiO ₂	Eg of CdS	Eg of TiO ₂ /CdS
CBD	3.7	2.7	3.02
SILAR	3.6	2.7	3.0

2.7 Downshifting

Downshifting is an ability of quantum dot materials like CdS, which can be exploited for improvement of solar cells. Lopez-Delgado R, et al. (2017) synthesized CdSe/CdS nanoparticles via hot injection method for improvement of Si solar cells, employing QD downshifting abilities. The Si solar cells showed improvement in PCE when QD's were used. Short circuit current density (J_{sc}) improved from 32.5 to 37.0 mA/cm², this led to an approximately 13% increase in the PCE, from 12.0 to 13.5%. High-energy wavelengths were absorbed and then emitted as lower energy wavelengths to be absorbed by the Si absorber layer, as shown in figure 2.2.

Flores-Pacheco A, et al. (2020) analyses the use of various QD layers on silicon solar cells, to use its downshifting abilities for the efficiency improvement of solar cells. When used, ZnO QD layer was shown to absorb wavelengths of high-energy light (unabsorbable by Si due to small band gap) and emit the light at lower wavelengths that can be absorbed by Si, as shown in figure 2.3.

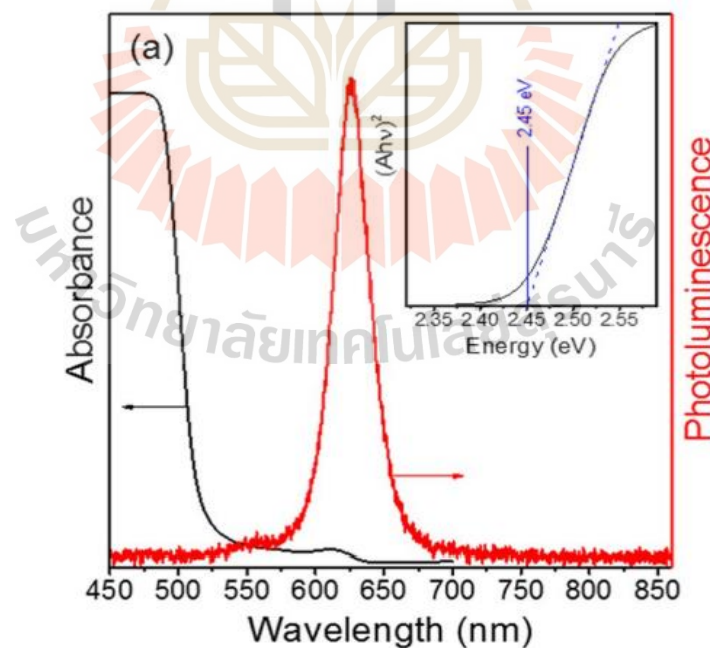


Figure 2.2 Absorbance and photoluminescence emission spectra of synthesized CdSe/CdS QD's. (Lopez-Delgado et al., 2017)

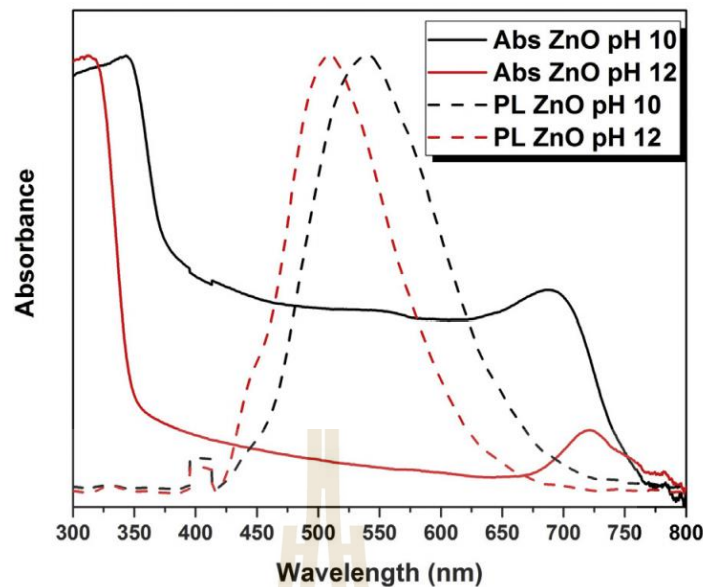


Figure 2.3 Absorbance and photoluminescence (PL) emission spectra of synthesized ZnO QDs with different pH values. The PL spectrum was obtained using an excitation wavelength of 340 nm. (Flores-Pacheco et al., 2020).

2.8 Cadmium sulphide in heterojunction solar cells

2.8.1 Cadmium sulphide with crystalline silicon

Using CdS as the n-type material in a heterojunction cell with p-type Si has shown promising results, owing to the reduced thickness of the cell and different band gap, compared to conventional bulk Si cells. Arya, et al. (1982), researched P-Si/CdS heterojunction solar cells using various methods of deposition, as shown in table 4. Lattice mismatch was investigated, finding that a higher lattice mismatch would result in a lower efficiency. Cubic structured CdS allows for a low lattice mismatch with the diamond cubic structure of Si; a 7.7% lattice mismatch yielded an 11% PCE from single source evaporation deposition of CdS. Saha, et al (2015), used spin coating technique to deposit CdS onto P-Si, achieving hexagonal structured CdS, 8nm in diameter. The efficiency achieved by the heterojunction cell was 0.51%. Gao, et al (2018) deposited CdS by evaporation, to create a P-Si/CdS solar cell, achieving efficiencies up to 10.64%.

Table 2.4 Methods of deposition for P-Si/CdS (Arya et al., 1982).

Method of deposition	Temperature (°C)	PCE (%)
Single Source evaporation	175	11
Vacuum evaporation	-	5.5
Electron beam	-	7
Multisource evaporation (In and Cd)	200-250	9.5

2.8.2 Cadmium sulphide with cadmium tellurium

E.W. Jones, et al. (2009), used chemical vapour deposition (CVD) for film deposition and SCAPS software simulation to calculate various parameters. The improvement of CdTe solar cells by using a CdS and cadmium zinc sulphide ($\text{Cd}_{0.9}\text{Zn}_{0.1}\text{S}$) was investigated. When a 1 μm thick CdTe layer was used with a 250 nm thick CdS window layer, CdTe/CdS showed a PCE of 7.31%, while $\text{Cd}_{0.9}\text{Zn}_{0.1}\text{S}$ showed PCE of 11.42%. Hodgson SD, et al. (2013) investigated QD luminescent downshifting by applying a $\text{Cd}_{1-x}\text{Zn}_x\text{S}$ window layer to a CdTe thin film solar cell. Using the window layer showed high the number of charge carriers generated for wavelengths ranging from 470 – 850 nm, ultimately improving the external quantum efficiency (EQE). Light in the blue region was blocked due to the band gap of the window layer. Dhatchinamurthy, et al. (2019) dip coated glass substrates to achieve hexagonal shaped CdS, determining that CdS nanostructure thin films were suitable for window layer applications due to its “impact of quantum confinement and the shifts in optical band gap”. As a window layer in a CdTe/CdS solar cell a 4.81% PCE was achieved.

2.8.3 Cadmium sulphide with lead sulphide

Bandhari et al. (2013) used CdS as the n-type material in a heterojunction p-n junction thin film PbS/CdS solar cell. The RF sputtering deposition technique was used, achieving an efficiency of 3.3%. Patel J, et al. (2014) used spin coating technique to deposit lead sulphide (PbS) and CdS films, reporting high transmittance in visible light region of the light spectrum, making it suitable for window layer applications in a heterojunction solar cell. The reported band gap for deposited

CdS was 2.5 eV. A PCE of 0.24% for spin coated PbS/CdS p-n junction solar cell was achieved.

2.8.4 Cadmium sulphide with perovskite

CdS has also shown potential as an n-type window layer in perovskite solar cells. Peng, et al. (2016) investigated the use of CdS as an electron transport layer (ETL) for perovskite solar cells. PCE of 16.1% was achieved, comparable to TiO₂ based devices. It was determined that CdS-based devices presented a higher recombination resistance than TiO₂-based devices, reducing carrier recombination (ultimately reducing losses) and increasing open circuit voltage. The entire device was achieved with temperature lower than 100°C, making it a sustainable option for use in perovskite solar cells. Wang, et al. (2017), investigated the effect of Urea (complexing agent) on the properties of the CdS ETL, as part of a spiro-OMeTAD/perovskite/CdS solar cell. It was found that a higher concentration of urea decreased the grain size of the CdS and affected the final PCE. Highest PCE obtained was 2.27%. Wessendorf, et al. (2018) investigated the use of a CdS thin film layer as an electron transport layer (ETL) for perovskite solar cells, comparing it to a TiO₂ ETL. It was found that CdS strongly suppressed hysteresis losses, showing possibility of reversing hysteresis, as a result of the higher electron mobility of CdS, compared to TiO₂. TiO₂ had more oxygen vacancies, allowing for recombination. Optimal CdS film thickness was found to be 50 nm, with band gap assumed to be 3.8 eV.

2.9 Zinc oxide thin films

Rattanawichai, et al. (2018) synthesized nanocrystalline zinc oxide films doped with bismuth (nc-ZnO:Bi) through sol-gel processing and then by spin coating method. ZnO:Bi films showed transmittances over than 80 % in the wavelength range of 390-800 nm and low effective reflectance, less than 17%. Films had current density of 3.98×10^2 mA/cm² (at 0.8V). Band gap is approximately 3.33 – 3.38 eV.

2.10 Summary

The previous research done, relating to cadmium sulphide, although not the same as the research in this thesis, can be referenced for methods of deposition, factors affecting optical properties, and to compare results. The results from papers in this chapter is summarized in table 2.5.

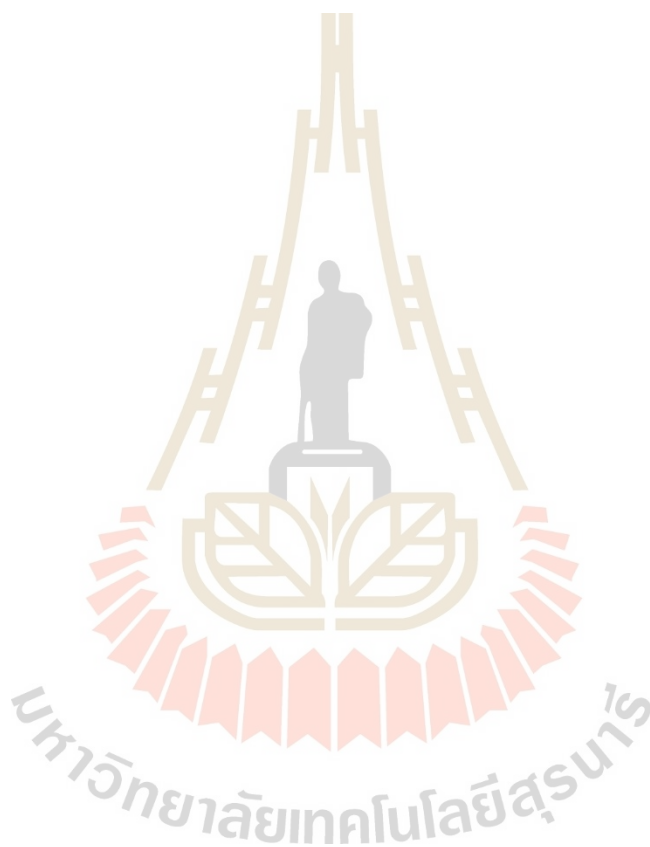


Table 2.5 Summary of results achieved from previous experiments

Source	Material	CdS deposition method	Annealing temperature (°C)	CdS film thickness (nm)	Grain size (nm)	CdS Band gap (eV)	PCE (%)
Arya, et al. (1982)	P-Si/CdS	Single source evaporation	175	-	-	-	11
Tsai. C.T., et al., (1996)	CdS	RF sputtering	-	400	28	2.45	-
F. Boakye, et al. (1997)	CdS	Thermal evaporation	30 - 200	250 - 400	-	3.24 - 2.46	-
S. Varghese, et al. (2002)	CdS	CBD	0 - 300	610	-	2.4 - 2.25	-
E.W. Jones, et al. (2009)	CdTe/CdS	CVD	400	240	-	2.4	7.31
Bakiyaraj, et al. (2011)	CdS	CBD	0 - 500	-	6.48 -14.71	3.5 - 2.9	-
Bandhari et al. (2013)	PbS/CdS	RF sputtering	-	70	-	2.4	3.3

Table 2.5 Summary of results achieved from previous experiments (Continued)

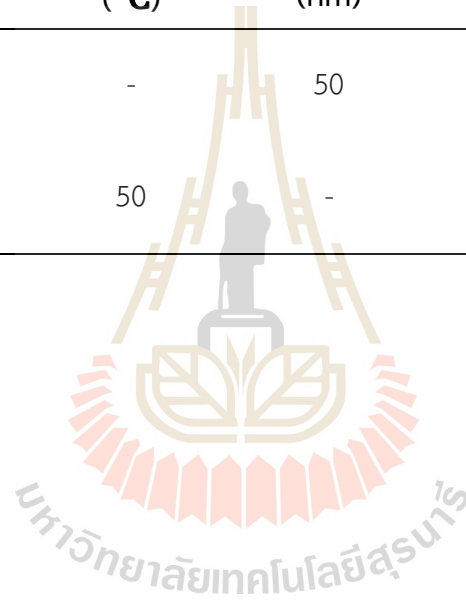
Source	Material	CdS deposition method	Annealing temperature (°C)	CdS film thickness (nm)	Grain size (nm)	CdS Band gap (eV)	PCE (%)
Saha, et al. (2015)	P-Si/CdS	Spin coating	60	-	8	3.42	0.51
Raj F.M, et al (2015)	CdS	Chemical precipitation method	200	-	7	3.81	-
Arunraja, et al. (2016)	CdS	Chemical precipitation method	300 – 500	-	21 – 41.5	-	-
Qutub N, et al. (2016)	CdS	Chemical precipitation method	-	-	10.18 – 3.9	2.61 – 3.0	-
Peng, et al. (2016)	Perovskite/ CdS	CBD	100	-	-	-	16.1
K. Veerathangam, et al. (2017)	TiO ₂ /CdS	SILAR (15 cycles)	-	-	6.8	2.26	1.8
Al-Jawad, et al. (2017)	TiO ₂ /CdS	CBD	-	-	-	3.02	-
		SILAR	-	-	-	3.0	-
	CdS	CBD	-	-	-	2.7	-
		SILAR	-	-	-	2.7	-

Table 2.5 Summary of results achieved from previous experiments (Continued)

Source	Material	CdS deposition method	Annealing temperature (°C)	CdS film thickness (nm)	Grain size (nm)	CdS Band gap (eV)	PCE (%)
Alkuam, et al. (2017)	TiO ₂ /CdS	Electrodeposition					2.7
		CBD					0.86
Devamani, et al. (2017)	CdS	Chemical precipitation	-	--	31.54	3.0	-
Wang, et al. (2017)	OMeTAD/ Perovskite/ CdS P-	CBD	90	≈200	-	3.8	2.27
Gao, et al. 2018)	Si/CdS/AZ O	Evaporation		60-300	-	-	10.64
Balaji, et al. (2018)	CdS	Hot wall	300	-	60	2.4	-
Rattanawichai, et al. (2018)	ZnO:Bi	Spin coating	350 – 550	118 – 202	10 – 20	3.3 – 3.8	-

Table 2.5 Summary of results achieved from previous experiments (Continued)

Source	Material	CdS deposition method	Annealing temperature (°C)	CdS film thickness (nm)	Grain size (nm)	CdS Band gap (eV)	PCE (%)
Wessendorf, et al. (2018)	Perovskite/ CdS	CBD	-	50	-	3.8	11
Dhatchinamurthy, et al. (2019)	CdS	Dip coating	50	-	-	2.57	-



CHAPTER 3

METHODOLOGY

3.1 Introduction

The materials and processes of deposition used to create thin films for potential window layer applications are described in this chapter. The steps taken to analyse the properties of the films, to determine its viability, together with the factors affecting those properties are explained. Equipment used to perform tests, characterizing the thin films, and analytical methods are broken down. To determine if the ZnO:Bi and CdS films are suitable for window layer/ heterojunction applications, the films need to be analysed. By determining the factors that can affect the properties related to solar cells, and how they can be manipulated, we can optimize materials for use in solar cells.

3.2 Materials

For the ZnO thin film doped with (Bi), zinc acetate dihydrate ($\text{Zn}(\text{CH}_3\text{COO})_2 \cdot 2\text{H}_2\text{O}$) (CARLO ERBA) was used for the source of ZnO, while bismuth nitrate pentahydrate ($\text{Bi}(\text{NO}_3)_3 \cdot 5\text{H}_2\text{O}$) (Fluka) was used as the source of the dopant, with a solvent consisting of ethylene glycol ($\text{C}_2\text{H}_6\text{O}_2$) (CARLO ERBA) and monoethanolamine (MEA) ($\text{HOCH}_2\text{CH}_2\text{NH}_2$) (CARLO ERBA).

For cadmium sulphide thin films, cadmium acetate dihydrate ($\text{Cd}(\text{CH}_3\text{COO})_2 \cdot 2\text{H}_2\text{O}$) (CARLO ERBA) was used as the source of cadmium, while sodium sulphide nonahydrate ($\text{Na}_2\text{S} \cdot 9\text{H}_2\text{O}$) (CARLO ERBA) was used as the source of sulphur. Deionized (DI) water was used as a solvent for both solutions. For optical measurements, fused quartz was used as substrates to deposit thin films onto. To incorporate the window layer into a photovoltaic device, polycrystalline PN silicon wafers from Solartron PLC were used as the substrate to deposit ZnO:Bi and/or CdS.

3.3 Procedure

3.3.1 Zinc oxide preparation

For a Bismuth-doped Zinc Oxide (ZnO:Bi) buffer layer, the ZnO:Bi solution was prepared by sol-gel method, using low amounts of Bi dopant source to avoid initial phase segregation of Bi_2O_3 , further explained in our previous work (Krongarrom et al., 2012b).

Zinc acetate of 0.7M was dissolved in a solution consisting of ethylene glycol-MEA, with a ratio of Zn:MEA at 1:1. The solution was then stirred for 10 minutes at 80°C , bismuth nitrate pentahydrate at a concentration of 0.2 at. % was then added. The mixture was stirred continuously for 1 hour at 80°C , after which 0.823mM of CTAB was slowly added drop-wise, for quality enhancement of the ZnO films. After further stirring for 30 minutes to ensure that the complete sol-gel is homogenous, the solution was left to rest at room temperature for 24 hours. Fused quartz substrates were cleaned using the Ratio Corporation of America (RCA) process. After resting, layers of ZnO:Bi solution were deposited onto the quartz substrate via spin coating, with speed a of 2500rpm for 30 seconds, then dried at 250°C for 30 minutes. The ZnO:Bi films were annealed at 550°C for 2 hours, using a ramp rate of $1^\circ\text{C}/\text{min}$ for both drying and annealing. The synthesis process is summarized in figure 3.1.

3.3.2 Cadmium sulphide preparation

For the cation solution of CdS, 0.1 M of cadmium acetate dihydrate was used, while 0.1 M of sodium sulphide was used for the anion solution, with both being dissolved in DI water. Both solutions were stirred for 30 minutes, at 70°C .

The CdS thin films were deposited onto cleaned quartz substrates, 25 mm x 25 mm, by spin coating. The quartz substrates were held on the spin coating chuck at room temperature for the deposition of the CdS films. The speed was set to an initial 500 rpm for 10 seconds, then to 2500 rpm for 30 seconds to obtain homogenous films. After spinning the cation solution, the anion solution was spun, creating one layer of CdS; the process was repeated for multiple layers, the samples were then dried at 200°C for 2 hours. Quartz substrate was used to deposit CdS, after deposition of ZnO:Bi buffer layer. Samples contained various numbers of CdS layers

— 3 layers (3L), 5 layers (5L), 8 layers (8L) and 11 layers (11L). The ZnO:Bi buffer layers are used for all samples to improve film quality; without the buffer layer, the CdS film is non-homogenous and difficult to analyse. The deposition process for CdS is summarized in figure 3.2.

When the cadmium acetate reacts with the sodium sulphide, the following reaction occurs:

Cadmium Acetate + Sodium sulphide = Cadmium Sulphide + Sodium acetate

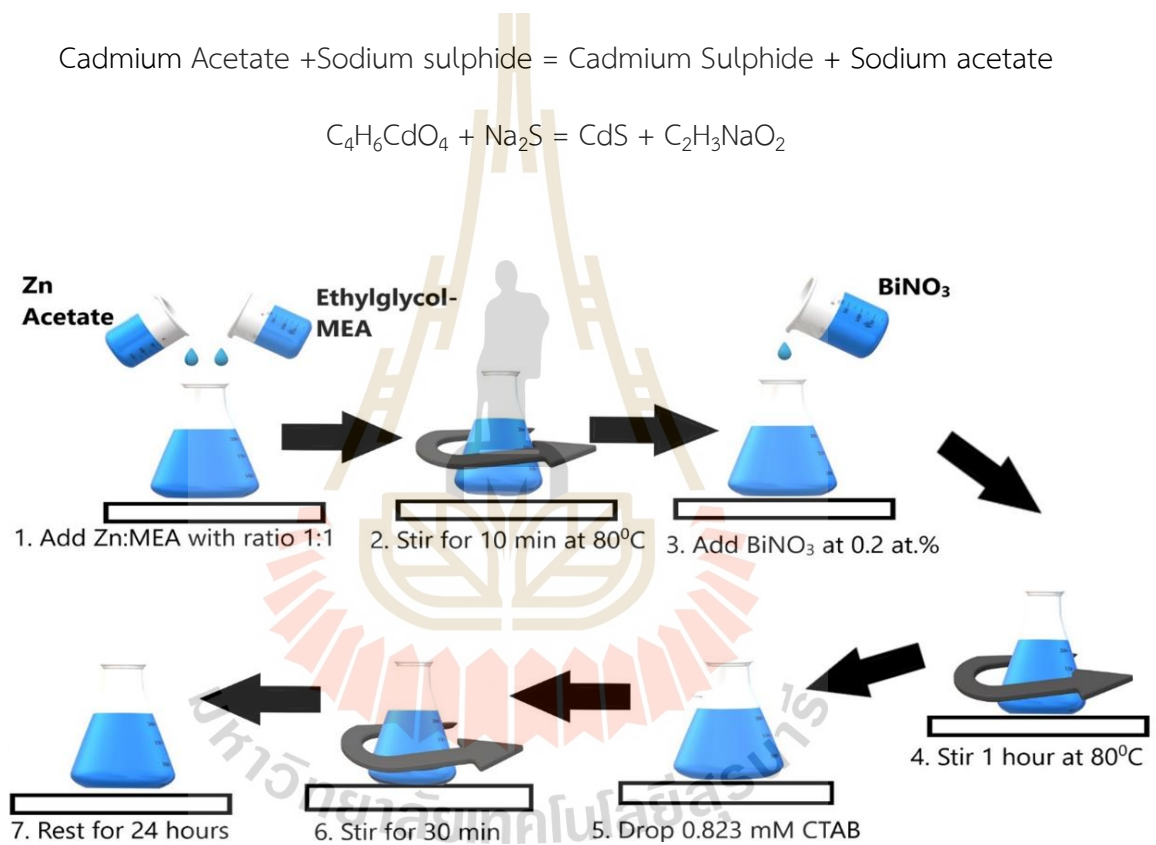
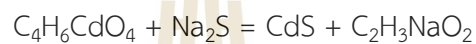


Figure 3.1 Process for synthesizing bismuth doped zinc oxide.

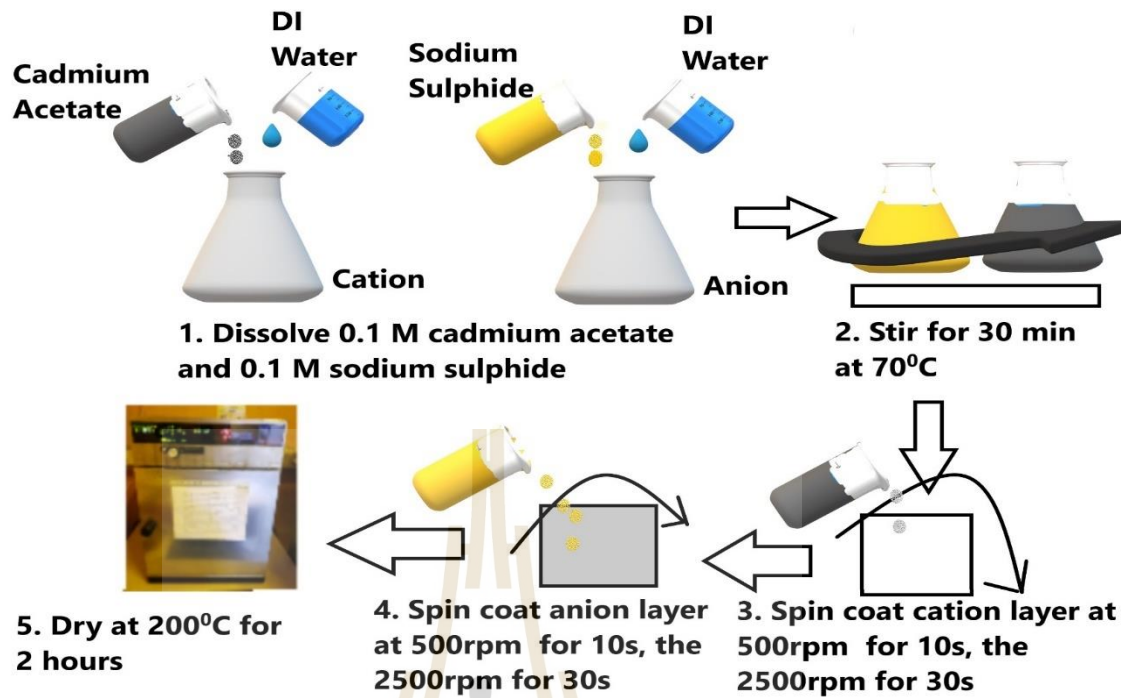


Figure 3.2 Process of depositing cadmium sulphide thin film by spin coating.

3.3.3 Characterizing thin films

The CdS and ZnO:Bi films were first deposited onto quartz substrates to analyse their properties — Electrical, optical, and structural — and determine if it is viable for solar cell applications.

For structural properties: Fourier Transform Infrared Spectroscopy (FTIR) analysis, field emission scanning electron microscope (FESEM) and X-ray diffraction (XRD), was conducted, to study the chemical compositions of the fabricated thin films, the crystal structure, as well as the functional groups and types of bonds present in the nanostructures, through vibrations of chemical bonds.

The two-probe method (Keithley a Tektronix Electrometer 2400), shown in Figure 3.3, was used to determine the photocurrent-voltage (I-V) measurements, which together with the thickness measured by optical profiler, was used to calculate the current density, conductivity, resistivity, and electrical behaviour. The Electrometer applies voltage to the thin film and the current that passes through gets measured. Measured current will be used to calculate the current density.

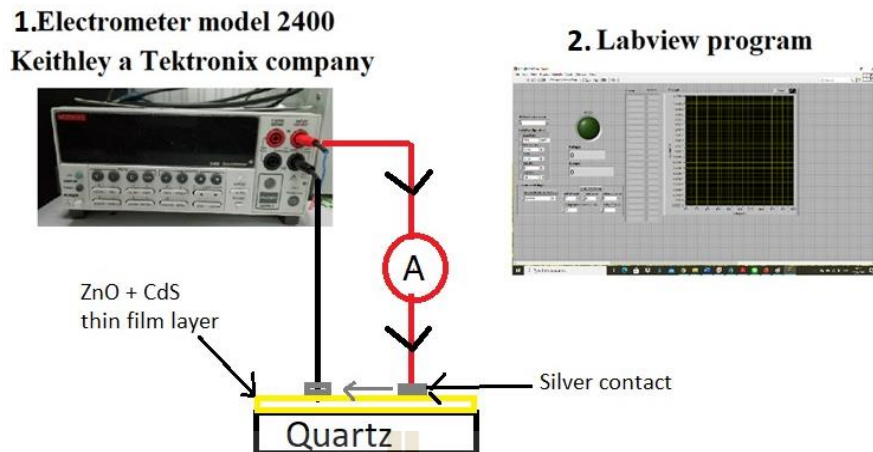


Figure 3.3 Keithley a Tektronix Electrometer 2400 used for two-probe method to find current density

Current density was calculated using equation 2:

$$J = \frac{I}{A} \quad (2)$$

where J is the current density (A/cm^2), I is the current (A), and A is the cross-sectional area (cm^2), which was obtained with the radius of the contact and thickness of the films.

The photocurrent gain, used to plot the J-V curve (figure 4.9) for each sample, was calculated using equation 3:

$$\text{Photocurrent gain} = \frac{J_{\text{Illumination}}}{J_{\text{Dark}}} \quad (3)$$

where $J_{\text{Illumination}}$ is the current density under illuminated conditions and J_{Dark} is the current density in dark conditions.

The electrical conductivity and resistivity of all samples were calculated using equation 4:

$$\rho = \frac{R' \times A}{l} = \frac{1}{\sigma} \quad (4)$$

where ρ is resistivity ($\Omega \cdot \text{cm}$), σ is conductivity (S/cm), l is length between contacts (cm) and R' is resistance (Ω).

Ultraviolet-Visible (UV-VIS) spectrophotometer model Cary 300 was used for analyzing the optical properties of the film, in the range of 200 to 850 nm, with an incident angle of 0° , in an integrating sphere mode. Optical properties determined from this analysis include transmission, absorption, reflectance, and energy band gap.

Absorption coefficient (α) was calculated using equation 5 (Rattanawichai et al., 2018) :

$$\alpha = \frac{1}{t} \ln \left(\frac{\sqrt{(1-R)^4 + 4T^2R^2} - (1-R)^2}{2TR^2} \right) \quad (5)$$

where t is the thickness of the film, T and R are the transmittance and reflectance of the film, respectively.

The Tauc plot for the fabricated samples was plotted using their respective energy band gaps, estimated using equation 6 (Rattanawichai et al., 2018; Veerathangam et al., 2017):

$$\alpha h\nu = C(h\nu - E_g)^{\frac{1}{2}} \quad (6)$$

where C is a constant for a direct transition and photon energy, E_g is the band gap of material, $h\nu$ is the photon energy (eV), and the exponent n is equal to $\frac{1}{2}$ for direct band gap materials.

Refractive indices (n) were estimated using equation 3 (Pankove, 2010):

$$n = \frac{-(2R+2) \pm \sqrt{((2R+2)-4(R-1)(RK^2-K^2+R-1))}}{2(R-1)} \quad (4).$$

where K is a constant, the absorption coefficient.

For film quality the samples were analysed using field emission scanning electron microscope (FESEM), to closely inspect the film surface. Together with the FESEM, an energy dispersive x-ray spectrometer was used to determine the type of materials and compounds present in the surface of the films.

After depositing films onto silicon wafers, screen printing is used to create silver and aluminum contacts on the front and rear of the wafer. The screen-printing technique is depicted in figure 3.4. Fast firing was used to ensure a good contact between the metal and the wafer. For fast firing, three stages were used to increase temperature: stage 1 at 300°C for 10 seconds, stage 2 at 600°C for 10 seconds, and stage 3 at 915°C for 7seconds.

To test the PN junction and the behaviour of the solar cell, a bias voltage from the Keithley electrometer was applied across the cell. Figure 3.5 shows the process of applying the bias voltage to the solar cell, showing holes and electrons migrating across the junction when the voltage exceeds the threshold voltage of the cell, creating a flow of current. If the cell works as a solar cell, carriers will migrate in the opposite direction.

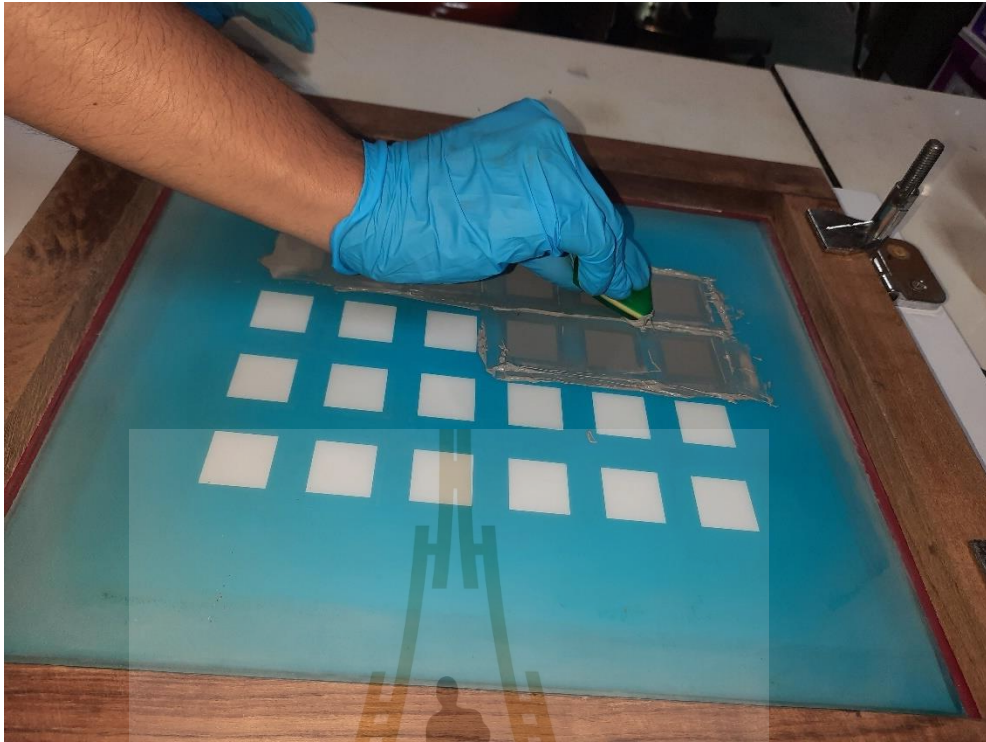


Figure 3.4 Screen-printing technique used for metal contacts

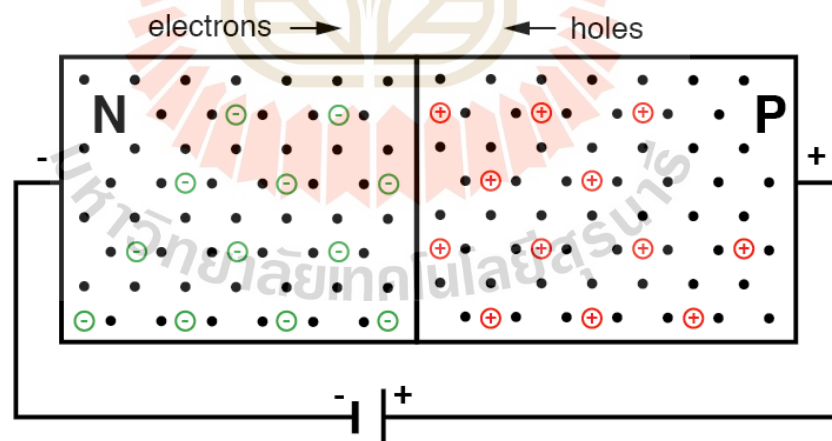


Figure 3.5 Diode behaviour when a bias voltage is applied to solar cell to test PN junction properties

The samples were prepared and analysed as follows:

- 1) ZnO:Bi films with 1-4 layers were deposited onto quartz and the properties were analysed via UV-Vis and SEM imaging.
- 2) CdS was spin coated onto quartz, both with and without a precoated ZnO:Bi film, to determine if the ZnO:Bi buffer would improve homogeneity.
- 3) The ZnO:Bi/CdS thin films on quartz were characterised by XRD and FTIR to assess the structural properties, SEM imaging for film quality, UV-Vis for the optical analysis, and two-probe method for electrical properties.
- 4) The number of CdS layers was increased to determine the effect of the number of layers on the band gap.
- 5) The drying temperature of CdS was varied between 100°C-300°C, to determine the effect of increased temperature on the film. 200°C was used as the default temperature for CdS, based on previous literature reviewed.
- 6) The ZnO:Bi/CdS with varying layers was deposited onto P-N junction Si wafers. Silver front contacts and aluminium rear contacts were made to collect charge carriers. Samples were then analysed using UV-Vis for optical properties, and Keithley electrometer for P-N junction quality.

3.4 Summary

Thin films consisting of ZnO:Bi and/or CdS will be deposited by spin coating technique onto quartz to have various properties analysed, through analytical equipment such as FTIR, XRD, SEM, UV-Vis and Keithley two-probe method. The results will be process using various analytical methods, to characterize the films and determine if the properties discovered can be beneficial to solar cells.

CHAPTER 4

RESULTS AND DISCUSSION

4.1 Introduction

To determine the viability of ZnO:Bi and CdS for solar cell applications, specifically window layers; properties related to solar cell efficiency need to be analysed. The use of a ZnO:Bi buffer layer, the effect of the number of layers on the optical properties, and the electrical properties, are investigated. Factors affecting the band gap of quantum dots are also analysed, attempting to understand how to tune band gaps to the desired width. A heterojunction solar cell prototype with ZnO:Bi and Si is attempted.

4.2 Analysis of bismuth doped zinc oxide multilayers

Prior to using the bismuth doped zinc oxide as a buffer layer, the films need to be independently analysed to determine it will be beneficial or detrimental to improvement of solar cell efficiency. The optical properties are analysed through UV-Vis and structural properties are obtained through FTIR. The number of layers used also affect the properties of the film which are important in light absorption. In figure 4.1 we can see the transmittance rates of ZnO:Bi, with 1-4 layers. The transmittance generally decreases with more layers used, especially in the near-UV region, while remaining high in the visible region of the spectrum. This shows that if used a buffer layer, the number of layers need to be kept at a minimum so as to not significantly reduce transmission.

Reflectance is shown in figure 4.2, where the film with 4 layers shows an increased reflection around the 400 nm wavelength, which would negatively impact the absorption of light in silicon cells.

Figure 4.3 shows the FTIR spectra for different number of layers of zinc oxide, the samples containing more layers show stronger bonds at 540nm compared to 485 nm. Indicating that more layers can result in increased zinc-oxygen bonds.

The FESEM results depicted in figures 4.4 and 4.5 show the ZnO:Bi_1L and ZnO:Bi_4L, respectively. Magnification shows that the more layers used, the more continuous and homogenous the film would be.

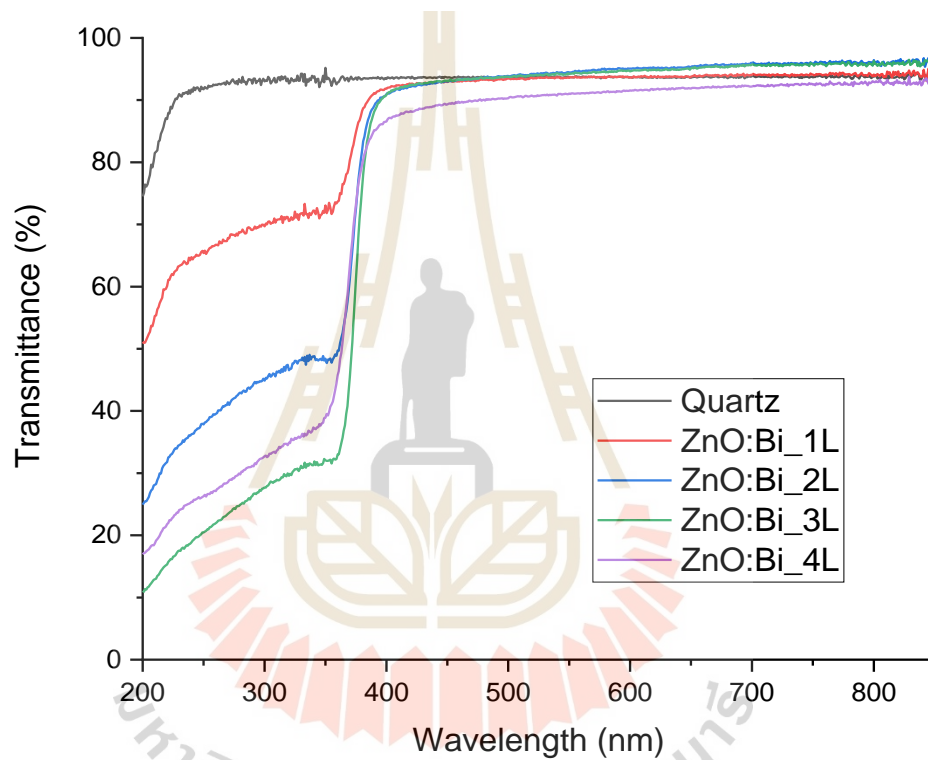


Figure 4.1 Transmittance rates of bismuth doped zinc oxide with different number of layers, for varying wavelengths.

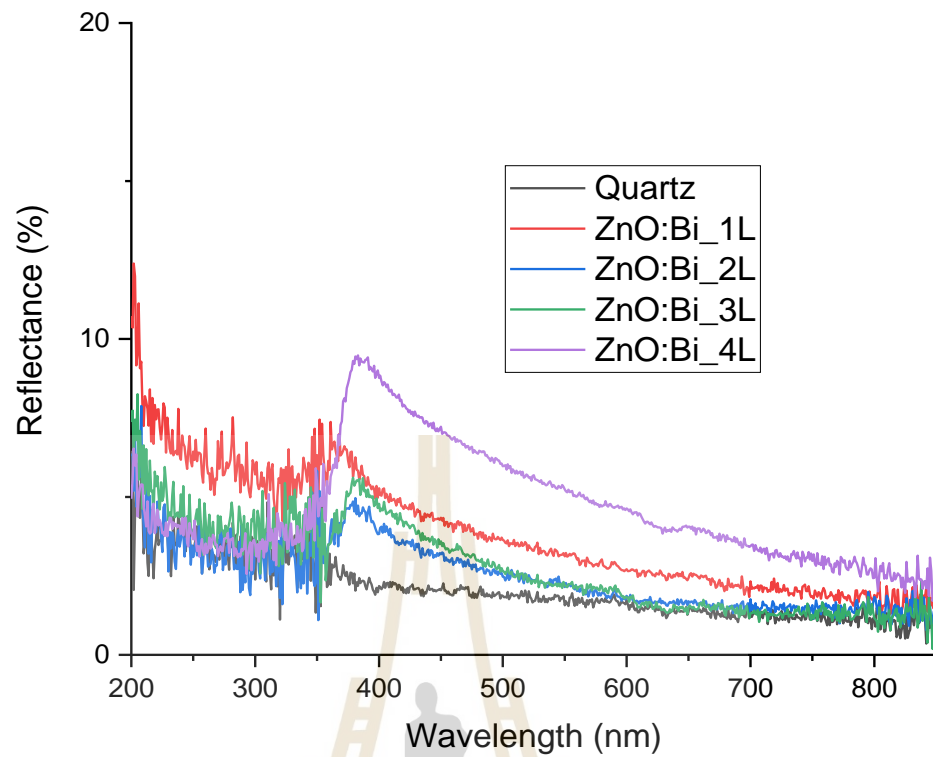


Figure 4.2 Reflectance rates of bismuth doped zinc oxide with different number of layers, for varying wavelengths.

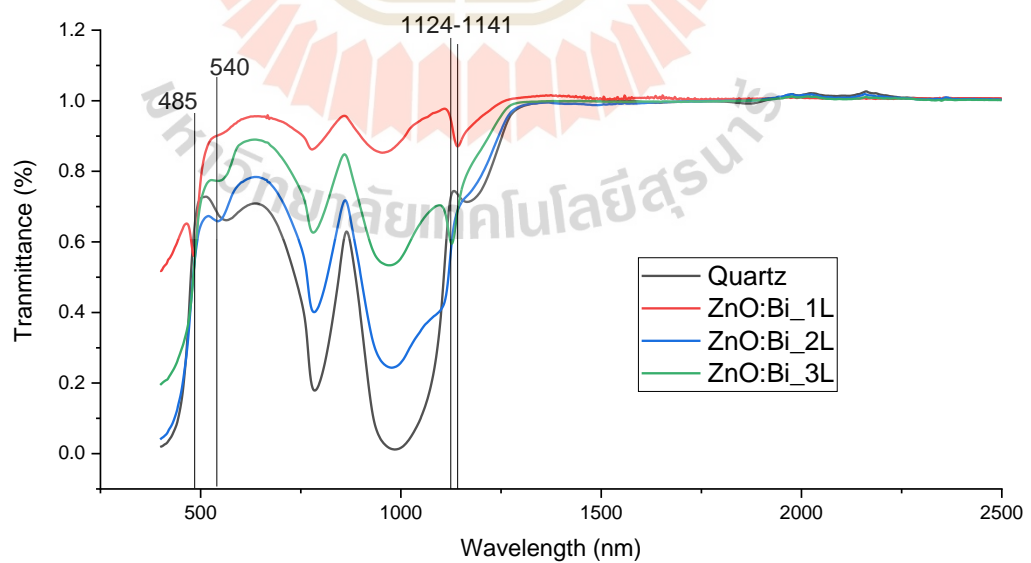


Figure 4.3 FTIR spectra of ZnO:Bi thin films on quartz with varied number of layers.

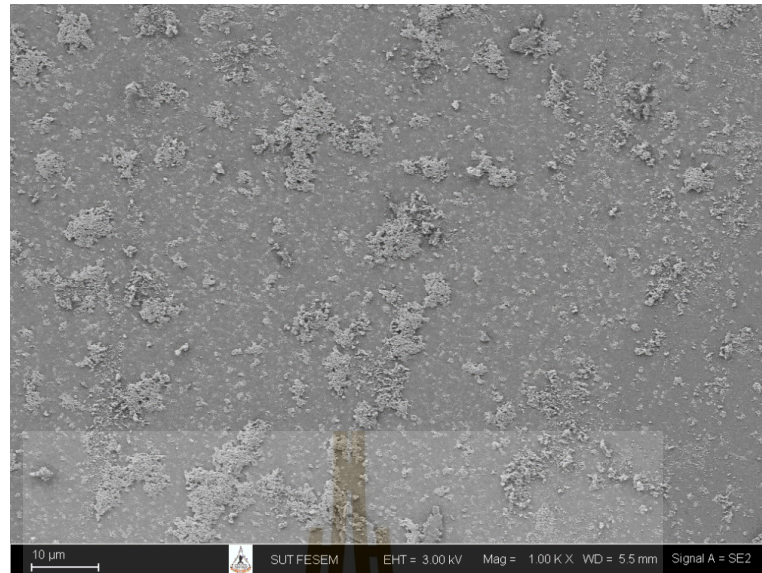


Figure 4.4 FESEM image of 1 layer bismuth doped zinc oxide on quartz substrate magnified 1000 times.



Figure 4.5 FESEM image of 4-layer bismuth doped zinc oxide on quartz substrate magnified 1000 times.

4.3 Using bismuth doped zinc oxide as a buffer layer for cadmium sulphide

4.3.1 Determining the ideal number of layers of ZnO:Bi for the buffer layer

Figure 4.6 shows the positive effect (homogeneity) of the ZnO:Bi buffer layer between the quartz substrate and CdS film, If CdS is deposited directly onto the quartz substrate, the film is non-homogenous, but if the ZnO:Bi buffer layer is deposited onto the quartz substrate prior to deposition of CdS, the CdS film quality improves, becoming homogenous.

4.3.1.1 Structural properties

FTIR analysis depicted in figure 4.7 shows broad weak absorption valley at 3385 cm^{-1} is attributed to O-H stretching (strong bonds) (Akhtar et al., 2020; Devamani et al., 2017b; Ghosh et al., 2018; Qutub et al., 2016), which only starts to appear for the ZnO:Bi_3L/CdS_3L film, possibly as a result of more H and O being absorbed. Weak absorption valley at 1372 cm^{-1} - 1561 cm^{-1} can indicate the bending vibrations of O-H/H₂O molecules (hydroxyl group) (Ghosh et al., 2018), the valley intensity increases with the increase in number of layers, possibly due to higher H₂O absorption (Devamani et al., 2017b).

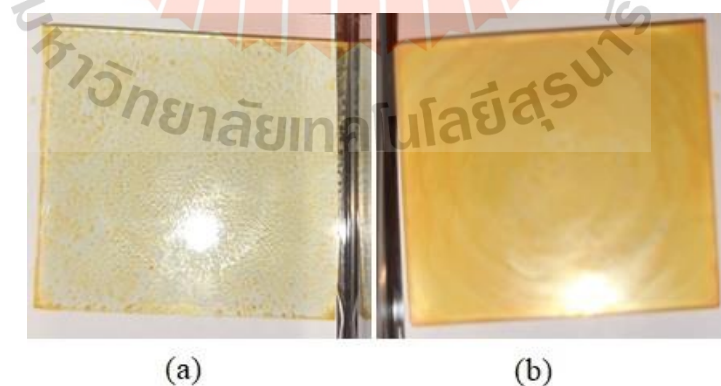


Figure 4.6 Comparison of surface homogeneity between 3 CdS layer samples deposited (a) directly onto quartz substrate and (b) onto ZnO:Bi buffer layer.

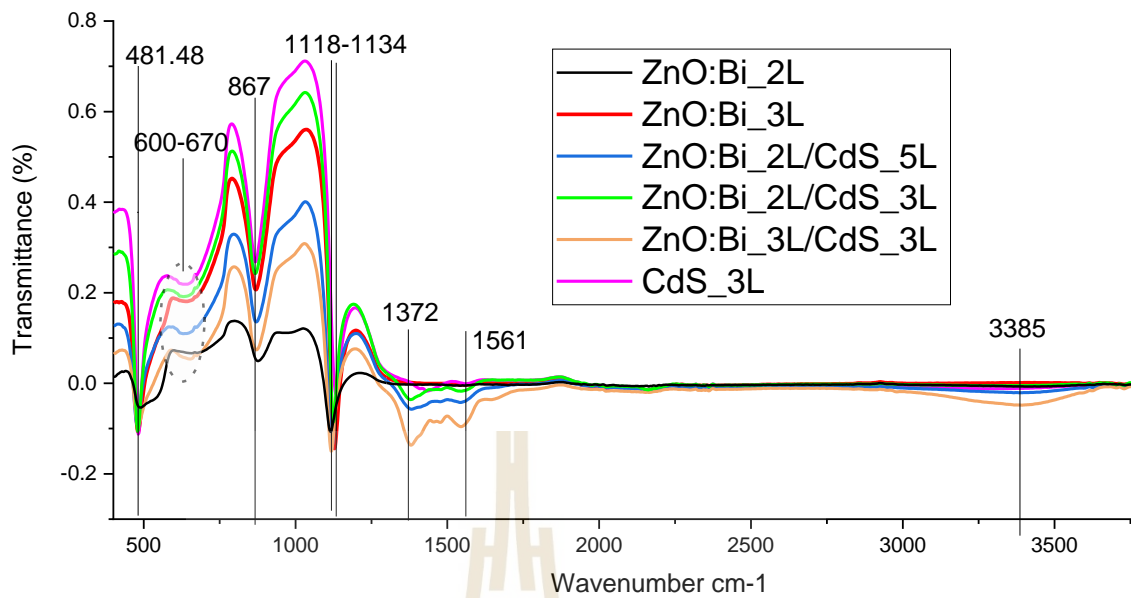


Figure 4.7 FTIR spectra of fabricated ZnO:Bi and CdS nanostructure thin films.

Valleys at the absorption bands 1134 cm^{-1} - 1118 cm^{-1} , attributed to C-O/S-O stretching (Devamani et al., 2017b; Qutub et al., 2016; Veerathangam et al., 2017), move from higher to lower wave numbers as number of layers on the samples increase, meaning an increase in the number of molecules with C-O/S-O bonds as the number of layers increase, potentially a result of a thicker film having more particles interacting with O_2 and CO_2 in the atmosphere.

Sharp absorption band at 867 cm^{-1} was assigned to bending vibrations of S-S and stretching vibrations of C-H bonds (Qutub et al., 2016; Veerathangam et al., 2017).

Very weak, broad valleys in the absorption range of 600 cm^{-1} - 670 cm^{-1} —only visible for samples containing CdS, are attributed to Cd-S bonds stretching (Arunraja et al., 2016; Choudhary & Verma, 2019; Ghosh et al., 2018; Kamble et al., 2020; Rafic et al., 2017; Raut et al., 2012; Ubale et al., 2012; Yeole et al., 2015). A sharp intense valley at the absorption band of 481.48 cm^{-1} represent Zn-O bonds stretching (Akhtar et al., 2020; Ghosh et al., 2018) and Cd-S bonds stretching (Akhtar et al., 2020; Arunraja et al., 2016; Devamani et al., 2017b; Ghosh et al., 2018; Kamble et

al., 2020; Pandian et al., 2011; Qutub et al., 2016; Rafic et al., 2017), indicating ZnO:Bi and CdS nanoparticles presences.

The CdS films on quartz with/without ZnO:Bi buffer layer were characterized. The various valleys on the FTIR spectra, as shown in figure 4.7 are a result of the thin film sample, indicating bonds present, together with their strength. Table 4.1 contains the wavenumber of the valley and the corresponding bonds they represent.

Table 4.1 Interpretation of the valleys obtained by the FTIR spectra of the synthesized CdS/ZnO:Bi nanostructures

Possible types of bonds	Intensity of valley	Valley wavenumber (cm ⁻¹)	Reference
Cd-S stretching Zn-O stretching	Sharp	481.48	(Akhtar et al., 2020; Arunraja et al., 2016; Devamani et al., 2017b; Ghosh et al., 2018; Kamble et al., 2020; Pandian et al., 2011; Qutub et al., 2016; Rafic et al., 2017)
Cd-S stretching	Small Broad	600-670	(Arunraja et al., 2016; Choudhary & Verma, 2019; Ghosh et al., 2018; Kamble et al., 2020; Rafic et al., 2017; Raut et al., 2012; Ubale et al., 2012; Yeole et al., 2015)
C-H bending S-S bending	Sharp	867	(Ghosh et al., 2018; Qutub et al., 2016)
C-O bonds S-O bonds	Sharp	1118-1134	(Devamani et al., 2017b; Qutub et al., 2016; Veerathangam et al., 2017)

Table 4.1 Interpretation of the valleys obtained by the FTIR spectra of the synthesized CdS/ZnO:Bi nanostructures (Continued)

Possible types of bonds	Intensity of valley	Valley wavenumber (cm ⁻¹)	Reference
H bonds/water molecules bending	Medium broad	1372-1561	(Ghosh et al., 2018)
H bonds O-H stretching	Broad	3385	(Fthenakis et al., 2020; Ghosh et al., 2018; Pankove, 2010; Qutub et al., 2016)

4.3.1.2 Electrical properties

Linearity of the J-V curve (figure 4.8) illustrates the ohmic contact behaviour of the samples. For the ZnO:Bi₃L/CdS₃L sample, ohmic contact behaviour is displayed under both illuminated and dark conditions, while all other samples had significantly lower current densities under both conditions, resulting in unobservable linearity of the J-V curves. Ohmic contact behaviour signifies the potential of the film to be used as a window layer, due to the low resistivity.

From the J-V plot (figure 4.8), all samples displayed photocurrent gains, however, when considering samples which displayed good curves for both the dark and illuminated test, the ZnO:Bi₃L/CdS₃L sample showed the highest photocurrent gain. It can also be observed that while the ZnO:Bi₃L sample had the highest photocurrent gain overall, it had bad current density under dark condition tests, improving with the addition of CdS in the ZnO:Bi₃L/CdS₃L sample. Sample ZnO:Bi₃L/CdS₃L also showed an increased current density for illuminated conditions, due to a higher absorption range being achieved with the addition of the CdS layer (Candelise et al., 2012).

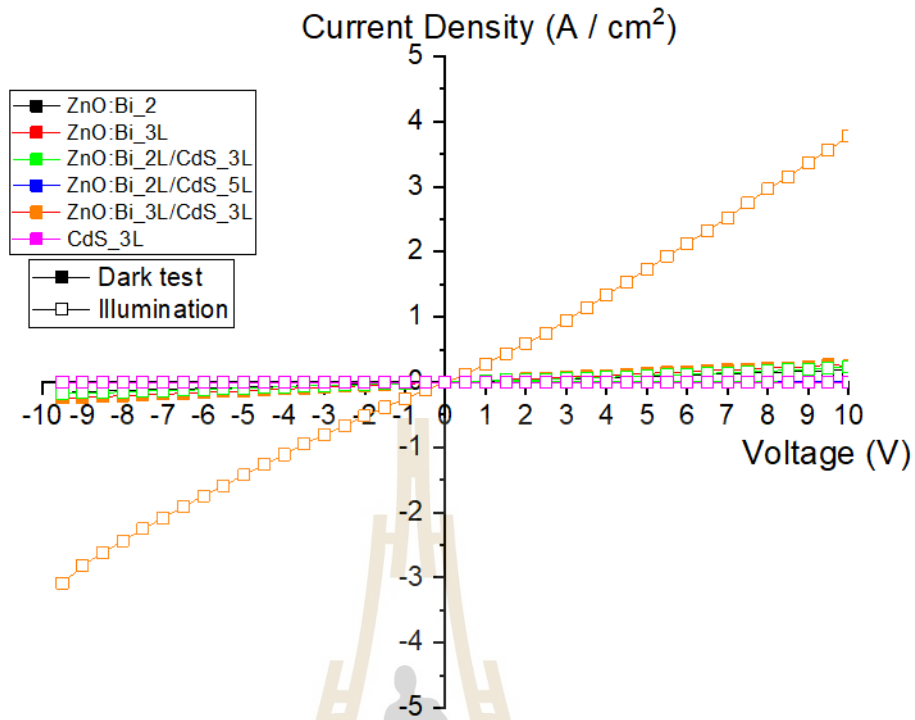


Figure 4.8 J-V curve for all samples under dark vs illumination test for determination of ohmic/non-ohmic behaviour.

Although the ZnO:Bi₃L/CdS₃L sample has the best conductivity under illumination conditions, it has the second-best conductivity under dark condition. The sample that achieved the best conductivity under dark conditions is the ZnO:Bi₂L/CdS₃L sample, this is due to decreased thickness and less ZnO:Bi, which resulted in a lower band gap, improving absorption of lower energy photons (Richter et al., 2013). Conductivity and current densities for all samples under different conditions are displayed in table 4.2, together with their respective cross-sectional areas.

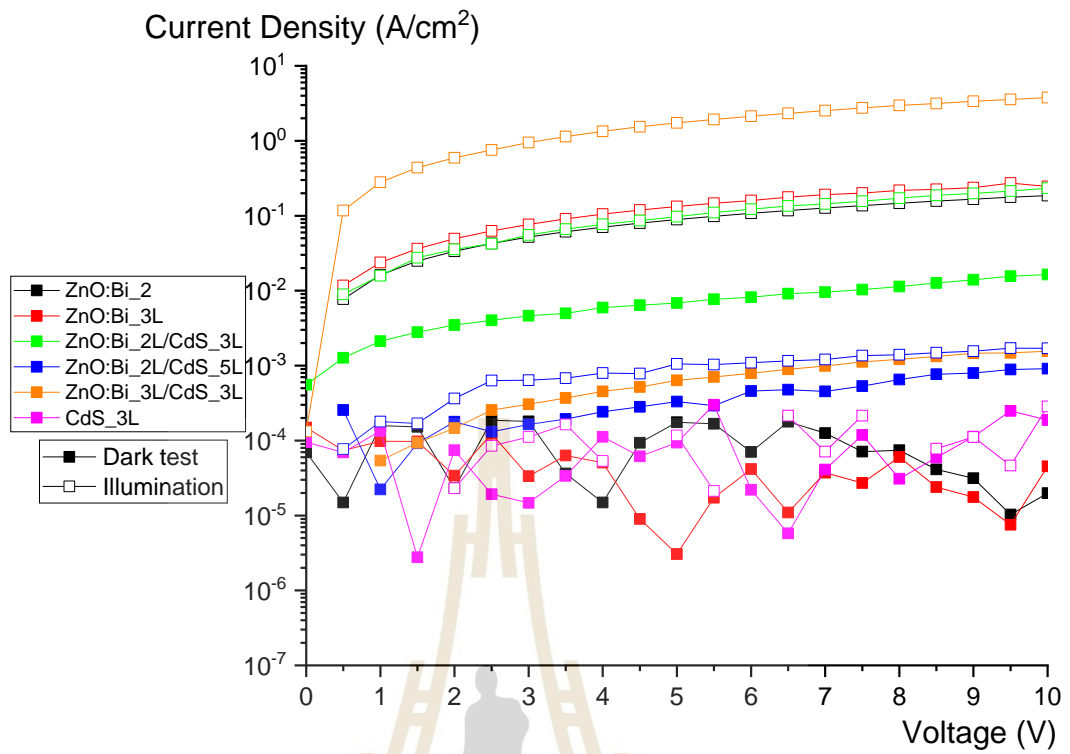


Figure 4.9 J-V plot in dark vs illumination test for photocurrent gain.

Table 4.2 Thickness and electrical properties of nanostructure thin films fabricated.

Type of thin film	Average thickness (nm)	Current density at 5V (A/cm ²)			Conductivity (S/cm)	
				Photocurrent gain		
		Dark	Illumination		Dark	Illumination
CdS_3L	Non-homogenous	9.37×10^{-5}	1.17×10^{-4}	1.25	2.56×10^{-5}	3.25×10^{-5}
ZnO_2L	131.03	1.76×10^{-4}	8.91×10^{-2}	5.07×10^2	1.64×10^{-5}	1.72×10^{-2}
ZnO_3L	259.94	3.05×10^{-6}	1.33×10^{-1}	4.36×10^4	1.81×10^{-5}	2.63×10^{-2}
ZnO_2L/CdS_3L	171.07	6.83×10^{-3}	9.73×10^{-2}	1.42×10^1	1.75×10^{-3}	2.00×10^{-2}
ZnO_2L/CdS_5L	330.03	3.32×10^{-4}	1.05×10^{-3}	3.16	7.41×10^{-5}	2.02×10^{-4}
ZnO_3L/CdS_3L	282.03	6.36×10^{-4}	1.74	2.73×10^3	1.39×10^{-4}	3.34×10^{-1}

4.3.1.3 Optical properties

Figure 4.10 and figure 4.11 show the transmittance and reflectance spectra of CdS and ZnO:Bi thin film layers in the range of 200 – 850 nm. It shows that all fabricated samples have a low transmittance for shorter wavelengths (< 400 nm). The transmittance increases toward 90% (considering $\approx 5\%$ transmittance drop caused by quartz substrate) in the visible to near-infrared light range (400 – 1100 nm), which is good since the film is for use as a window layer and the visible to near-infrared region of light is the range most absorbed by Si solar cells (Green, 2008; Sproul & Green, 1991).

Samples containing both the ZnO:Bi buffer layer and CdS window layer, have the lowest transmittance relative to other fabricated samples, due to increased thickness (Table 7). However, the transmittance of the visible to near-infrared region is high enough to allow light to reach the absorber layer on Si solar cells. The transmittance in the blue to UV range is low, being lowest for combined buffer and CdS layers. A low transmittance of low-wavelength photons (< 450 nm), exceeding the band gap of Si (1.1 eV), will lower losses in the Si solar cell, improving efficiency (Trupke et al., 2002).

While reflectance in the visible to near-infrared wavelength range is high for CdS samples containing the ZnO:Bi buffer layer (ZnO:Bi_2L/CdS_3L, ZnO:Bi_2L/CdS_5L, ZnO:Bi_3L/CdS_3L), relative to other fabricated samples, it is still low enough (< 10%) (taking $\approx 2\%$ reflectance of quartz substrate into consideration) to be used as a window layer for Si solar cells. Reflectance for shorter wavelengths is higher than the in the visible region, for all samples, which will potentially reduce heat losses caused by high-energy photons that exceed the absorption range of Si solar cells (Akhtar et al., 2020; Ramalingam & Indulkar, 2017).

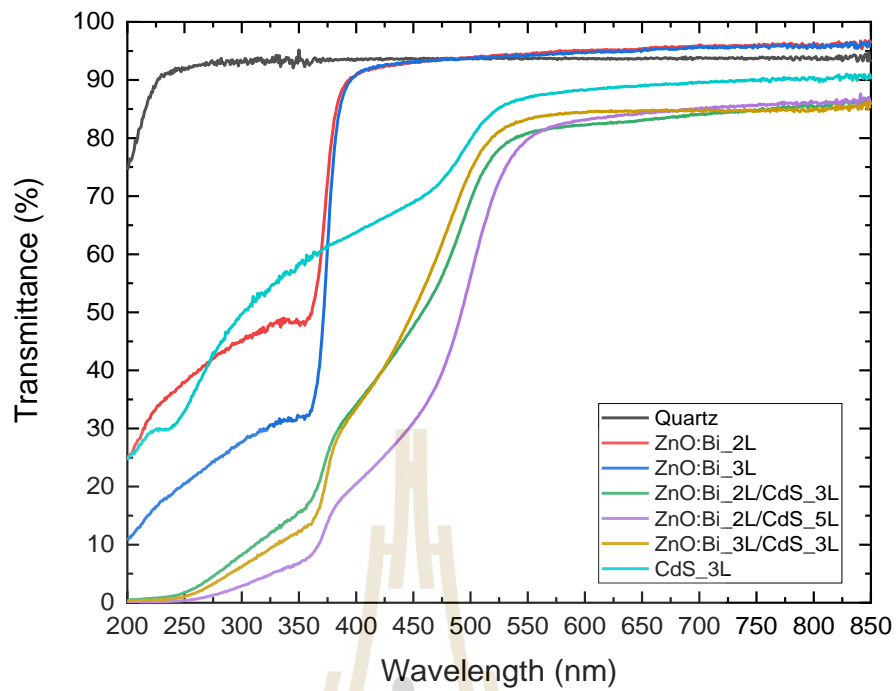


Figure 4.10 Transmittance spectra of CdS window layer and ZnO:Bi buffer layer with samples containing varying number of layers.

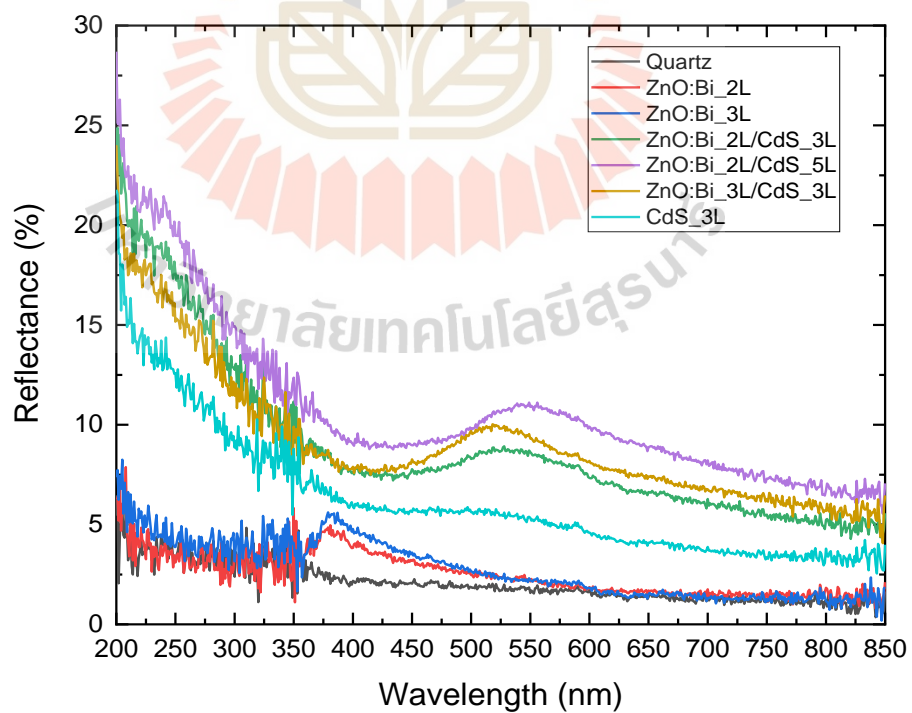


Figure 4.11 Reflectance spectra of CdS window layer and ZnO:Bi buffer layer with samples containing varying number of layers.

Samples only containing ZnO:Bi display an absorption edge at wavelength of 380 nm. The samples containing only CdS display an absorption edge at wavelength of 535 nm. When ZnO:Bi is used as the buffer layer for CdS, the absorption edge shifts to wavelengths shorter than that of CdS and longer than that of ZnO:Bi. With an increase in the number of CdS layers added to the buffer layer, the absorption edge shifts to shorter wavelengths. With an absorption edge between, 500–550 nm, as seen in figure 4.12, the window layer can potentially improve the absorption in the visible region, for Si solar cells (Green, 2008; Schinke et al., 2015; Sproul & Green, 1991).

It is observable from the Tauc plot in figure 4.13 that when ZnO:Bi is used as the buffer layer, the band gap broadens.

For ZnO:Bi_2L/CdS_3L and ZnO:Bi_3L/CdS_3L samples the band gaps are 2.61 eV and 2.69 eV, indicating that an increase in ZnO:Bi layers, increased the band gap. This results from the increase in concentration of ZnO:Bi nanoparticles that have a larger band gap (3.29 eV), compared to CdS (2.49 eV).

For ZnO:Bi_2L/CdS_3L and ZnO:Bi_2L/CdS_5L the band gaps are 2.61 eV and 2.56 eV, indicating that an increase in CdS layers decreased the band gap. A decrease in the band gap can be attributed to the increase in CdS particle size when more layers are used (Veerathangam et al., 2017).

Linearity of the curves in figure 4.13 provide confirmation of the direct band gap of the materials (Ubale et al., 2012)

A broadened band gap can increase the photon energy efficiency of Si solar cells by allowing higher energy photons to be converted to electricity (Ramalingam & Indulkar, 2017).

Refractive indices of ZnO:Bi_2L and ZnO:Bi_3L samples are the lowest (Figure 4.14); the refractive index of CdS_3L is higher than ZnO:Bi samples, but lower than CdS samples containing the ZnO:Bi buffer layer. All samples show refractive indices below 2 (considering refraction of quartz substrate), in the visible to near-infrared region of the spectrum, with increased refraction for high-energy photons (<400

nm). Refractive indices of the films are lower than that of Si (≈ 4 at 600 nm), therefore if used as a window layer, it would comply with Snell's law (Boccard et al., 2014; Bryant, 1958). By complying with the law, light is refracted toward the normal of the absorber layer, instead of away, potentially reducing surface recombination losses. This shows that the number of high-energy photons converted to heat by Si can potentially be reduced by the it's refraction through the window layer (Ramalingam & Indulkar, 2017).

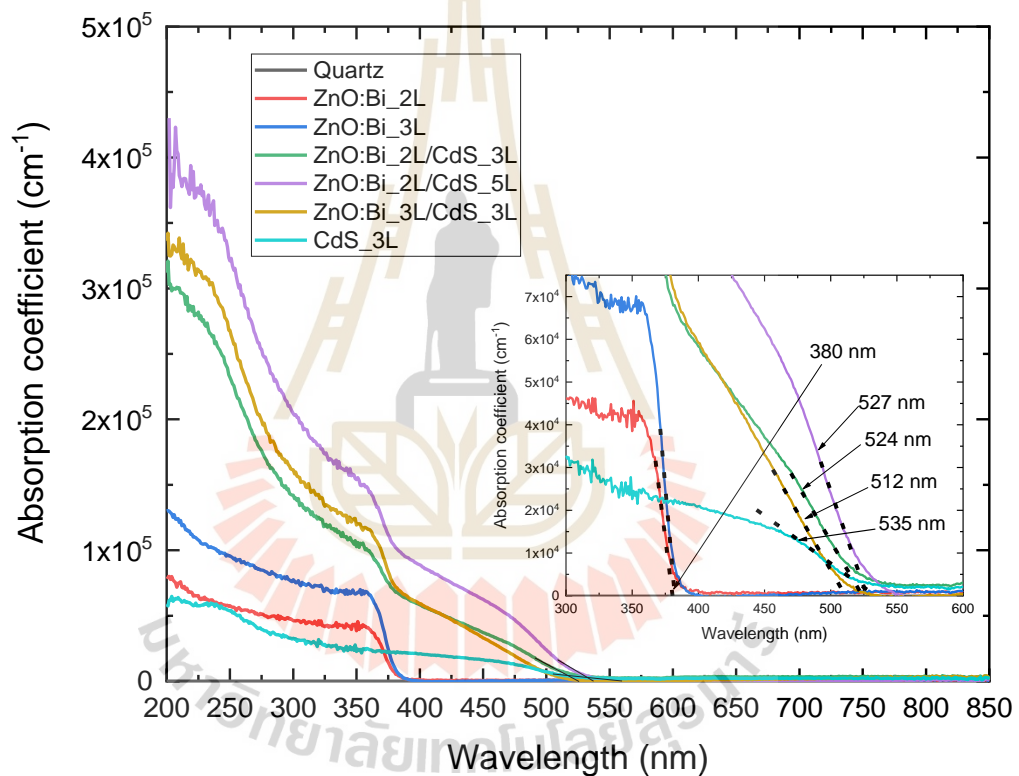


Figure 4.12 Absorption coefficients for fabricated samples at different wavelengths and inset are the estimated wavelengths for absorption edges

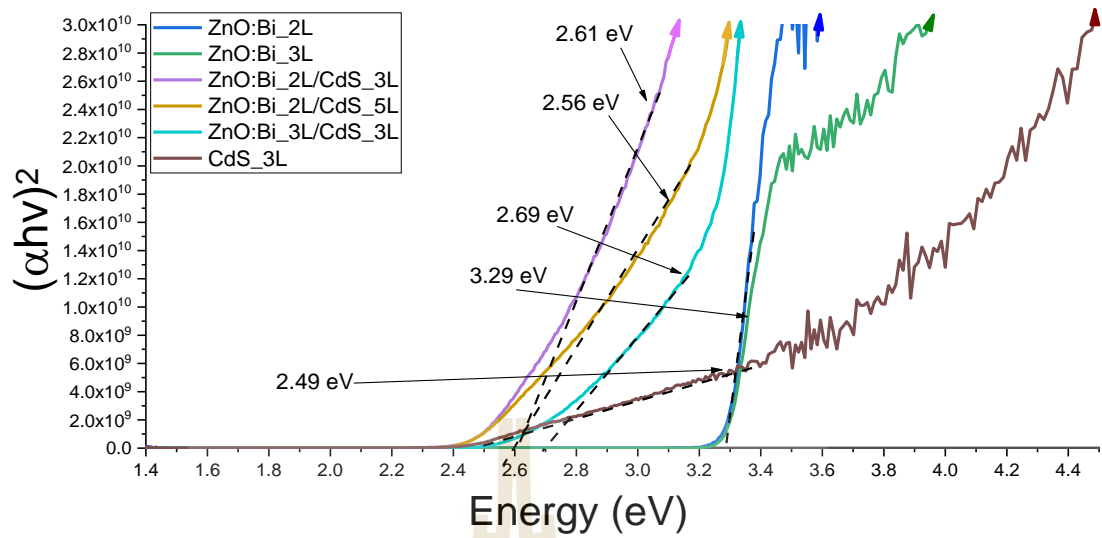


Figure 4.13 $(\alpha h\nu)^2$ versus $(h\nu)$ curve for all samples (Tauc plot to determine band gap)

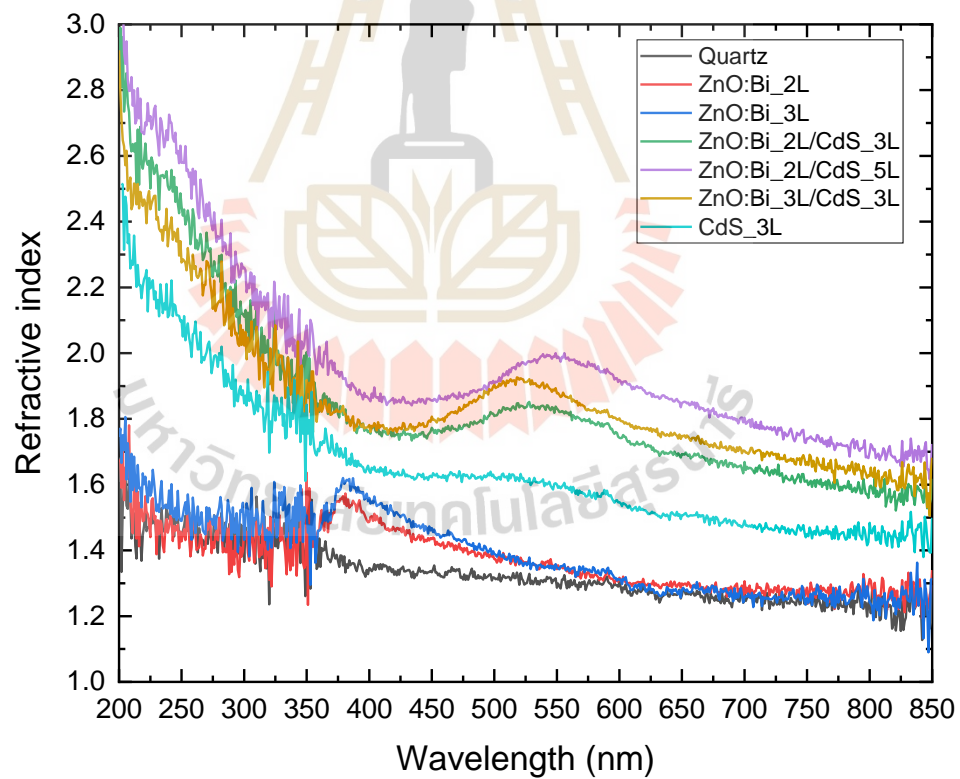


Figure 4.14 Refractive index for all fabricated samples.

4.3.2 The effect of a varied temperature for drying cadmium sulphide

While drying the cadmium sulphide thin films — deposited onto quartz substrates by spin coating — the drying temperature was varied. Three different temperatures were used while keeping time constant and 30 minutes, and ramp rate constant at 1°C/min. The number of layers in the film was also kept constant, with 1 layer of ZnO:Bi and 5 layers of CdS. Figure 4.15 show the results from FESEM analysis, in which we can see that increased temperature results in fewer cracks present in the surface, which would be a better quality of film. The sample prepared at 300°C (Figure 4.15.C) shows crystals forming.

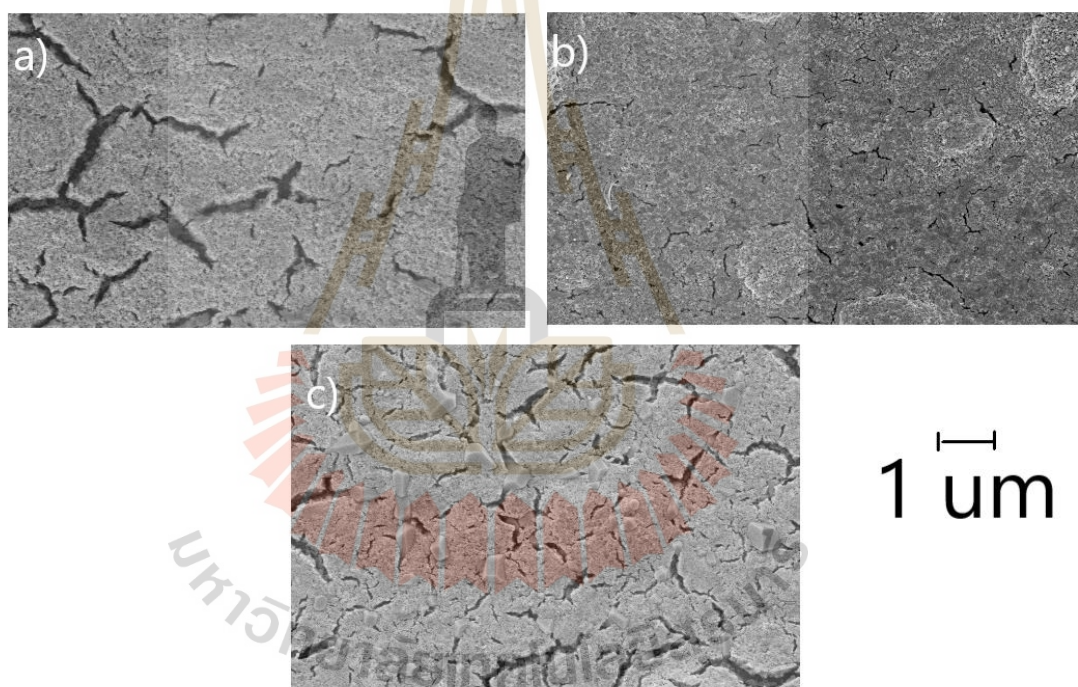


Figure 4.15 FESEM images showing surface of ZnO:Bi_1L/CdS_5L prepared at a)100°C, b)200°C and c)300°C.

From the EDS analysis we can see that these crystals in figure 4.16.a correspond to sodium and zinc concentrations, in figures 4.16.c and 4.16.d, respectively. The crystals are possibly formed by sodium acetate ($C_2H_3NaO_2$), from the reaction to obtain cadmium sulphide. These crystals represent phase separation

occurring when higher temperatures are used. Figure 4.16.d shows an even spread of sulphur and figure 4.16.e shows an even spread of cadmium, these concentrations represent a homogenous cadmium sulphide deposition.

The XRD analysis shown in figure 4.17, of the samples prepared at different temperatures, show a cubic face structure for all samples, with peaks being more visible for samples prepared at lower temperature. This could be a result of a hanging in structure from cubic to hexagonal, with the higher temperature used.

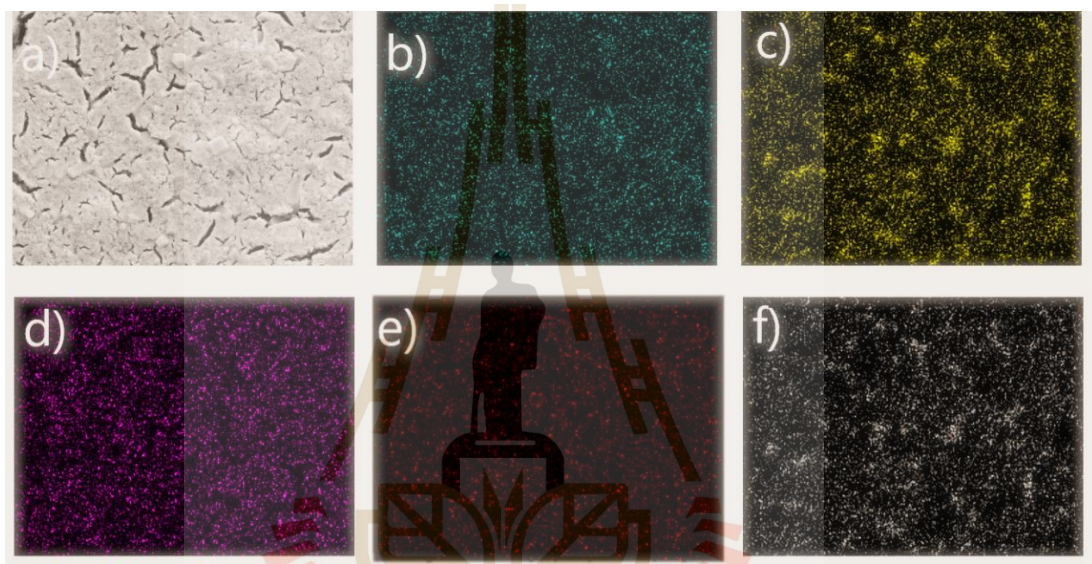


Figure 4.16 EDS data for film prepared at 300°C, showing the concentration of different elements on the ZnO_1L/CdS_5L film, proving the crystals formed are of sodium acetate. a) captured image from electron microscope, b) Oxygen concentration, c) Sodium concentration, d) Sulphur concentration, e) Cadmium concentration, f) Zinc concentration.

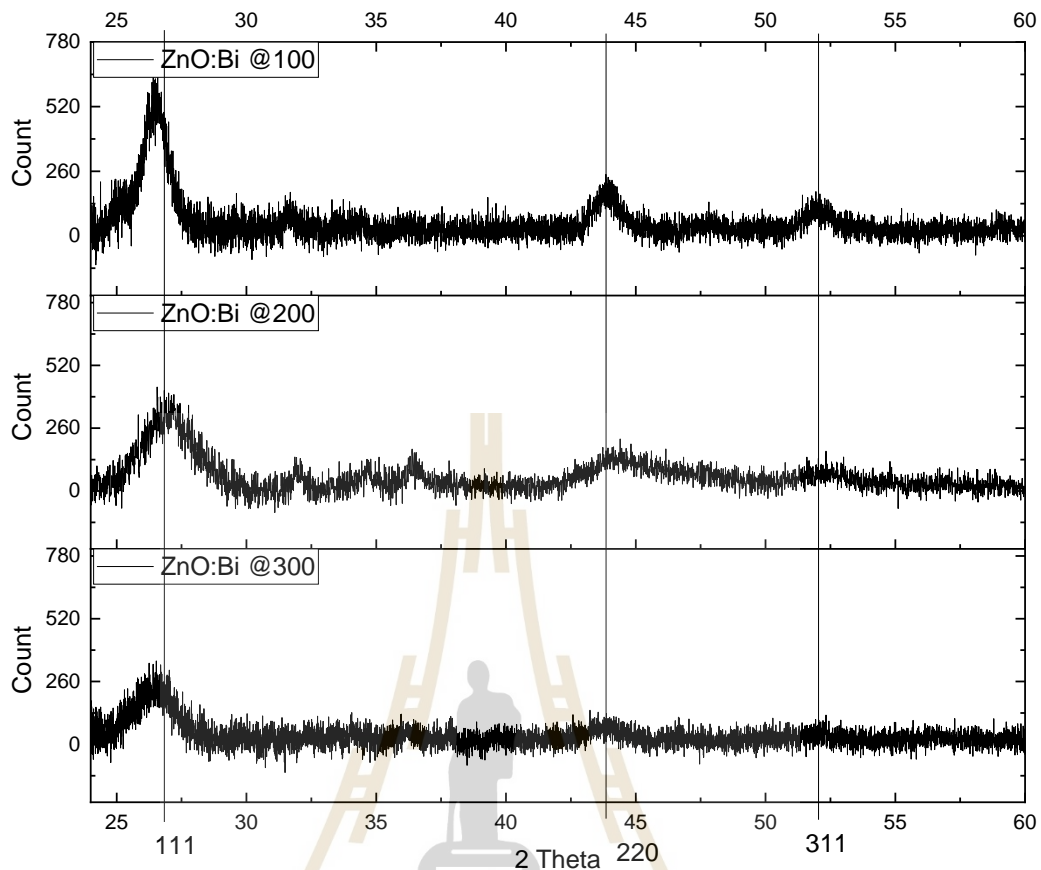


Figure 4.17 XRD analysis of ZnO:Bi_3L/CdS_5L at 100°C, 200°C and 300°C.

4.3.3 The effect of a varied number of layers for cadmium sulphide

The number of ZnO:Bi layers were kept constant at 3 layers, while variations of 3, 5, 8 and 11 layers of cadmium sulphide were used, to determine the effect of the number of layers, on the characteristics of the film.

The surface morphology of the fabricated films was studied by FESEM analysis (Figure 4.18). It is observable that the thicker film (more layers) has more cracks in the surface, showing a correlation between the number of layers and the frequency of cracks. Changes in the film thickness are observed to affect the optical properties such as transmittance.

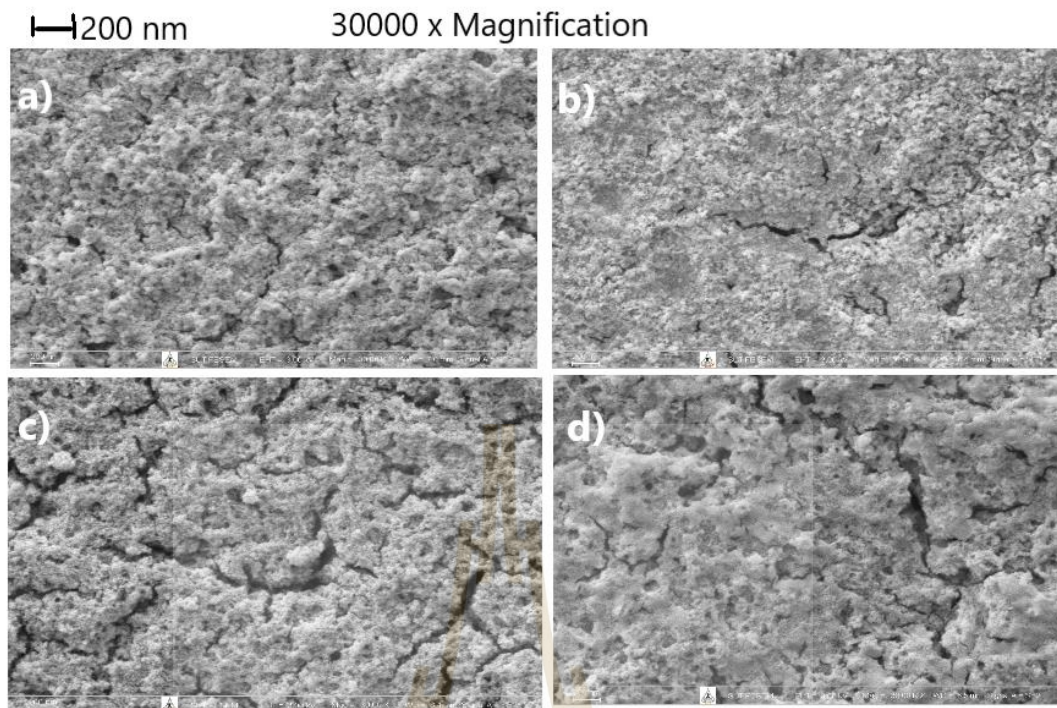


Figure 4.18 SEM images of CdS films at 30000 x magnification; a) CdS_3L, b) CdS_5L, c) CdS_8L, d) CdS_11L.

From XRD analysis, the broad peaks of CdS nanostructures (Figure 4.19) at 26.77° , 44° , and 52.1° are in good correspondence with the (111), (220), and (311) planes of cubic phase CdS crystal structures, respectively, following the JCPDS data cards (No. 80-0019). Because of the smaller crystals, the diffraction lines have become broadened, the number of its lattice planes and thus the extent of orderly arrangement also decrease. (Gupta & Pal, 2012)

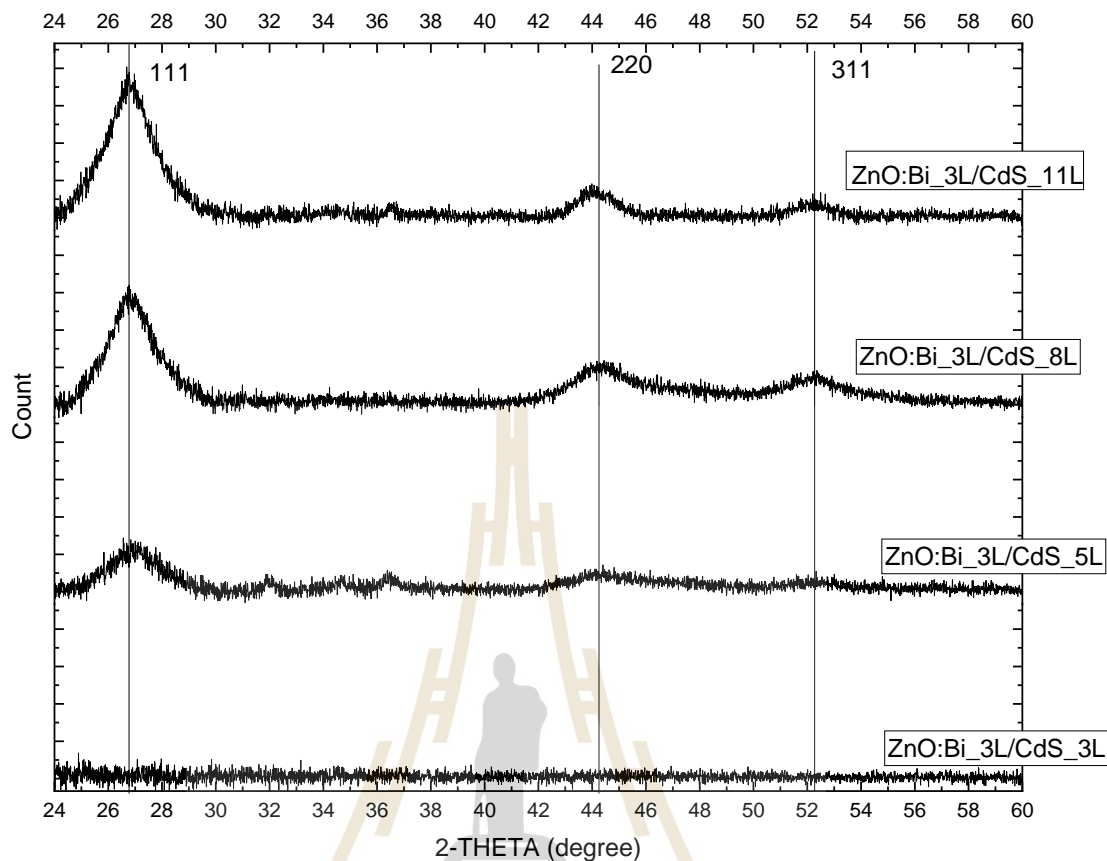


Figure 4.19 XRD results from samples containing various number of layers of CdS on 3 ZnO:Bi layers.

It is observable from the Tauc plot in Figure 4.21, that the band gaps correspond to the absorption edges from Figure 4.20.

For ZnO:Bi_3L and ZnO:Bi_3L/CdS_3L samples, the band gaps are 3.30 eV and 2.71 eV, respectively, indicating that the addition of ZnO:Bi layers, increased the band gap. This results from the increase in concentration of ZnO:Bi nanoparticles that have a larger band gap (3.30 eV), compared to cubic CdS ($\approx 2.4\text{-}2.7$ eV).

When the number of CdS layer increases, the calculated band gap is tunable from 2.71eV to 2.41 eV. A decrease in the band gap can be attributed to the increase in CdS grain size when more layers are used (Veerathangam et al., 2017).

Linearity of the curves in Figure 4.21 confirms the direct band gap of the materials (Ubale et al., 2012). All band gaps illustrated maintain a band gap greater than that of Si solar cells. A broadened band gap can increase the photon energy efficiency of Si solar cells by allowing higher energy photons to be converted to electricity (Ramalingam & Indulkar, 2017).

Correlation between the absorption edges, band gaps, grain sizes and the number of deposition cycles used can be seen in table 4.3.

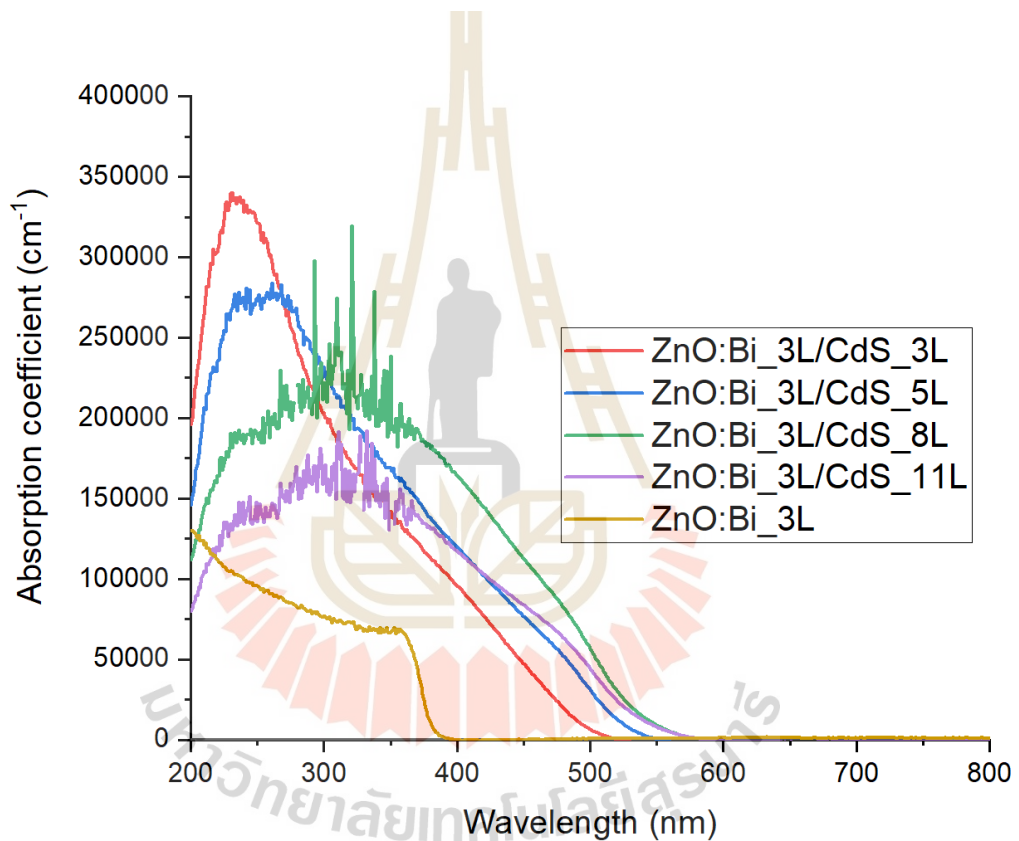


Figure 4.20 Absorption coefficients of CdS window layer and ZnO:Bi buffer layer with samples containing varying number of layers.

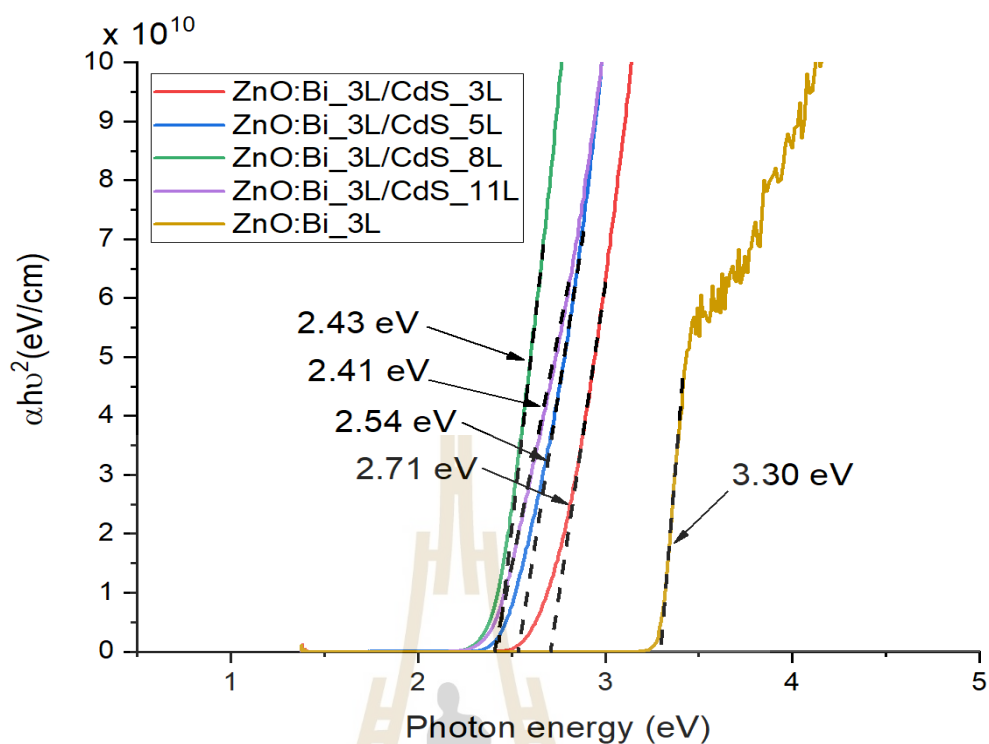


Figure 4.21 $(\alpha hv)^2$ versus (hv) curve for all samples (Tauc plot to determine band gap)

Table 4.3 Correlation between the number of layers of CdS and the grain size, absorption edge and band gap.

Number of CdS layers	Estimated grain size (nm)	Absorption edge wavelength (nm)	Band gap (eV)
3	5	500	2.71
5	6.5	530	2.54
8	8.54	550	2.43
11	9.46	560	2.41

The structural and optical properties show that an increase in the number of CdS layers will affect the performance of the thin films as part of a solar cell. The correlation between the band gap, grain size, and the number of layers was

determined in this experiment; an increase in the number of CdS layers will result in an increased grain size, which subsequently decreases the band gap.

4.4 Cadmium sulphide deposited by spin coating onto PN Silicon

ZnO:Bi and CdS were deposited onto PN silicon wafers by spin coating method, metal contacts were then made on the front and rear. The resulting solar cell was subjected to an external bias voltage to test the diode PN junction. The structure of post-firing and pre-firing samples are shown in Figure 4.22 (a) and (b), respectively.

In figure 4.23, the diode results of the pre-firing cell samples showed I-V characteristics indicative of a non-rectify property, with high metal-contact resistance from the illustrated low I-V slope. When the post-firing sample without cut edges obtains a non-rectify property, since a PN junction short circuit exists. This severe effect was dealt with by cutting the edges. The cut edged sample under the post-firing process provides a diode rectify behavior, due to shallow diffusion of contact metals with 0.25V threshold voltage which is less than a typical PN diode at 0.5-0.6V.

The tested PN Si solar cells (6.45 cm² area size) with varying ZnO:Bi/CdS layers were measured under the 1sun simulator test (1000 Watt/m²), which showed the I-V curve in figure 4.24. It was found that the increase in CdS film thickness strongly affects the power conversion performance of PN Si/ZnO:Bi/CdS cells. The power conversion is shown to decrease with the increase of CdS layer thickness. This is due to low transmittance of the light through the 11 CdS layers.

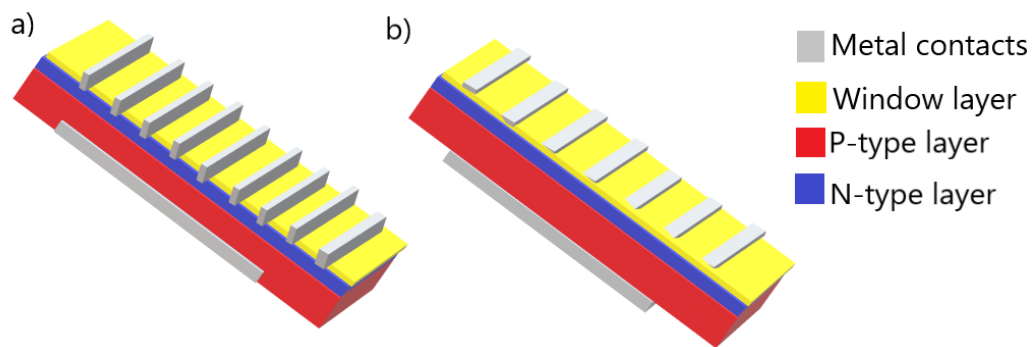


Figure 4.22 Structure of prototype photovoltaic cell where metal makes a) contact on PN -junction, and b) non-firing contact

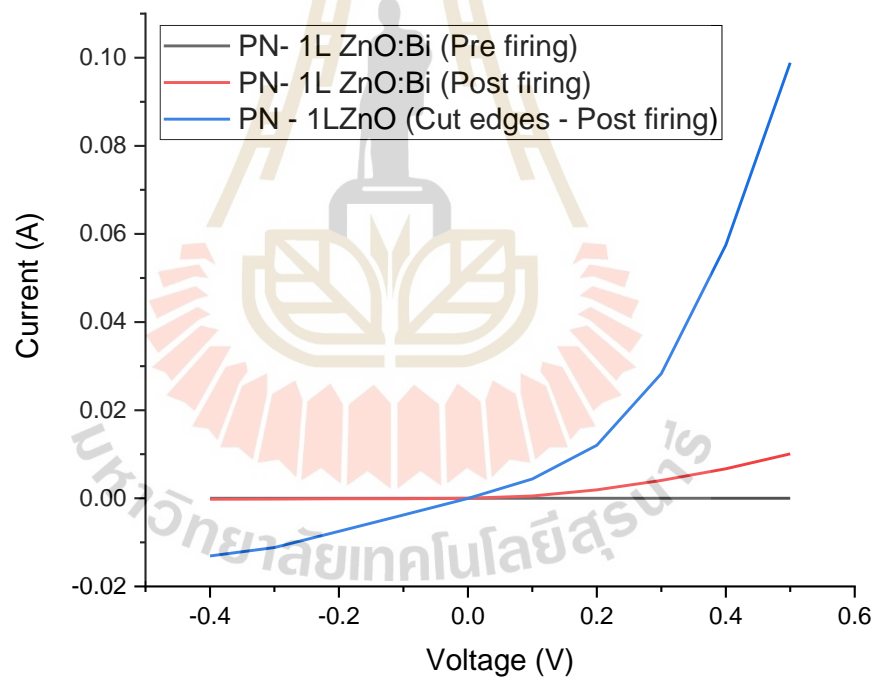


Figure 4.23 Curve from bias voltage applied to a PN-Si/ZnO:Bi diode

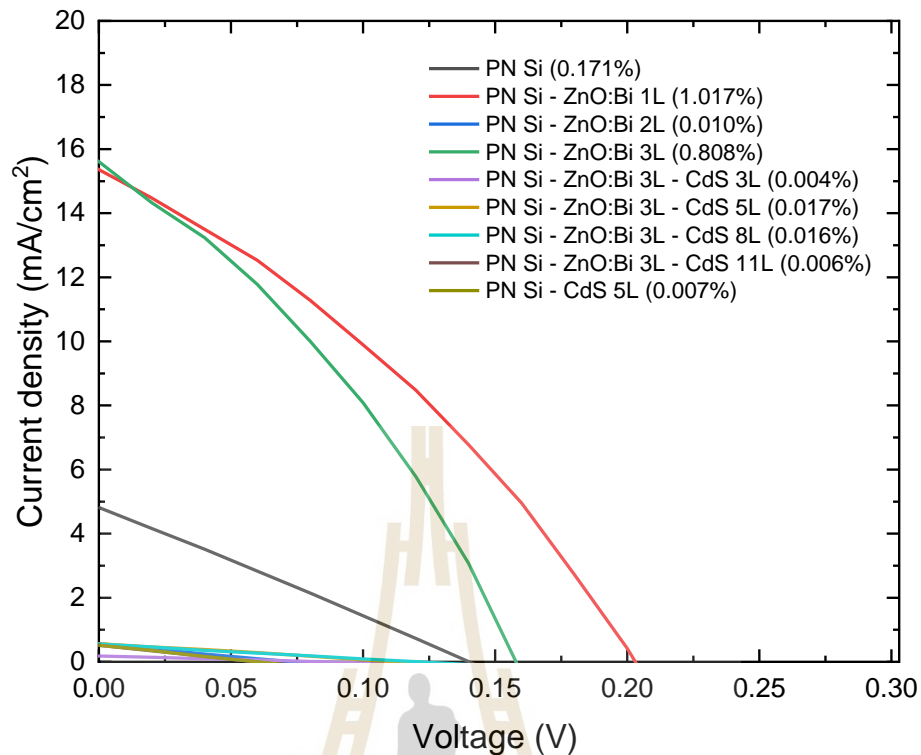


Figure 4.24 Current density and voltage of samples, with efficiencies, measured under solar simulator.

4.5 Summary

The structural, optical, and electrical analyses show properties of the ZnO:Bi/CdS as suitable for window layer applications in solar cells. The structural properties show Cd-S bonds in the cadmium sulphide films, and Zn-O bonds from the ZnO:Bi films, proving the effectiveness of the fabrication technique. Band gap is shown to be affected by the number of layers of the films used, which also affects the particle sizes. Optical analyses show desirable transmittance, reflectance, and refractive properties, with relation to window layer applications.

Application of the window layer on the prototype PN-Si shows that the metal contacts were not making good contact on the PN-junction, resulting in the detection of charge carriers across the electric field of the two n-layers being measured — rather than the charge carriers migrating across the PN-junction.

CHAPTER 5

CONCLUSIONS AND RECOMMENDATIONS

The need for an economical solution to improve the efficiency of current solar cell technology is clear. By incorporating quantum dots into existing solar cells, there is a potential to improve efficiency, through downshifting or through generating more electron-hole pairs. Besides being used as a window layer on PN silicon, quantum dots can also be used in heterojunction solar cells, being the active layer in a thin film solar cell. By having a direct band gap, the absorption coefficients are lower, meaning that photons don't have to penetrate the cell as deep as with bulk materials.

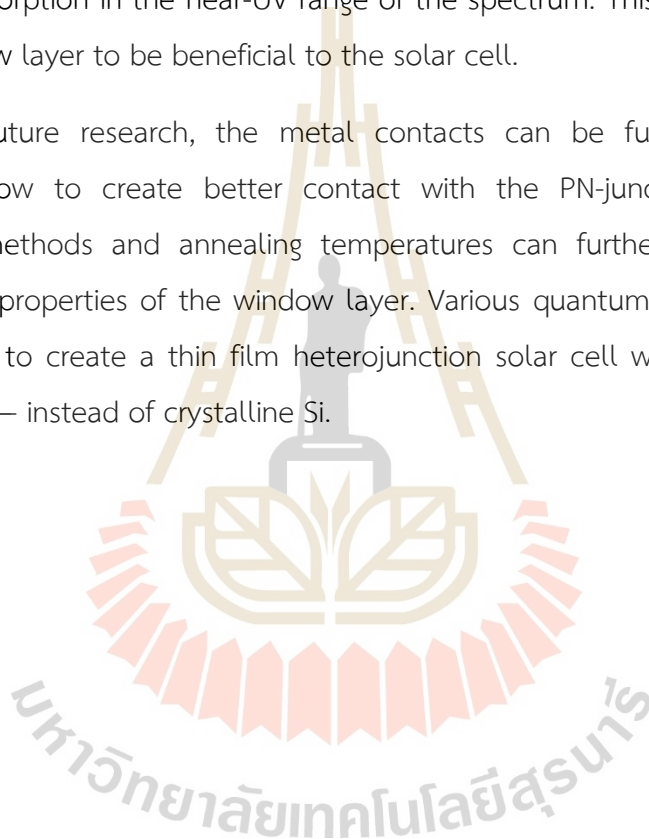
From this research, we can conclude that the CdS films, together with ZnO:Bi show good structural properties — having strong bonds, similar to other related research, and showing crystal structures in line with previous research using similar techniques — proving the method of fabrication is effective in creating a good quality film. The ZnO:Bi buffer layer enables the CdS film to be homogenous, with fewer cracks in the surface, while also contributing to reducing reflectance and widening the band gap.

From the analysis of optical properties of ZnO:Bi/CdS films, we can see that they have the potential to be used as a window layer in heterojunction solar cells. The reflectance is low in the visible light region of the spectrum, minimizing the parasitic losses from a window layer. Transmission is high in the visible region while being reduced in the near-UV region, indicating absorption and possible downshifting of high-energy light. Absorption of light in regions outside of the absorption range of the band gap of Si, is what an ideal window layer should do, and what we can observe through the analysed films.

The factors affecting properties of the film, including the grain size, temperature, and number of layers were investigated, showing that by manipulating these factors we can achieve the desired characteristics of the material.

A good quality film was achieved, proving the spin coating deposition technique successful. Characterization of the thin films are achieved in this thesis, proving that cadmium sulphide can be used as a window layer material, showing properties needed to improve the efficiency of a singly junction silicon solar cell. While the PN-junction silicon with the window layer has not shown the desired electrical properties, due to short circuit and metal contact faults — which are not a result of the window layer — the optical properties show that the window layer reduces reflectance in all areas and improves absorption in the near-UV range of the spectrum. This proves the potential of the window layer to be beneficial to the solar cell.

For future research, the metal contacts can be further investigated to determine how to create better contact with the PN-junction. Using different deposition methods and annealing temperatures can further be investigated to improve the properties of the window layer. Various quantum dot p-type materials can be used to create a thin film heterojunction solar cell with the window layer investigated — instead of crystalline Si.



References

- Abid, M., Abid, Z., Sagintayev, Z., Murtaza, R., Dastan, S., & Shabbir, M. (2018). Prospects of floating photovoltaic technology and its implementation in Central and South Asian Countries. *International Journal of Environmental Science and Technology*, 16, 1755-1762
- Ahmed, R., Will, G., Bell, J., & Wang, H. (2012). Size-dependent photodegradation of CdS particles deposited onto TiO₂ mesoporous films by SILAR method. *Journal of Nanoparticle Research*, 14.
- Akhtar, S., Rehman, S., Asiri, S. M., Khan, F. A., Baig, U., Hakeem, A. S., & Gondal, M. A. (2020). Evaluation of bioactivities of zinc oxide, cadmium sulfide and cadmium sulfide loaded zinc oxide nanostructured materials prepared by nanosecond pulsed laser. *Materials Science and Engineering: C*, 116, 111156.
- Al-Jawad, S. M. H. (2017). Comparative study between CBD and SILAR methods for deposited TiO₂, CdS, and TiO₂/CdS core-shell structure. *Materials Science in Semiconductor Processing*, 67, 75–83.
- Alkuam, E., Mohammed, M., & Chen, T.-P. (2017a). Enhanced synthesis of cadmium sulfide by electrodeposition in dye-sensitized solar cells. *Solar Energy*, 157, 342–348.
- Alkuam, E., Mohammed, M., & Chen, T.-P. (2017b). Enhanced synthesis of cadmium sulfide by electrodeposition in dye-sensitized solar cells. *Solar Energy*, 157, 342–348.
- Amin, N., Sopian, K., & Konagai, M. (2007). Numerical modeling of CdS/CdTe and CdS/CdTe/ZnTe solar cells as a function of CdTe thickness. *Solar Energy Materials and Solar Cells*, 91, 1202–1208.
- Andreani, L. C., Bozzola, A., Kowalczewski, P., Liscidini, M., & Redorici, L. (2019). Silicon solar cells: Toward the efficiency limits. *Advances in Physics: X*, 4(1), 1548305.
- Arunraja, L., Thirumoorthy, P., Arumugam, K., Sriram, G., VENKATACHALAM, R., & Edwinpaul, L. (2016). Structural and Electrical Properties of Cadmium Sulfide

- Nanoparticles: A Simple Chemical Route. *Synthesis and Reactivity in Inorganic, Metal-Organic, and Nano-Metal Chemistry*, 46, 1642-1646.
- Arya, R. R., Sarro, P. M., & Loferski, J. J. (1982). Efficient cadmium sulfide on silicon solar cells. *Applied Physics Letters*, 41(4), 355–357.
- Awasthi, A., Shukla, A. K., S.r., M. M., Dondariya, C., Shukla, K. N., Porwal, D., & Richhariya, G. (2020). Review on sun tracking technology in solar PV system. *Energy Reports*, 6, 392–405.
- Bakiyaraj, G., Gopalakrishnan, N., & Dhanasekaran, R. (2011). Influences of thermal annealing on the structural, optical and electrical properties of nanostructured cadmium sulphide thin films. *Chalcogenide Letters*, 8, 419–426.
- Balaji, G., Balasundaraprabhu, R., Prasanna, S., Prabavathy, N., Venkatraman, M. R., Asokan, V., Muthukumarasamy, N., Kannan, M. D., & Sivakumaran, K. (2018). Investigations on Hot-wall deposited Cadmium Sulphide buffer layer for thin film solar cell. *Materials Letters*, 222, 82–87.
- Balkus, K. J. (2013). Chapter 9—Metal Oxide Nanotube, Nanorod, and Quantum Dot Photocatalysis. In S. L. Suib (Ed.), *New and Future Developments in Catalysis* (pp. 213–244).
- Bhandari, K. P., Roland, P. J., Mahabaduge, H., Haugen, N. O., Grice, C. R., Jeong, S., Dykstra, T., Gao, J., & Ellingson, R. J. (2013). Thin film solar cells based on the heterojunction of colloidal PbS quantum dots with CdS. *Solar Energy Materials and Solar Cells*, 117, 476–482.
- Bin Rafiq, M. K. S., Amin, N., Alharbi, H. F., Luqman, M., Ayob, A., Alharthi, Y. S., Alharthi, N. H., Bais, B., & Akhtaruzzaman, M. (2020). WS 2: A New Window Layer Material for Solar Cell Application. *Scientific Reports*, 10(1), 771.
- Boakye, F., & Nusenu, D. (1997a). The energy band gap of cadmium sulphide. *Solid State Communications*, 102(4), 323–326.
- Boakye, F., & Nusenu, D. (1997b). The energy band gap of cadmium sulphide. *Solid State Communications*, 102(4), 323–326.
- Boccard, M., Despeisse, M., Escarre, J., Niquille, X., Bugnon, G., Hänni, S., Bonnet-Eymard, M., Meillaud, F., & Ballif, C. (2014). High-Stable-Efficiency Tandem Thin-Film Silicon Solar Cell With Low-Refractive-Index Silicon-Oxide Interlayer. *IEEE Journal of Photovoltaics*, 4(6), 1368–1373.

- Bouraiou, A., Hamouda, M., Chaker, A., Mostefaoui, M., Lachtar, S., Sadok, M., Boutasseta, N., Othmani, M., & Issam, A. (2015). Analysis and evaluation of the impact of climatic conditions on the photovoltaic modules performance in the desert environment. *Energy Conversion and Management*, 106, 1345–1355.
- BP, p. l. c. (2020). *Bp Statistical Review of World Energy 2020*. 68.
- Breeze, P. (2019). *Power Generation Technologies* (3rd ed.). Elsevier science and technology.
- Britt, J., & Ferekides, C. (1993a). Thin-film CdS/CdTe solar cell with 15.8% efficiency. *Applied Physics Letters*, 62(22), 2851–2852.
- Britt, J., & Ferekides, C. (1993b). Thin-film CdS/CdTe solar cell with 15.8% efficiency. *Applied Physics Letters*, 62(22), 2851–2852.
- Bruchez, M., Moronne, M., Gin, P., Weiss, S., & Alivisatos, A. P. (1998). Semiconductor nanocrystals as fluorescent biological labels. *Science (New York, N.Y.)*, 281(5385), 2013–2016.
- Bryant, F. (1958). Snell's Law of Refraction. *Physics Bulletin*, 9(12), 317–317.
- Candelise, C., Winkler, M., & Gross, R. (2012). Implications for CdTe and CIGS technologies production costs of indium and tellurium scarcity. *Progress in Photovoltaics: Research and Applications*, 20(6), 816–831.
- Capellán-Pérez, I., Castro, C., & Arto, I. (2017). Assessing vulnerabilities and limits in the transition to renewable energies: Land requirements under 100% solar energy scenarios. *Renewable and Sustainable Energy Reviews*, 77, 760–782.
- Chopra, K. L., Paulson, P. D., & Dutta, V. (2004). Thin-film solar cells: An overview. *Progress in Photovoltaics: Research and Applications*, 12(2–3), 69–92.
- Choudhary, R. B., & Verma, A. (2019). Augmented structural, optical and electrical properties of CdS decorated PANI/rGO nanohybrids. *Optical Materials*, 96, 109310.
- Chuu, D.-S., & Dai, C.-M. (1992). Quantum size effects in CdS thin films. *Physical Review B*, 45(20), 11805–11810.
- Comello, S., Reichelstein, S., & Sahoo, A. (2018). The road ahead for solar PV power. *Renewable and Sustainable Energy Reviews*, 92, 744–756.

- Devamani, R. H. P., Kiruthika, R., Mahadevi, P., & Sagithapriya, S. (2017a). Synthesis and Characterization of Cadmium Sulfide Nanoparticles. *International Journal of Innovative Science, Engineering & Technology*, 4(1), 181-185.
- Dhatchinamurthy, L., Thirumoorthy, P., Arunraja, L., & Karthikeyan, S. (2019). Synthesis and characterization of cadmium sulfide (CdS) thin film for solar cell applications grown by dip coating method. *Materials Today: Proceedings*, 26.
- Esteve-Turrillas, F. A., & Abad-Fuentes, A. (2013). Applications of quantum dots as probes in immunosensing of small-sized analytes. *Biosensors & Bioelectronics*, 41, 12–29. <https://doi.org/10.1016/j.bios.2012.09.025>
- Ferekides, C. S., Marinskiy, D., Viswanathan, V., Tetali, B., Palekis, V., Selvaraj, P., & Morel, D. L. (2000). High efficiency CSS CdTe solar cells. *Thin Solid Films*, 361–362, 520–526.
- Fernandez, A. (2021). *How a Solar Cell Works*. American Chemical Society. <https://www.acs.org/content/acs/en/education/resources/highschool/chemmatters/past-issues/archive-2013-2014/how-a-solar-cell-works.html>
- Flores-Pacheco, A., Álvarez-Ramos, M. E., & Ayón, A. (2020). Chapter Thirteen—Downshifting by quantum dots for silicon solar cell applications. In F. Enrichi & G. C. Righini (Eds.), *Solar Cells and Light Management* (pp. 443–477).
- Fthenakis, V., Athias, C., Blumenthal, A., Kulur, A., Magliozzo, J., & Ng, D. (2020). Sustainability evaluation of CdTe PV: An update. *Renewable and Sustainable Energy Reviews*, 123, 109776.
- Fuhs, W. (2005). ZnO Window Layers for Solar Cells. In N. H. Nickel & E. Terukov (Eds.), *Zinc Oxide—A Material for Micro- and Optoelectronic Applications* (pp. 197–209). Springer Netherlands.
- Gao, B., Zhao, Y., Cai, L., Liu, P., Liang, Z., & Shen, H. (2018). Fabrication of cadmium sulfide/p type silicon heterojunction solar cells under 300 °C with more than 10% efficiency. *Solar Energy*, 173, 635–639.
- Ghosh, B., Datta, A., Das, D., Kumbhakar, D., & Pramanik, A. (2018). Assessment of nanoparticles (copper, cadmium sulphide, copper oxide and zinc oxide) mediated toxicity in a plant system (*Indigofera tinctoria* L.; Fabaceae). *RESEARCH JOURNAL OF CHEMISTRY AND ENVIRONMENT*, 22, 34–48.

- Gray, J. L. (2011). The Physics of the Solar Cell. In A. Luque & S. Hegedus (Eds.), *Handbook of Photovoltaic Science and Engineering* (pp. 82–129). John Wiley & Sons, Ltd.
- Green, M. A. (1982). *Solar Cells: Operating Principles, Technology, and System Applications*. Prentice-Hall.
- Green, M. A. (2008). Self-consistent optical parameters of intrinsic silicon at 300K including temperature coefficients. *Solar Energy Materials and Solar Cells*, 92(11), 1305–1310.
- Gupta, N., & Pal, B. (2012). The synthesis, structure, optical and photocatalytic properties of silica-coated cadmium sulfide nanocomposites of different shapes. *Journal of Colloid and Interface Science*, 368(1), 250–256.
- Hod, I., & Zaban, A. (2014). Materials and Interfaces in Quantum Dot Sensitized Solar Cells: Challenges, Advances and Prospects. *Langmuir*, 30(25), 7264–7273.
- Hodgson, S. D., Brooks, W. S. M., Clayton, A. J., Kartopu, G., Barrioz, V., & Irvine, S. J. C. (2013). Enhancing blue photoresponse in CdTe photovoltaics by luminescent down-shifting using semiconductor quantum dot/PMMA films. *Nano Energy*, 2(1), 21–27.
- Huo, H., Zhang, Q., Wang, M. Q., Streets, D. G., & He, K. (2010). Environmental Implication of Electric Vehicles in China. *Environmental Science & Technology*, 44(13), 4856–4861.
- Hur, S.-G., Kim, E.-T., Lee, J.-H., Kim, G.-H., & Yoon, S.-G. (2008). Characterization of photoconductive CdS thin films prepared on glass substrates for photoconductive-sensor applications. *Journal of Vacuum Science & Technology B: Microelectronics and Nanometer Structures Processing, Measurement, and Phenomena*, 26(4), 1334–1337.
- Jäger, K.-D., Isabella, O., Smets, A. H. M., Swaaij, R. A. C. M. M. van, & Zeman, M. (2016). *Solar energy: Fundamentals, technology and systems*.
- Jain, N., & Hudait, M. K. (2014). III–V Multijunction Solar Cell Integration with Silicon: Present Status, Challenges and Future Outlook. *Energy Harvesting and Systems*, 1(3–4), 121–145.
- Jasim, K. E. (2015). *Solar Cells: New Approaches and Reviews* (L. A. Kosyachenko, Ed.). InTech Open Access.

- Jones, E. W., Barrioz, V., Irvine, S. J. C., & Lamb, D. (2009). Towards ultra-thin CdTe solar cells using MOCVD. *Thin Solid Films*, 517(7), 2226–2230.
- Kamble, M. M., Rondiya, S. R., Bade, B. R., Kore, K. B., Nasane, M. P., Dzade, N. Y., Funde, A. M., & Jadkar, S. R. (2020). Optical, structural and morphological study of CdS nanoparticles: Role of sulfur source. *Nanomaterials and Energy*, 9(1), 72–81.
- Kassim, M., Al-Obaidi, K., C. Munaaim, M. A., & Salleh, A. (2015). Feasibility Study on Solar Power Plant Utility Grid under Malaysia Feed-in Tariff. *American Journal of Engineering and Applied Sciences*, 8.
- Kengpol, A., Rontlaong, P., & Tuominen, M. (2013). A Decision Support System for Selection of Solar Power Plant Locations by Applying Fuzzy AHP and TOPSIS: An Empirical Study. *Journal of Software Engineering and Applications*, 06, 470–481.
- Kereush, D., & Perovych, I. (2017). Determining criteria for optimal site selection for solar power plants. *Geomatics, Landmanagement and Landscape*, 4.
- Khalis, M., Masrour, R., Khrypunov, G., Kirichenko, M., Kudiy, D., & Zazoui, M. (2016). Effects of Temperature and Concentration Mono and Polycrystalline Silicon Solar Cells: Extraction Parameters. *Journal of Physics: Conference Series*, 758, 012001.
- Klimov, V. I., Mikhailovsky, A. A., Xu, S., Malko, A., Hollingsworth, J. A., Leatherdale, C. A., Eisler, H.-J., & Bawendi, M. G. (2000). Optical Gain and Stimulated Emission in Nanocrystal Quantum Dots. *Science*, 290(5490), 314–317.
- Kodigala, S. R. (2010). 7—Fabrication and Properties of Window Layers For Thin Film Solar Cells. In S. R. Kodigala (Ed.), *Thin Films and Nanostructures* (Vol. 35, pp. 393–504). Academic Press.
- Krongarrom, P., Rattanachan, S., & Fangsuwannarak, T. (2012a). ZnO Doped with Bismuth in Case of In-Phase Behavior for Solar Cell Application. *Engineering Journal*, 16.
- Krongarrom, P., Rattanachan, S. T., & Fangsuwannarak, T. (2012b). ZnO Doped with Bismuth in Case of In-Phase Behavior for Solar Cell Application. *Engineering Journal*, 16(3), 59–70.

- Lekha, P., Balakrishnan, A., Subramanian, K. R. V., & Nair, S. V. (2013). Size dependent electron transfer from CdTe quantum dots linked to TiO₂ thin films in quantum dot sensitized solar cells. *Materials Chemistry and Physics*, 141(1), 216–222.
- Lopez-Delgado, R., Zhou, Y., Zazueta-Raynaud, A., Zhao, H., Pelayo, J. E., Vomiero, A., Álvarez-Ramos, M. E., Rosei, F., & Ayon, A. (2017). Enhanced conversion efficiency in Si solar cells employing photoluminescent down-shifting CdSe/CdS core/shell quantum dots. *Scientific Reports*, 7(1), 14104.
- Mey, A. (2019, March 9). *Average U.S. construction costs for solar generation continue to decrease—Today in Energy—U.S. Energy Information Administration (EIA)*. <https://www.eia.gov/todayinenergy/detail.php?id=41153>
- Molina, M. G. (2017). Energy Storage and Power Electronics Technologies: A Strong Combination to Empower the Transformation to the Smart Grid. *Proceedings of the IEEE*, 105(11), 2191–2219.
- Nagai, T., Kanemitsu, Y., Ando, M., Kushida, T., Nakamura, S., Yamada, Y., & Taguchi, T. (2002). Optical Properties of Cubic CdS. *Physica Status Solidi (b)*, 229(1), 611–614.
- Nelson, V. C., & Stacher, K. L. (2015). *Introduction to Renewable Energy* (2nd ed.). CRC Press.
- Nicolay, A., Lanzutti, A., Poelman, M., Ruelle, B., Fedrizzi, L., Dubois, Ph., & Olivier, M.-G. (2015). Elaboration and characterization of a multifunctional silane/ZnO hybrid nanocomposite coating. *Applied Surface Science*, 327, 379–388.
- Olekseyuk, I. D., Davidyuk, H. Y., Parasyuk, O. V., Voronyuk, S. V., Halka, V. O., & Oksyuta, V. A. (2000). Phase diagram and electric transport properties of samples of the quasi-binary system CuInS₂-CdS. *Journal of Alloys and Compounds*, 1–2(309), 39–44.
- Oreski, G., Moulai, F., Khan, A., Jaunich, M., Agroui, K., Arfi, W., & Barretta, C. (2018). *Optical and thermal analysis of PVB encapsulant polymer functionalized with luminescent organic dyes*. 10759.
- Özer, T., & Köse, S. (2009). Some physical properties of Cd_{1-x}Sn_xS films used as window layer in heterojunction solar cells. *International Journal of Hydrogen Energy*, 34(12), 5186–5190.

- Pandian, S. R. K., Deepak, V., Kalishwaralal, K., & Gurunathan, S. (2011). Biologically synthesized fluorescent CdS NPs encapsulated by PHB. *Enzyme and Microbial Technology*, 48(4), 319–325.
- Pankove, J. I. (2010). *Optical Processes in Semiconductors* (2nd ed.). Dover Publications.
- Park, N. C., Oh, W. W., & Kim, D. H. (2013). Effect of Temperature and Humidity on the Degradation Rate of Multicrystalline Silicon Photovoltaic Module. *International Journal of Photoenergy*, 2013, e925280.
- Patel, J., Mighri, F., Aji, A., Tiwari, D., & Chaudhuri, T. (2014). Spin-coating deposition of PbS and CdS thin films for solar cell application. *Applied Physics A*, 117, 1791–1799.
- Peng, H., Sun, W., Li, Y., Yan, W., Yu, P., Zhou, H., Bian, Z., & Huang, C. (2016). High-performance cadmium sulphide-based planar perovskite solar cell and the cadmium sulphide/perovskite interfaces. *Journal of Photonics for Energy*, 6(2), 022002.
- Philippis, S. P., Dimroth, F., & Bett, A. W. (2018). High-Efficiency III–V Multijunction Solar Cells. In *McEvoy's Handbook of Photovoltaics* (pp. 439–472). Elsevier.
- Qutub, N. (2013). *CADMIUM SULPHIDE NANOPARTICLES*. A.M.U.
- Qutub, N., Pirzada, B. M., Umar, K., & Sabir, S. (2016). Synthesis of CdS nanoparticles using different sulfide ion precursors: Formation mechanism and photocatalytic degradation of Acid Blue-29. *Journal of Environmental Chemical Engineering*, 4(1), 808–817.
- Rafic, S. N., Al-Jawad, S. M. H., & Muhsen, M. M. (2017). Synthesized and Study the Structural and Morphological Properties of Polyaniline-Cadmium Sulfide Nanocomposite. *Al-Nahrain Journal of Science*, 20(3), 91–98.
- Raj, F. M., & Rajendran, A. J. (2015). *Synthesis and Characterization of Cadmium Sulfide Nanoparticles for the Applications of Dye Sensitized Solar Cell*, 4(1), 56-60.
- Ramalingam, K., & Indulkar, C. (2017). Chapter 3—Solar Energy and Photovoltaic Technology. In G. B. Gharehpetian & S. M. Mousavi Agah (Eds.), *Distributed Generation Systems* (pp. 69–147). Butterworth-Heinemann.
- Ramanathan, K., Contreras, M., Perkins, C., Asher, S., Hasoon, F., Keane, J., Young, D., Romero, M., Metzger, W., Noufi, R., Ward, J. S., & Duda, A. (2003). Properties of

- 19.2% efficiency ZnO/CdS/CuInGaSe₂ thin-film solar cells. *Progress in Photovoltaics*, 11, 225–230.
- Rattanawichai, P., & Rattanachan, S. T. (2015). High Photocurrent Gain of Spherical Nano-crystalline ZnO:Bi Film for Advanced Solar Cells Application. *Chiang Mai J. Sci.*, 10.
- Rattanawichai, P., Rattanachan, Sirirat. T., & Fangsuwannarak, T. (2018). High Photocurrent Gain of Spherical Nano-crystalline ZnO:Bi Film for Advanced Solar Cells Application. *Chiang Mai J. Sci.*, 45, 1995–2004.
- Raut, B. T., Chougule, M. A., Sen, S., Pawar, R. C., Lee, C. S., & Patil, V. B. (2012). Novel method of fabrication of polyaniline–CdS nanocomposites: Structural, morphological and optoelectronic properties. *Ceramics International*, 38(5), 3999–4007.
- Richter, A., Hermle, M., & Glunz, S. W. (2013). Reassessment of the Limiting Efficiency for Crystalline Silicon Solar Cells. *IEEE Journal of Photovoltaics*, 3(4), 1184–1191.
- Rosa-Clot, M., & Tina, G. M. (2018). Chapter 5—The Floating PV Plant. In M. Rosa-Clot & G. M. Tina (Eds.), *Submerged and Floating Photovoltaic Systems* (pp. 89–136).
- Saga, T. (2010). Advances in crystalline silicon solar cell technology for industrial mass production. *NPG Asia Materials*, 2(3), 96–102.
- Saha, S., Bhattacharya, R., & Bhunia, A. (2015). *FABRICATION OF CdS/Si HETEROJUNCTION SOLAR CELL*. 5, 1–6.
- Saidan, M., Albaali, A. G., Alasis, E., & Kaldellis, J. K. (2016). Experimental study on the effect of dust deposition on solar photovoltaic panels in desert environment. *Renewable Energy*, 92, 499–505.
- Sainthiya, H., & Beniwal, N. (2017). *Different types of cooling systems used in photovoltaic module solar system: A review*, 2017, 1500–1506.
- Santos Andrade, T., Papagiannis, I., Dracopoulos, V., César Pereira, M., & Lianos, P. (2019). Visible-Light Activated Titania and Its Application to Photoelectrocatalytic Hydrogen Peroxide Production. *Materials*, 12(24), 4238.
- Schinke, C., Christian Peest, P., Schmidt, J., Brendel, R., Bothe, K., Vogt, M. R., Kröger, I., Winter, S., Schirmacher, A., Lim, S., Nguyen, H. T., & MacDonald, D. (2015). Uncertainty analysis for the coefficient of band-to-band absorption of crystalline silicon. *AIP Advances*, 5(6), 067168.

- Senthil, K., Mangalaraj, D., & Narayandass, Sa. K. (2001). Structural and optical properties of CdS thin films. *Applied Surface Science*, 169–170, 476–479.
- Shah, A. V., Schade, H., Vanecek, M., Meier, J., Vallat-Sauvain, E., Wyrsh, N., Kroll, U., Droz, C., & Bailat, J. (2004). Thin-film silicon solar cell technology. *Progress in Photovoltaics: Research and Applications*, 12(2–3), 113–142.
- Shah, A. V., Schade, H., Vanecek, M., Meier, J., Vallat-Sauvain, E., Wyrsh, N., Kroll, U., Droz, C., & Bailat, J. (2004). Thin-film silicon solar cell technology. *Progress in Photovoltaics: Research and Applications*, 12(2–3), 113–142.
- Shalaeva, D. S., Kukartseva, O. I., Tynchenko, V. S., Kukartsev, V. V., Aponasenko, S. V., & Stepanova, E. V. (2020). Analysis of the development of global energy production and consumption by fuel type in various regions of the world. *IOP Conference Series: Materials Science and Engineering*, 952(1), 012025.
- Shockley, W., & Queisser, H. J. (1961). Detailed Balance Limit of Efficiency of p-n Junction Solar Cells. *Journal of Applied Physics*, 32(3), 510–519.
- Singh, U., & Patra, S. (2010). Progress in Polycrystalline Thin-Film Cu(In,Ga)Se₂ Solar Cells. *International Journey of Photoenergy*, 2010.
- Soltani, N., Gharibshahi, E., & Saion, E. (2012). Band gap of cubic and hexagonal cds quantum dots-experimental and theoretical studies. *Chalcogenide Letters*, 9(7), 321-328.
- Sproul, A. B., & Green, M. A. (1991). Improved value for the silicon intrinsic carrier concentration from 275 to 375 K. *Journal of Applied Physics*, 70(2), 846–854.
- Sui, X., Tao, H., Lou, X., Wang, X., Feng, J., Zeng, T., & Zhao, X. (2013). CdS quantum dots-sensitized TiO₂ nanotube arrays for solar cells. *Journal of Wuhan University of Technology-Mater. Sci. Ed.*, 28(1), 17–21.
- Tan, J. J., Li, Y., & Ji, G. F. (2011). High-Pressure Phase Transitions and Thermodynamic Behaviors of Cadmium Sulfide. *Acta Physica Polonica A*, 120(3), 501–506.
- Trupke, T., Green, M. A., & Würfel, P. (2002). Improving solar cell efficiencies by down-conversion of high-energy photons. *Journal of Applied Physics*, 92(3), 1668–1674.
- Tsai, C. T., Chuu, D. S., Chen, G. L., & Yang, S. L. (1996a). Studies of grain size effects in rf sputtered CdS thin films. *Journal of Applied Physics*, 79(12), 9105–9109.

- Tsai, C. T., Chuu, D. S., Chen, G. L., & Yang, S. L. (1996b). Studies of grain size effects in rf sputtered CdS thin films. *Journal of Applied Physics*, 79(12), 9105–9109.
- Ubale, A. U., Chipade, K. S., Bhute, M. V., Raut, P. P., Malpe, G. P., Sakhare, Y. S., & Belkhedkar, M. R. (2012). Structural, Optical and Electrical Properties of Nanostructured CdS:CuS Composite Thin Films Grown by CBD Method. *International Journal of Materials and Chemistry*, 2(4), 165–172.
- Varghese, S., Iype, M., Mathew, E. J., & Menon, C. S. (2002). Determination of the energy band gap of thin films of cadmium sulphide, copper phthalocyanine and hybrid cadmium sulphide/copper phthalocyanine from its optical studies. *Materials Letters*, 56(6), 1078–1083.
- Veerathangam, K., Pandian, M., & Ramasamy, P. (2017). Size-dependent photovoltaic performance of cadmium sulfide (CdS) quantum dots for solar cell applications. *Journal of Alloys and Compounds*, 735, 202–208.
- Wang, J., Liu, L., Liu, S., Yang, L., Zhang, B., Feng, S., Yang, J., Meng, X., Fu, W., & Yang, H. (2017). Influence of a compact CdS layer on the photovoltaic performance of perovskite-based solar cells. *Sustainable Energy & Fuels*, 1(3), 504–509.
- Wessendorf, C. D., Hanisch, J., Müller, D., & Ahlswede, E. (2018). CdS as Electron Transport Layer for Low-Hysteresis Perovskite Solar Cells. *Solar RRL*, 2(5), 1800056.
- What is coal & where is it found?* (2020, February 15). World Coal Association. <https://www.worldcoal.org/coal-facts/what-is-coal-where-is-it-found/>
- Xiao, J., Wen, B., Melnik, R., Kawazoe, Y., & Zhang, X. (2014). Phase transformation of cadmium sulfide under high temperature and high pressure conditions. *Physical Chemistry Chemical Physics*, 16(28), 14899–14904.
- Yeole, B., Sen, T., Hansora, D. P., & Mishra, S. (2015). Effect of electrical properties on gas sensitivity of polypyrrole/cds nanocomposites. *Journal of Applied Polymer Science*, 132(32).
- Zhao, J., Wang, A., & Green, M. A. (1999). 24.5% Efficiency silicon PERT cells on MCZ substrates and 24.7% efficiency PERL cells on FZ substrates. *Progress in Photovoltaics: Research and Applications*, 7(6), 471–474.

Vitae

Mr Nikhil Jaden Naidoo was born on October 4, 1996, in Durban, South Africa. He received his bachelor's degree in Electrical Engineering from Durban University of Technology, South Africa, in 2019. Afterwards, he attended Suranaree University of Technology, Nakhon Ratchasima, Thailand, to pursue a master's degree in Electrical Engineering. His research interests include photovoltaic solar cell efficiency, thin film solar cells, and quantum dot technology.

